NMR spectroscopic investigations of diffusion in mixtures of small molecules, fluorinated drugs, and biomolecules in a membrane mimetic environment

A THESIS

submitted by

MATSYENDRANATH SHUKLA

for the award of the degree

of

DOCTOR OF PHILOSOPHY

Department of Physical Sciences
Indian Institute of Science Education & Research (IISER) Mohali
Mohali - 140306 (India)

February 2013

DECLARATION

The work presented in this thesis has been carried out by me under the guidance of Dr. Kavita Dorai at the Indian Institute of Science Education and Research Mohali.

This work has not been submitted in part or in full for a degree, diploma or a fellowship to any other University or Institute. Whenever contributions of others are involved, every effort has been made to indicate this clearly, with due acknowledgement of collaborative research and discussions. This thesis is a bonafide record of original work done by me and all sources listed within have been detailed in the bibliography.

Matsyendranath Shukla

Place :
Date :

In my capacity as the supervisor of the candidate's PhD thesis work, I certify that the above statements by the candidate are true to the best of my knowledge.

Dr. Kavita Dorai
Associate Professor
Department of Physical Sciences
IISER Mohali

Place :
Date :

ACKNOWLEDGEMENTS

First I would like to thank God for giving me an opportunity to do a PhD. Realizing this thesis would never have been possible without all support, inspiration and encouragement from my close surroundings. I would like to thank all the people who helped me and encouraged me during my PhD.

I would like to thank my supervisor Prof. Kavita Dorai for her guidance and many helpful discussions throughout my PhD. She has always encouraged exploration and free thinking. My heartiest thanks goes to her for inspiration, encouragement and support.

I wish to thank my director Prof.N Sathyamurthy, for providing an excellent opportunity and encouragement to work in a new area of science, which made the current work so interesting and worthwhile. It is a pleasure to thank Dean Students Prof. Arvind for his motivation and inspiration during the course of my doctoral study. I thank IISER Mohali for its financial support and facilities to pursue my research.

My thanks also reach out to the many friends who have contributed to the completion of this thesis, either directly or indirectly. The experience and knowledge of Dr.B.S.Joshi, Application Scientist Bruker Biospin Inc. who helped to install the spectrometers used in most part of this work is greatly appreciated.

I thank my labmates Amrita Kumari, Shruti, Navdeep and Harpreet for their help and support and for providing a friendly environment in the laboratory. I thank Mr. Rajesh, NMR lab assistant for his kind support.

Most gratefully, I would like to thank my wife, Abhilasha, she has stood by me every time. In truth I would not have succeeded without her. My special thanks to my friends Shukdeep Kumar, Jebarathinam, Ritabrata Sengupta, Debmalaya Das,for helpful discussions and cheerful moments during my stay in the campus. A special thanks to my collaborators and coauthors, especially summer intern Mr. Mahamaya

Singh and Mr Prashant Mishra during his MS project.

I wish to thank my doctoral committee members Dr. Kamal P. Singh and Dr. Rajeev Kapri for their encouragement. I thank Department of Science and Technology (DST) for providing me the financial support to attend an international conference.

I am also grateful for the help, support and time I have spent with my mother, father, brothers, sister and other close relatives.

—

TABLE OF CONTENTS

LIST OF PUBLICATIONS

1. Resolving overlaps in diffusion encoded spectra using band-selective pulses in a 3D BEST-DOSY experiment, Matsyendranath Shukla and Kavita Dorai, *J. Magn. Reson.*, 213, 69 (2011).

2. Disentangling diffusion information of individual components in a mixture with a 3D COMPACT-IDOSY NMR experiment, Matsyendranath Shukla and Kavita Dorai, *Magnetic Resonance in Chemistry*, 50, 341 (2012).

3. A novel multiple-quantum correlation NMR scheme to separate components of a mixture according to their diffusion coefficients, Matsyendranath Shukla, and Kavita Dorai, *Applied Magnetic Resonance*, 43, 485 (2012).

4. A facile protocol for the construction of novel bridged bisdioxins trioxabicyclo-[3.3.1]nonadienes: mechanistic insights using DFT analysis, Satyanarayana Reddy Jaggavarapur, Anand Solomon Kamalakaran, Matsyendranath Shukla, Kavita Dorai and Gopikrishna Gaddamanugu, **In Press, Tetrahedron (2013)**, **(doi: 10.1016/j.tet.2013.01.002)**.

5. Investigations of the stereochemistry and liposomal interaction of new-generation fluoroquinolone drugs using ^{19}F NMR, Matsyendranath Shukla, Navdeep Gogna and Kavita Dorai, **Manuscript in Preparation (2013)**.

6. NMR investigations of the diffusion of anti-oxidants in DPPC lipid bilayers, Matsyendranath Shukla, Navdeep Gogna and Kavita Dorai, **Manuscript in Preparation (2013)**.

WORK PRESENTED IN CONFERENCES

1. Efficiency of heteronuclear polarization transfer schemes in TROSY-like pulse sequences in biomolecules, Matsyendranath Shukla and Kavita Dorai, NMRS-2010, CBMR Lucknow, February 21-24, 2010.

2. Studies of diffusion coefficients in proteins, Matsyendranath Shukla and Kavita Dorai, NMRS-2011, GNDU Amritsar, March 1-4, 2011.

3. 3D COMPACT-IDOSY: A new tool for the analysis of complex mixtures, Matsyendranath Shukla and Kavita Dorai, NMRS-2012, IISc Bangalore, February 5-8, 2012.

4. 3D BEST-DOSY, 3D COMPACT-IDOSY and 3D MQ-DOSY: New tools for the analysis of complex mixtures, Matsyendranath Shukla and Kavita Dorai, 53rd Experimental nuclear magnetic resonance conference (ENC), Florida USA, April 15-20, 2012.

Abstract

NMR spectroscopy is a very powerful technique for the investigation of molecular structure, conformation and dynamics. This thesis describes a detailed study of NMR diffusion processes in several systems and also includes the construction of novel 2D and 3D pulse sequences in the field of diffusion NMR. The main objective was to carry out detailed experiments to measure accurate self-diffusion coefficients of solution systems ranging in size from molecules to micelles. Diffusion-ordered spectroscopy (DOSY) is based on the pulse-field gradient spin-echo NMR sequence and can be used to separate the individual NMR spectra of a molecules in a mixture according to their diffusion coefficients. The strength of DOSY is that it can be used as a non-invasive method to obtain both physical and chemical information. The 2D DOSY experiment has limited potential to differentiate between severely overlapped signals in a mixture, which can lead to inaccurate estimates of diffusion coefficients. Several 3D DOSY experiments have been designed that achieve resolution of overlaps by concatenating a diffusion pulse sequence with common 2D pulse sequences. We have designed 3D BEST-DOSY, 3D COMPACT-IDOSY and 3D MQ-DOSY type of pulse sequences to circumvent the overlap problem in several molecular mixtures.

Chapter 1

This chapter deals with fundamentals of NMR spectroscopy, fundamentals of diffusion, a brief description of the pulsed-field gradient NMR and application of PFG NMR, the basic spin echo experiment, 2D DOSY and its applications.

Chapter 2

This chapter describes a pulse sequence we developed called 3D BEST-DOSY. This method focuses on exploiting the sensitivity-enhanced BEST-HMQC technique to achieve resolution of overlaps in a novel 3D heteronuclear ^{13}C-^{1}H diffusion ordered experiment with good sensitivity and a substantial reduction in experiment time. This pulse sequence has been applied on a mixture of molecules with similar diffusion coefficients, a mixture of amino acids and a mixture of commercial gasoline.

Chapter 3

This chapter describes a new 3D I-DOSY type of pulse sequence we developed called COMPACT-IDOSY which includes a diffusion encoding sequence within a sensitivity enhanced HMBC-type pulse sequence. The direct incorporation of diffusion-encoding into the heteronuclear coherence transfer sequence gives a substantial time and sensitivity advantage over standard 3D DOSY methods. The scheme has been experimentally demonstrated on a rutin trihydrate and quercetin dihydrate mixture, wherein the diffusion coefficients of the two molecular species are very similar.

Chapter 4

This chapter deals with the incorporation of a novel multiple-quantum/single-quantum correlation experiment into a DOSY sequence which we call the MQ-DOSY pulse sequence. This pulse sequence has been applied on small molecules and achieves good resolution of severely overlapped multiplets, leading to the accurate estimation of diffusion coefficients.

Chapter 5

This chapter shows that drugs that have little or no difference in diffusion coefficients in simple solution may readily be resolved in DOSY experiments in solutions containing micelles. Two fluorinated drugs prulifloxacin and pazufloxacin were chosen as a test case. Their diffusion properties and T_1 and T_2 relaxation properties were investigated in DMSO-D6 solutions, and in solutions containing micelles.

Chapter 6

This chapter deals with the extraction of diffusion information using PFGNMR of two anti-oxidants: alpha-tocopherol and curcumin, diffusing inside DPPC lipid bilayer. The relevance of diffusion NMR study of lipid-soluble antioxidants in lipid bilayer membrane models and micellar structures is discussed.

Chapter 7

A brief outline of the main results of the thesis are summarized and some prospects for future extensions of the work are described in this chapter.

Appendix

A brief tutorial on how to install and calibrate the Diff30 diffusion probe as well protocols for diffusion data processing using the Bruker Topspin softare as well as the DOSY Toolbox software package, are given in the Appendix.

LIST OF TABLES

LIST OF FIGURES

List of Abbreviations

NMR - Nuclear Magnetic Resonance
RF - Radio Frequency
FID - Free Induction Decay
FFT- Fast Fourier Transform
ILT- Inverse Laplace Transform
PFG - Pulsed Field Gradient
PGSE - Pulsed Field Gradient Spin-Echo
STE - Stimulated-Echo
COSY - Correlated Spectroscopy
HSQC - Heteronuclear Single-Quantum Correlation
HMQC - Heteronuclear Multiple-Quantum Correlation
HMBC - Heteronuclear Multiple-Bond Correlation
TOCSY - Total Correlation Spectroscopy
CPMG - Carr-Purcell-Meiboom-Gill
PGSTE-WATERGATE - Pulsed Field Gradient Stimulated-Echo-Water Suppression by Gradient Tailored Excitation.
BPPSTE - Bipolar Pulse Pair Stimulated-Echo
DOSY - Diffusion-Ordered Spectroscopy
BEST-DOSY - Band-Selective Excitation Short-Transient Diffusion-Ordered Spectroscopy
COMPACT-IDOSY - Cross Polarization Optimized Multisite Polarized Accelerated Time-IDOSY
MQ-DOSY - Multiple-Quantum-Diffusion-Ordered Spectroscopy
MAD - Matrix Assisted Diffusion-Ordered NMR Spectroscopy
SDS - Sodium Dodecyl Sulfate
DPPC - Dipalmitoylphosphatidylcholine
DNA - Deoxyribonucleic Acid
DECRA - Direct Exponential Curve Resolution Algorithm
CORE - Component Resolved

CHAPTER 1

Introduction

1.1 Fundamentals of NMR

The physical foundation of nuclear magnetic resonance (NMR) spectroscopy lies in the magnetic properties of atomic nuclei. The explanation of NMR uses quantum mechanics to arrive at a description of nuclear response to a static, external magnetic field and applied radio frequency (RF) radiation. This chapter will briefly cover the fundamental aspects of NMR and the reader is referred to several books and review articles for an in-depth analysis of NMR theory [4, 5, 6, 7, 8, 9, 10, 11, 12, 13, 14, 15, 16].

Quantum mechanically, subatomic particles (protons, neutrons and electrons) have spin. The spin properties of protons and neutrons in the nuclei of heavier elements combine to define the overall spin of the nucleus. When both the number of protons (atomic number) and the sum of the protons and neutrons (atomic mass) are even, the nucleus has no magnetic properties, i.e. its spin quantum number (I) is zero. In several atoms (e.g ^{12}C, ^{14}N, ^{16}O), the spins are paired and cancel out each other, so that the nucleus of the atom has no overall spin and therefore are invisible to the NMR experiment. When either the atomic number or the atomic mass is odd, or both are odd, the nucleus has magnetic properties and is said to be spinning. In many atoms (^{1}H, ^{13}C, ^{15}N, ^{19}F, ^{31}P etc) the nucleus does possess an overall spin. A spinning nucleus acts as a tiny bar magnet oriented along the spin rotation axis. When this small magnet is placed in the field of a much larger magnet its orientation will no longer be random [16]. The most favorable orientation would be the low-energy state (α- spin state) and the less favorable orientation be the high-energy state (β- spin state). Figures 1.1 and 1.2 show the respective orientations of a nucleus in a magnetic field. This picture is purely classical. However, nuclear spins are really quantum objects. In Dirac notation, the states a spin can be denoted by $|\alpha\rangle$ for a spin in the ground state (along z), and by $|\beta\rangle$ for a spin in the excited state (along -z). The two states have well defined energies and the energy level

splitting of the spin in the magnetic field is known as the Zeeman splitting. A spin-1/2 particle is not restricted to these states, but may be in a superposition of the two energy eigenstates:

$$|\psi\rangle = c_\alpha|\alpha\rangle + c_\beta|\beta\rangle \tag{1.1}$$

where c_α, c_β are complex and $|c_\alpha|^2 + |c_\beta|^2 = 1$.

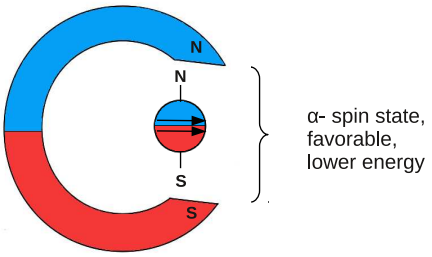

Figure 1.1: A spinning nucleus with its magnetic field aligned with the magnetic field of a magnet.

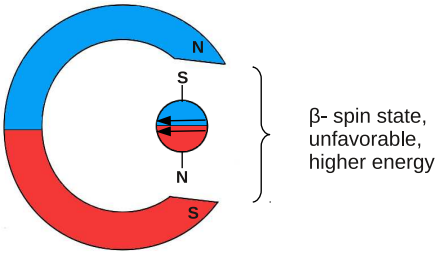

Figure 1.2: A spinning nucleus with its magnetic field aligned against the magnetic field of a magnet.

The hydrogen atom (denoted by ^{1}H), is composed of a single proton and a single electron. For the purpose of NMR, the key aspect of the hydrogen nucleus is its angular momentum. The spinning hydrogen nucleus is positively charged, it generates a magnetic field and possesses a magnetic moment μ.

The magnitude of the magnetic moment produced by a spinning nucleus varies from atom to atom in accordance with the equation $\mu = \gamma\hbar I$, where $\hbar$ is Planck's constant divided by 2π and γ is the gyromagnetic ratio which determines the resonant frequency of the nucleus for a given external field. Figure 1.3 depicts on the left a magnetic moment with a +z component, and a magnetic moment with a -z component on the right. The force of B_0 causes the magnetic moment to precess in a cone about the +z direction in the first case and about the -z direction in the second. The magnetic field B_0 in the z direction operates on the x components of μ to create a force in the y direction. The spin angular momentum confers a magnetic moment on a nucleus and therefore a given energy in a magnetic field. The nuclear magnetic moment (μ) is given by

$$\mu = \gamma P \tag{1.2}$$

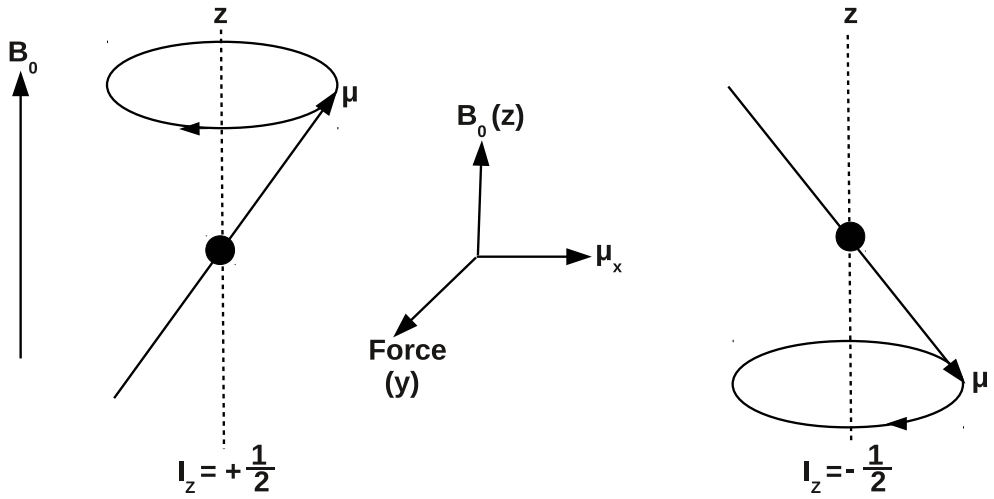

Figure 1.3: Orientation of the nuclear spin dipole.

The allowed values or eigenvalues of the maximum component of the angular momentum in the z direction are defined by

$$P_z = (h/2\pi)m_I \tag{1.3}$$

where m_I is the magnetic quantum number. In a magnetic field, a nucleus of spin *I* has 2*I* + 1 possible orientations which has values [10]

$$m_I = I, I-1, I-2, ..., -I \tag{1.4}$$

We can visualize a spin $\frac{1}{2}$ nucleus as a small bar magnet which when placed in a static field has an energy which varies with orientation to the field. The possible energies are quantized, with the two possible values of m_I $\left(\pm\frac{1}{2}\right)$ corresponding to parallel and antiparallel orientations of this small magnet and the external field (Figure 1.4). The population ratio between the number of nuclei in the higher and lower energy levels is described by the Boltzmann relationship which is dependent upon the absolute temperature T of the sample.

$$\frac{N_\alpha}{N_\beta} = \exp\left(\frac{\Delta E}{k_B T}\right) \tag{1.5}$$

where k_B is the Boltzmann's constant, ΔE is the energy difference between the spin states. The precessional motion of the magnetic moment around B_0 occurs with angular frequency ω_0, called the Larmor frequency given by:

$$\omega_0 = \gamma B_0 \tag{1.6}$$

The energy separation (ΔE) between the two spin states is related to the Larmor frequency by the formula:

$$\Delta E = \hbar\omega_0 = h\nu_0 = \gamma\hbar B_0 \tag{1.7}$$

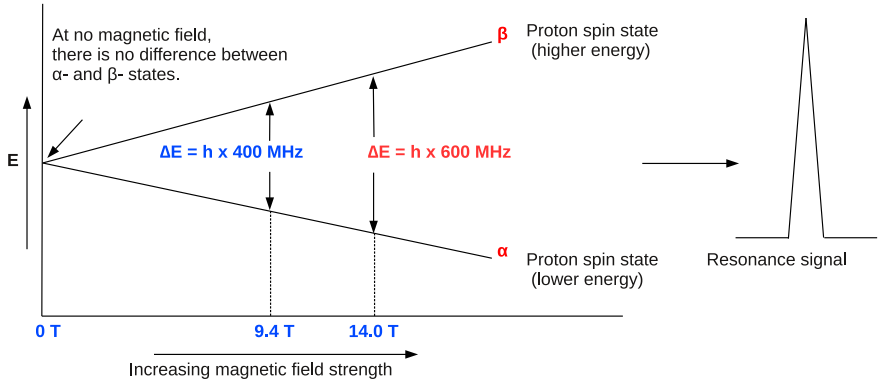

Figure 1.4: Energy separation between nuclear spin states.

Thus as the B_0 field increases, the difference in energy between the two spin states increases. The natural precession frequency of a spinning nucleus depends only on the nuclear properties contained in the gyromagnetic ratio and the applied magnetic field. For a proton in a magnetic field of 9.4 T, the frequency of precession is 400 MHz, and the difference in energy between the spin states is only 3.8×10^{-5} Kcal/mol. For higher fields, such as 14.0 T, the resonance frequency increases to 600 MHz.

In the NMR experiment the populations of the two energy states (Figure 1.4) are interconverted by applying a second magnetic field B_1 at radio frequencies. The absorption of energy occurs as $+\frac{1}{2}$ nuclei (α states) transition to $-\frac{1}{2}$ nuclei (β states), and emission occurs as $-\frac{1}{2}$ nuclei (β states) revert to $+\frac{1}{2}$ nuclei (α states). The process is called resonance. The NMR absorption is a consequence of transitions between the energy levels stimulated by RF radiation and can be detected, amplified and recorded as a

spectral line, called the resonance signal.

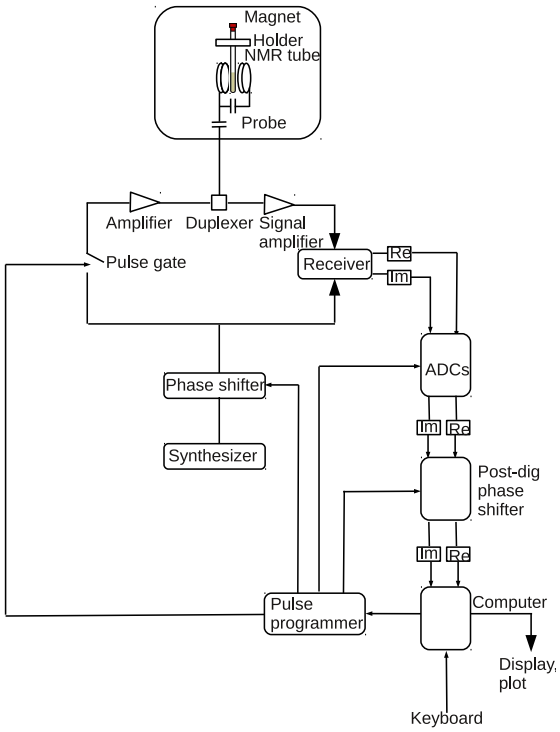

Figure 1.5: Block diagram of an NMR spectrometer.

1.1.1 NMR Magnetization

At thermal equilibrium, the vector sum of all the individual spins is called the magnetization $\mathbf{M}_0$, oriented along the magnetic field direction [15, 16]. Only 20 spins are shown on the surface of the double cone in the Figure 1.6(A), and the excess of $+\frac{1}{2}$ over $-\frac{1}{2}$ nuclei is exaggerated (12 to 8). When a second RF magnetic field is applied to the nuclei, the vector B_1 exerts a force on $\mathbf{M}_0$, (the force comes from the cross product $\mathbf{F} = \mathbf{M} \times \mathbf{B}$). The resonance frequency in the transverse (x-y) plane causes $\mathbf{M}_0$ to precess or "tip" only slightly off the z axis, moving toward the y axis are shown in Figure 1.6(C) as 11 nuclei of spin $+\frac{1}{2}$ and 9 of spin $-\frac{1}{2}$, after application of the B_1 field. The angle of rotation θ is given by

$$\theta = \gamma B_1 \tau \tag{1.8}$$

where θ is the tip angle which is dependent on the strength of the B_1 field excitation and τ is the duration of the B_1 field application. When the excitation pulse is stopped, the

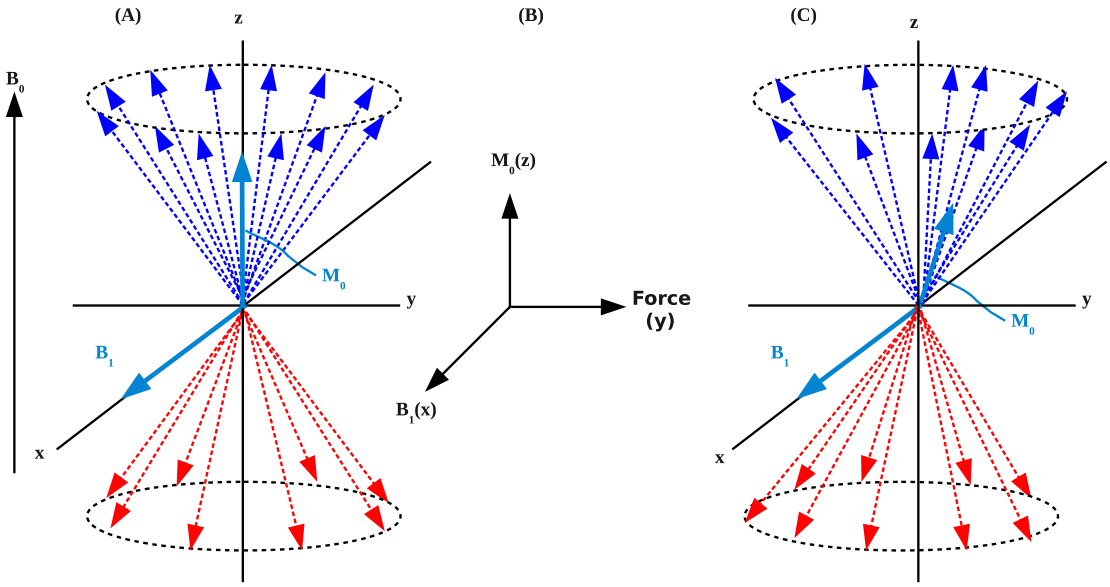

Figure 1.6: (A) A distribution of an ensemble of nuclear spins in the presence of a magnetic field applied along the z axis. (B) The vector B_1 exerts a force on $\mathbf{M}_0$ whose result is perpendicular to both vectors. (C) Nuclear spins immediately after application of the B_1 field.

individual nuclei begin to undergo relaxation by emitting the absorbed RF energy and re-establishing the thermal equilibrium Boltzmann population of the spins (Figure 1.6).

1.1.2 Free induction decay (FID)

After the B_1 pulse is turned off, the transverse magnetization precesses in the x-y plane around the $\mathbf{B}_0$ field. The transverse magnetization is coherent and gives rise to a non-zero magnetic moment in the x-y plane. A spin is considered to be on-resonance if its resonance frequency is the same as the frequency of the B_1 field. In this case, the signal does not oscillate, but decays exponentially with a time constant of T_2, the spin-spin relaxation time. An off-resonance spin is one whose resonance frequency is not equal to the frequency of the applied B_1 pulse. The precessing transverse magnetization induces a sinusoidally oscillating, exponentially decaying NMR signal in the RF coil. This signal is called the free induction decay, and is the product of a periodic function containing a mixture of frequencies and an exponential decay function [14]. In order to

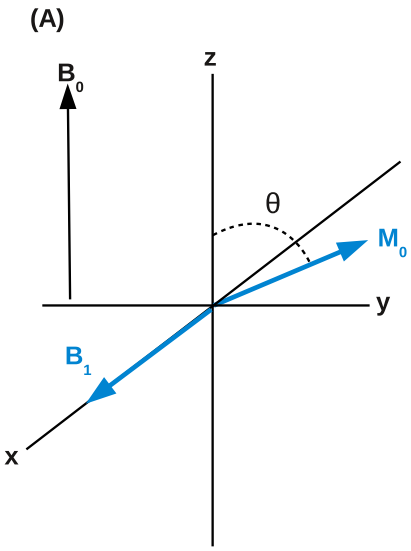

Figure 1.7: The second RF magnetic field $\mathbf{B}_1$ applied perpendicular to the $\mathbf{B}_0$ field. $\mathbf{M}_0$ precesses about the $\mathbf{B}_1$ field, and coherently tips the magnetization into the transverse plane at an angle θ.

transfer NMR data from time (FID) to frequency domain (spectrum), we have to apply a mathematical operation called the Fourier transformation. The Fourier transformation defines a relationship between one function in the time domain and another function in the frequency domain:

$$S(\omega) = Fs(t) = \int_{-\infty}^{\infty} s(t)e^{-i\omega t}dt; \tag{1.9}$$

$$S(\nu) = Fs(t) = \int_{-\infty}^{\infty} s(t)e^{-i2\pi\nu t}dt, \tag{1.10}$$

in which $\omega = 2\pi\nu$. The two functions $s(t)$ and $S(\omega)$ (or $s(t)$ and $S(\nu)$) are said to form a Fourier transform pair. The inverse Fourier transformations are defined by

$$s(t) = F^{-1}S(\omega) = \frac{1}{2\pi}\int_{-\infty}^{\infty} S(\omega)e^{i\omega t}d\omega; \tag{1.11}$$

$$s(t) = F^{-1}S(\nu) = \int_{-\infty}^{\infty} S(\nu)e^{i2\pi\nu t}d\nu, \tag{1.12}$$

The line intensities in the NMR spectrum are defined by the maximum FID amplitudes of the respective frequency components.

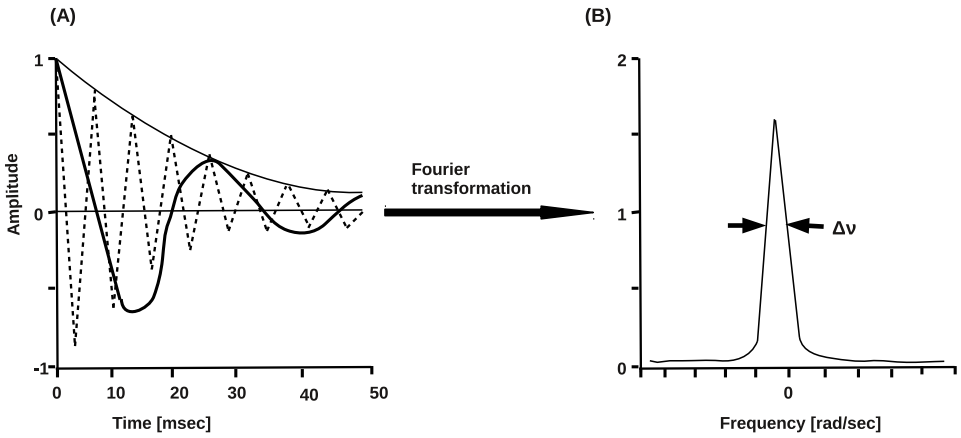

Figure 1.8: (A) FID showing on and off-resonance signals. (B) Lineshape of an NMR resonance. The Fourier transform of the FID is the Lorentzian function. The width of the Lorentzian at the half maximum, $\Delta\nu$, indicated and related to T_2.

The position of the resonance line in the spectrum depends on its precessional frequency. The lineshape of a resonance depends on how the signal decays with time (Figure 1.8). T_2 is the FID decay time constant and associated with the full width of the line at half-height, $\Delta\nu$ which is equal to [17]

$$\Delta\nu = \frac{1}{\pi T_2} \tag{1.13}$$

1.1.3 T_1 relaxation

Spin-lattice relaxation, also called T_1 or longitudinal relaxation is the irreversible evolution of a spin system toward thermal equilibrium, with the orbital degrees of freedom of the medium in which the spins are embedded, called the lattice [18, 17]. The most efficient T_1 relaxation occurs when a molecule is rotating or translating at a rate close to the Larmor frequency. The commonly used pulse sequence to measure spin-lattice relaxation is the 180° - τ - 90° sequence. It is known also as the inversion recovery (IR) pulse sequence (Figure 1.9). At time $\tau = 0$ the 180° RF pulse is applied at the Larmor frequency, which inverts the the magnetization vector $\mathbf{M}$. After this the magnetization $\mathbf{M}$ lies along the negative z axis and $\mathbf{M}$ = - $\mathbf{M}_z$. After the termination of the RF pulse the spin lattice relaxation makes the magnetization $\mathbf{M}_z$ increase during τ interval, and

the spins will dissipate their energy. This dissipation results in the return of $\mathbf{M}$ to the equilibrium position aligned parallel with the $\mathbf{B}_0$ field.

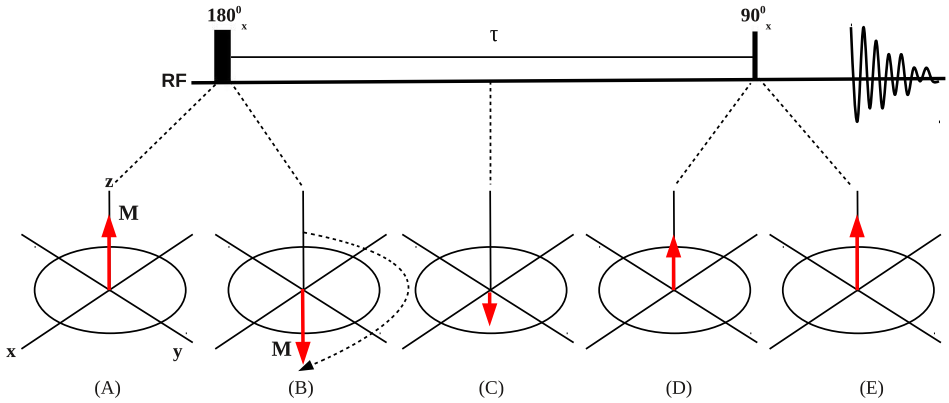

Figure 1.9: Top: Inversion-recovery pulse sequence for the measurement of T_1 relaxation [1]. Bottom: (A) Magnetization(M) lies along the z-axis (B) 180^0 radio frequency pulse tips magnetization (M) to -M_z. (C) $\rightarrow$ (D) Magnetization is relaxing back. (E) Magnetization has recovered to Mz.

The magnetization along the z-axis return to its equilibrium value, due to a random process and thus recovers exponentially as described by the value of M_z at a time τ (Figure 1.10):

$$M_z(\tau) = M_0\ (1 - \alpha e^{\frac{-\tau}{T_1}}) \tag{1.14}$$

where $\alpha = 1$ for a 90° and $\alpha = 2$ for a 180° pulse, respectively.

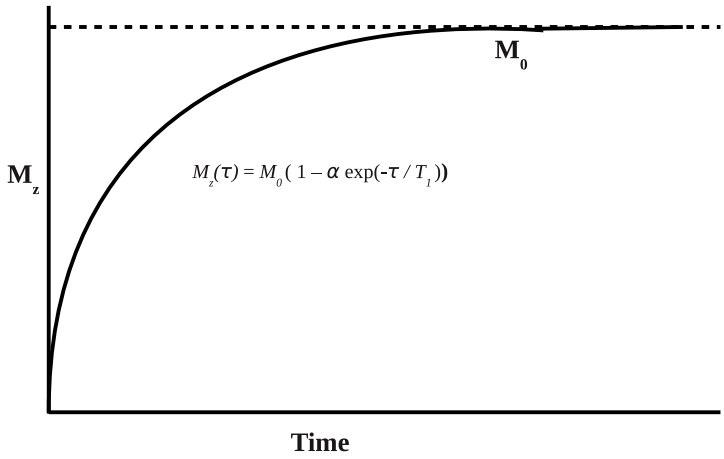

Figure 1.10: The exponential recovery of the longitudinal magnetization component M_z.

1.1.4 T_2 relaxation

A second type of relaxation mechanism is known as transverse relaxation, or spin-spin relaxation. T_2 relaxation occurs when spins in the high and low energy states exchange energy but do not lose energy to the surrounding lattice. Following application of a 90° RF pulse, the net magnetization in the samples begins to precess coherently in the transverse plane (Figure 1.11). The most efficient transverse relaxation occurs in the presence of a static or slowly fluctuating local magnetic fields within a sample. At the end of the excitation pulse, all of the spins precess in-phase in the transverse xy-plane. After some time, the individual nuclei undergo relaxation by exchange of the rf absorbed energy within the spin system, nuclear spins start fanning out and lose their phase coherence. This results in a decay of the total magnetization in the xy-plane (Figure 1.12):

$$\mathbf{M}_{x,y}(\tau) = \mathbf{M}_0 e^{\frac{-\tau}{T_2}} \tag{1.15}$$

The actual decay of the transverse magnetization is a combination of dipole-dipole interactions and magnetic field inhomogeneity (mainly caused by the differences in the magnetic susceptibility within the sample and possible paramagnetic impurities). The field inhomogeneity increases the rate of signal loss and the net decay is described by the apparent relaxation time T_2^*, which is always shorter than T_2:

$$\frac{1}{T_2^*} = \frac{1}{T_2} + \frac{1}{T_{2(sus)}} + \frac{1}{T_{2(in\ hom)}} + \frac{1}{T_{2(diff)}} \tag{1.16}$$

where $T_{2(sus)}$ is the transverse relaxation due to susceptibility, $T_{2(in\ hom)}$ is the transverse relaxation due to B_0 field inhomogeneities, and $T_{2(diff)}$ is the transverse relaxation due to molecule diffusion.

Measuring T_2 is more difficult because of the presence of local field inhomogeneities. One method involves using the Carr-Purcell-Meiboom-Gill (CPMG) spin-echo technique [19, 20]. In the CPMG sequence, the successive 180° pulses are coherent, and the phase of the 90° RF pulse is shifted 90° relative to the phase of the 180° pulse.

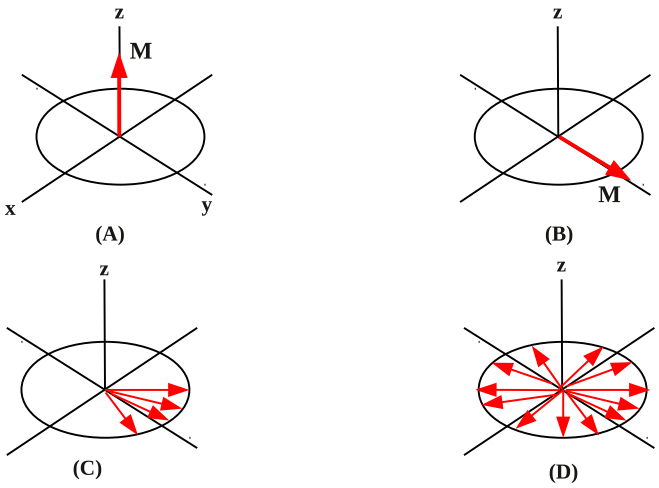

Figure 1.11: Schematic representation of transverse, or spin-spin relaxation mechanism. (A) Magnetization lies along the z axis. (B) Magnetization is tipped in to x-y plane. (C) Individual spins begin to dephase due to atomic interactions. (D) Spins are completely dephased.

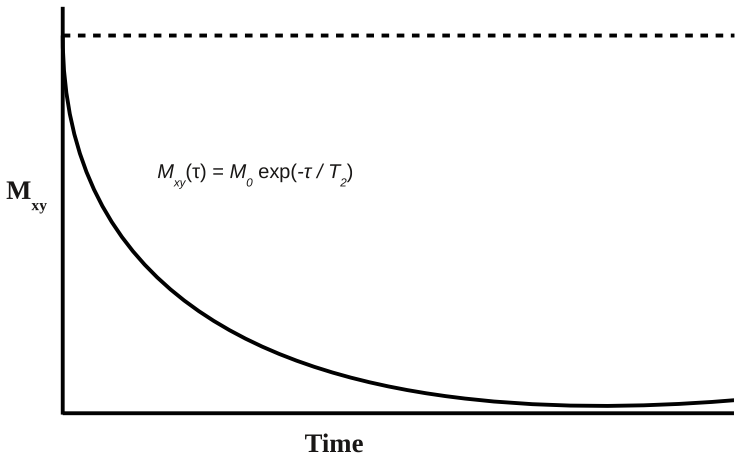

Figure 1.12: Schematic representation of the attenuation of echo signal amplitudes due to T_2 decay.

1.2 Fundamentals of Diffusion

Molecules in solution are in random motion. The random molecular motion in diffusion is because all molecules have energy of motion (kinetic energy) and are constantly colliding with each other [21]. Self-diffusion is the random translational motion of molecules driven by internal kinetic energy. Translational diffusion encodes the transport properties of molecules and ions and is responsible for all chemical reactions since the reacting species must collide before they can react. The diffusion coefficient "*D*" is critically dependent on (1) Sample temperature (2) Solvent viscosity (3) Molecular shape (4) Molecular size. The value of *D* may be approximated by the Stokes-Einstein equation. Diffusion is quantified as the translational (D_t) and rotational (D_r) diffusion coefficients. (D_t) and (D_r) are related to viscosity via the Stokes-Einstein Law:

$$D_t = \frac{k_B T}{f} \tag{1.17}$$

where k_B (JK^{-1}) is the Boltzmann constant, *T* is the absolute temperature (K) and f is the friction factor. For the special case of a spherical particle of hydrodynamic radius R_h in a solvent of viscosity η, the fractional coefficient $f = 6\pi\eta R_h$, and is described by the Stokes-Einstein Debye Law :

$$D_r = \frac{k_B T}{8\pi\eta R_h^3} \tag{1.18}$$

This thesis will focus on measurements of the translational diffusion coefficient. The quantification of the diffusion coefficient in NMR is related to the self diffusion of the molecule and mathematically can be described using a theory based on the change in molecular concentration along a diffusion gradient as described by Fick's Laws [22]. The amount of a property passing through a unit area per unit time is called flux e.g. moles m^{-2}s^{-1}. According to Fick's 1st Law, the flux is defined as

$$\mathbf{J}(\mathbf{r}, t) = -D\nabla c(\mathbf{r}, t) \tag{1.19}$$

The flux, $\mathbf{J}(\mathbf{r}, t)$, is equal to the gradient of concentration, $c(\mathbf{r}, t)$, at some diffusion

coefficient, in the direction of larger to smaller concentration (indicated by negative sign [23, 24]). According to the law of conservation of mass the number of molecules is conserved within the sample space. In general, the diffusion process is anisotropic and the isotropic diffusion coefficient *D* (scalar) is replaced by a rank two diffusion tensor [22]. Thus for Cartesian coordinates $\mathbf{D}$ is given by D_{ij} where *i* and *j* take each of the Cartesian directions and the equation can be written as:

$$\begin{bmatrix} J(x,t) \\ J(y,t) \\ J(z,t) \end{bmatrix} = \begin{bmatrix} D_{xx} & D_{xy} & D_{xz} \\ D_{yx} & D_{yy} & D_{yz} \\ D_{zx} & D_{zy} & D_{zz} \end{bmatrix} \begin{bmatrix} \frac{\partial c(x,t)}{\partial x} \\ \\ \frac{\partial c(y,t)}{\partial y} \\ \\ \frac{\partial c(z,t)}{\partial z} \end{bmatrix}$$

The diagonal elements of $\mathbf{D}$ (e.g. D_{xx}, D_{yy}, D_{zz}) scale concentration gradients and fluxes in the same direction, the off-diagonal elements couple fluxes and concentration gradients in orthogonal directions.

For a normal diffusion process, particles cannot be created or destroyed, which means the flux of particles into one region must be the sum of the particle flux flowing out of the surrounding regions. This is represented mathematically by the continuity equation

$$\frac{\partial c(\mathbf{r},t)}{\partial t} = -\nabla \cdot J(\mathbf{r},t) \tag{1.20}$$

Fick's 2 nd Law of diffusion is given by [25]

$$\frac{\partial c(\mathbf{r},t)}{\partial t} = D\nabla^2 c(\mathbf{r},t) \tag{1.21}$$

D is assumed to be essentially independent of the solute concentration, which is presumed to be low. It is appropriate to introduce the probability $P(\mathbf{r_0}, \mathbf{r_1}, t)$ that a solute molecule, which is initially at $\mathbf{r_0}$ will be at position $\mathbf{r_1}$ at time *t*. For ordinary isotropic diffusion, the 'propagator' $P(\mathbf{r_0}, \mathbf{r_1}, t)$ obeys [26]:

$$\frac{\partial P(\mathbf{r_0}, \mathbf{r_1}, t)}{\partial t} = D\nabla^2 P(\mathbf{r_0}, \mathbf{r_1}, t) \tag{1.22}$$

For the case of unbounded diffusion and for the starting condition $P(\mathbf{r_0}, \mathbf{r_1}, 0) = \delta(\mathbf{r_0} - \mathbf{r_1})$ (where $\delta(\mathbf{r_0} - \mathbf{r_1})$ is the Dirac delta function, indicating that as t $\rightarrow$ 0, c = 0 everywhere except at the origin $\mathbf{r_1}$ = 0) and the boundary condition $P(\mathbf{r_0}, \mathbf{r_1}, t) \rightarrow 0$ for $\mathbf{r_1} \rightarrow \infty$, the solution yields the dependence of the probability P on the displacement.

The solution to Fick's 2 nd Law in an isotropic, homogeneous medium turns out to be a Gaussian probability function:

$$P(\mathbf{r_0}, \mathbf{r_1}, t) = -(4\pi Dt)^{-3/2} \exp\left\{-\frac{(\mathbf{r_1} - \mathbf{r_0})^2}{4Dt}\right\} \tag{1.23}$$

where $\mathbf{r_0}$ and $\mathbf{r_1}$ are the initial and final spatial positions of diffusing molecule, respectively [23]. The probability that a molecule will diffuse a given distance is not dependent on the starting position $\mathbf{r_0}$ but rather on the net displacement $\mathbf{r_1} - \mathbf{r_0}$ of the molecules during the diffusion time *t*. At very short time-scales diffusion is a many-body problem, but at sufficiently large times it reduces to a single-body stochastic problem characterized by a single number, the self diffusion coefficient [27]

$$D = \lim_{t\rightarrow\infty} \frac{1}{nt} \langle (\mathbf{r_1} - \mathbf{r_0})^2 \rangle \tag{1.24}$$

where n is 2, 4, or 6 for one, two or three-dimensional diffusion, respectively. Hence the displacement resulting from diffusion is related to the diffusion coefficient and for the case of unhindered diffusion, the average square displacement increases linearly with the diffusion time t.

1.3 Pulsed-Field Gradient (PFG) NMR

One of the most commonly used NMR experiments is the pulsed gradient spin-echo (PGSE). The PGSE experiment is based on either a two-pulse spin-echo or a three-pulse stimulated echo RF pulse sequence. In the PFG method, the attenuation of the NMR signal resulting from the dephasing of the nuclear spins due to the combined effect of the translational motion and the imposition of spatially well-defined gradient pulses is used to measure molecular motion [28, 29, 30, 31, 32, 33, 34]. Since the static

magnetic field $\mathbf{B}_0$ is spatially homogeneous, a spatially-varying, linear magnetic field gradient $\mathbf{g}$ can be superimposed on $\mathbf{B_0}$ such that ω becomes spatially dependent,

$$\omega_{eff} = \omega_0 + \gamma(\mathbf{g}.\mathbf{r}) \tag{1.25}$$

where $\mathbf{r}$ is the spatial position of a molecule relative to the applied gradient and $\mathbf{g}$ is defined as

$$\mathbf{g} = \nabla\mathbf{B_0} = \frac{\partial \mathbf{B}_z}{\partial x}\mathbf{i} + \frac{\partial \mathbf{B}_z}{\partial y}\mathbf{j} + \frac{\partial \mathbf{B}_z}{\partial z}\mathbf{k} \tag{1.26}$$

where **i,j** and $\mathbf{k}$ are unit vectors of the laboratory frame of reference. The change in local magnetic field induces a spatially-dependent phase shift of the nuclear spins that is cumulatively defined as

$$\phi_t = \gamma\mathbf{B_0}t + \gamma\int_0^t \mathbf{g}(t').\mathbf{r}(t')dt' \tag{1.27}$$

The first term on the right-hand side of the equation corresponds to the phase shift due to the static field, and the second term represents the phase shift due to the effects of the gradients. In the rotating frame of reference, the static term in the equation goes to zero. The accumulated phase ϕ_t during the application of a magnetic field gradient can be used to spatially label the position of nuclei. The PFG method was first introduced by Stejskal and Tanner [35], who incorporated a pair of diffusion-sensitizing constant magnetic field gradients into a Hahn spin-echo sequence [36] in which equal rectangular gradient pulses of duration δ are inserted into each τ period (Figure 1.13). A perfect 90^0 RF pulse excites a uniform "comb" of transverse magnetization. Consider an ensemble of diffusing spins at thermal equilibrium. A π/2 rf pulse is applied which rotates the magnetization from the z axis into the x-y plane to create a magnetization ribbon in the rotating coordinate frame. During the first τ period at time t_1, a gradient pulse of duration δ and magnitude $\mathbf{g}$ is applied so that the effect of the gradient $\mathbf{g}$ is then to twist the ribbon in to a helix. The pitch of the helix is given by $\Lambda = 2\pi/\mathbf{q}$ where $\mathbf{q} = \gamma\mathbf{g}\delta/2\pi$ is the area of the gradient pulse. At the end of the first τ period the spin experiences a phase shift. The phase effect ϕ of a gradient pulse $\mathbf{g}$ of duration δ on a spin at position $\mathbf{r}$ is given by

$$\phi(\mathbf{r}) = \gamma\delta\mathbf{g}.\mathbf{r} \tag{1.28}$$

The scalar product arises because only motion parallel to the direction of the gradient will cause a change in the phase of the spin. The equation also ignores the effects of displacement during the gradient pulse and experimentally this condition is approximated by keeping $\delta \ll \Delta$. If during the first gradient pulse, the spin that was at position $\mathbf{r_0}$ and position $\mathbf{r_1}$ during the second then change in phase of this individual nuclear spin, $\Delta\phi$ moving from $\mathbf{r_0}$ to $\mathbf{r_1}$ is given by

$$\Delta\phi(\mathbf{r_1} - \mathbf{r_0}) = \gamma\delta\mathbf{g}.(\mathbf{r_1} - \mathbf{r_0}) \tag{1.29}$$

In the absence of diffusion, the phase difference $\Delta\phi$ is zero since the two identical gradient pulses exert an equal phase effect. This implies that the dephasing efficiency of a gradient pulse depends on the type of nucleus, the strength and duration of the gradient pulse, and the displacement of the spin along the gradient direction [37]. The final NMR signal attenuation resulting from molecular diffusion must include the cumulative residual phase shift and the probability function derived from Fick's 2^{nd} Law which describes the random diffusion process. A magnetization helix is uniquely described by its direction and tightness, together known as the diffusion wave vector $\mathbf{q}$.

The coherence of the order p evolves as $\exp(ip\omega_0 t)$. The term coherence is a generalization of the idea of transverse magnetization. Coherences can be classified by their coherence order p which can take the values $0, \pm1, \pm2....$ Longitudinal magnetization has coherence order p = 0, whereas transverse magnetization has p = $\pm$1. A π/2 pulse acting on equilibrium longitudinal magnetization excites p = +1 and -1 with equal weights. A π pulse inverts the sign of p. Detected signal is generated only by p = -1, hence only one of the initially excited components p = +1 and p = -1 gives rise to a detectable signal [15, 38]. A gradient pulse labels coherences with a phase that corresponds to the position and coherence order of the individual spins in the sample. This phase label can be removed by another gradient pulse, which is usually referred to as a refocusing gradient. The standard stimulated echo (STE) diffusion experiment is shown in Figure 1.14. The sequence contains three $90\,^\circ$ pulses, the echo after the third RF pulse was named by Hahn as the "stimulated echo". The signal intensity of the STE

diffusion experiment with rectangular pulse gradients is given by

$$I_{(G)} = (I_{(0)}/2) \exp\left[\left(\frac{-2\tau}{T_2}\right) - \left(\frac{T_M}{T_1}\right)\right] \tag{1.30}$$

It is clear that the effects of relaxation and diffusion can be separated in the signal decay in both the PFG experiments. The magnetic field generated by the applied gradient pulse varies across the sample, so that molecules in one area of the sample experience a magnetic field different to those in another region. The degree of attenuation is a function of the magnetic gradient pulse amplitude (g) and occurs at a rate proportional to the diffusion coefficient of the molecule.

$$I = I_0 \exp\left[-D\left(g\delta\gamma\right)^2\left(\Delta - \delta/3\right)\right] \tag{1.31}$$

Where *I* is the observed intensity, I_0 is the reference intensity, *D* is the diffusion coefficient, g is the amplitude of the applied gradient, δ is the duration of the applied gradient and Δ is the diffusion time. The molecular motion due to isotropic diffusion results in an attenuation of the signal and it is this effect that is used to measure diffusion coefficients that can be predicted by using the Bloch equations [39]. The Bloch equations for the decays of M_x and M_y in the xy-plane of the rotating frame.

$$\frac{dM_x}{dt} = -\frac{M_x}{T_2}, \qquad \frac{dM_y}{dt} = -\frac{M_y}{T_2} \tag{1.32}$$

For the consideration of the diffusion effect, an additional diffusion term needs to be included

$$\frac{dM_x}{dt} = -\frac{M_x}{T_2} + D\nabla^2 M_x, \tag{1.33}$$

$$\frac{dM_y}{dt} = -\frac{M_y}{T_2} + D\nabla^2 M_y, \tag{1.34}$$

where *D* is the diffusion constant, and $D\nabla^2 M = \nabla \cdot D\nabla M$ is the net diffusion influx which contributes to the time dependent quantity, dM/dt. T_2 is the transverse

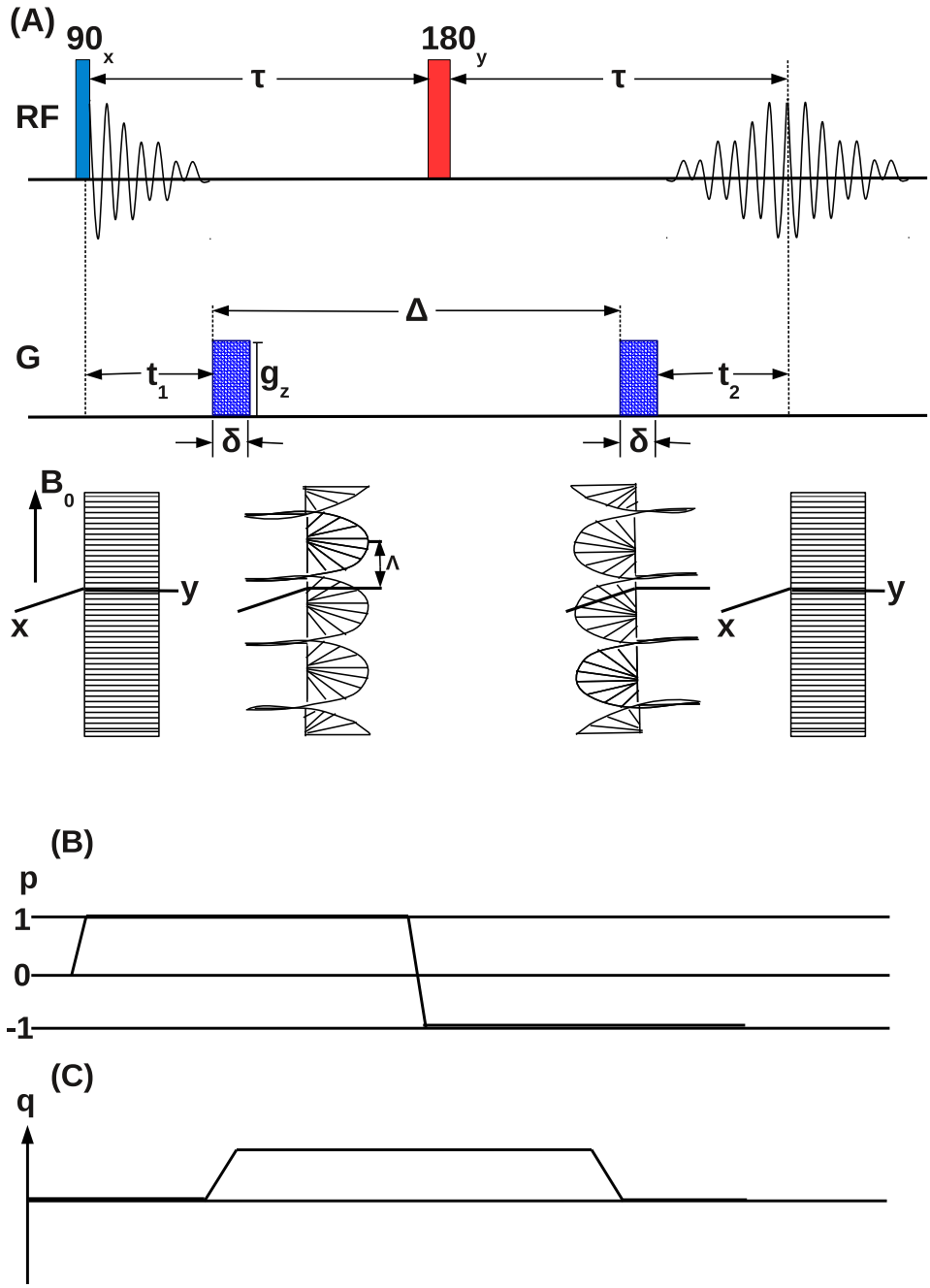

Figure 1.13: Schematics of the pulsed gradient spin-echo (PGSE) experiment (A) A Hahn spin-echo based PGSE sequence in which two equal gradient pulses of duration δ and direction and magnitude $\mathbf{g}$ are inserted into each τ period. (B) the selected coherence transfer pathway (C) time dependence of the amplitude of the wave vector $\mathbf{q}$.

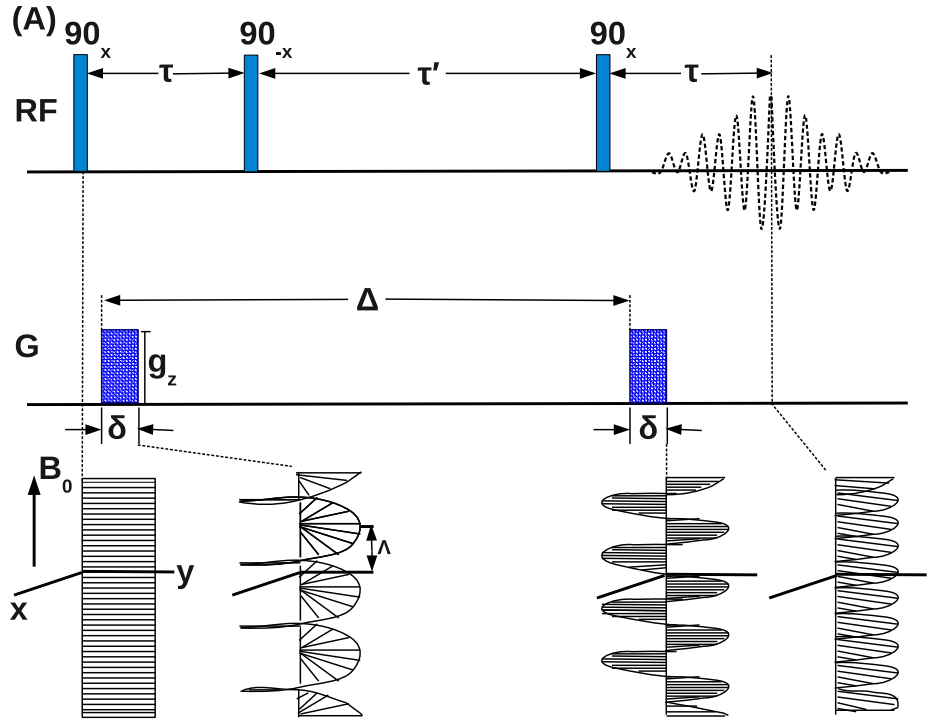

Figure 1.14: The pulsed field gradient stimulated echo (PFG-STE) pulse sequence with three $90\,^{\circ}$ pulses. τ and τ' are the time delays between RF pulses.

relaxation time and

$$M^{+} = M_x + iM_y \tag{1.35}$$

We can rewrite the previous equations in a concise form

$$\frac{dM^{+}}{dt} = -\frac{M^{+}}{T_2} + D\nabla^2 M^{+} \tag{1.36}$$

M_x and M_y are the x and y components of the magnetization, respectively. This equation applies for the case of a homogeneous magnetic field oriented along the z axis and in the absence of radiofrequency pulses. In the presence of an inhomogeneous magnetic field

$$\frac{\partial M^{+}(z,t)}{\partial t} = -\frac{M^{+}(z,t)}{T_2} - i\gamma B(z) M^{+}(z,t) + D\frac{\partial^2}{\partial z^2} M^{+}(z,t) \tag{1.37}$$

where *B(z)* is the contribution to the magnetic field at position z due to the gradient. The first of the additional terms accounts for the change in the Larmor frequency due to B(z), and the second term is analogous to Fick's second law. If there were no diffusion,

i.e., *D*=0 the following solution would hold:

$$M^{+} = \Psi(z,t)\exp(-i\omega_0 t - t/T_2) \tag{1.38}$$

$$\frac{\partial\Psi(z,t)}{\partial t} = -i\gamma g z\Psi(z,t) + D\nabla^2\Psi(z,t) \tag{1.39}$$

The effect of diffusion on the amplitude of the helix $\Psi(t)$ is obtained by

$$\Psi(z,t) = \Psi(t)\exp\left[-i\gamma z\int_0^t g(t')dt'\right] \tag{1.40}$$

$$ln\Psi(t) = -D\left[-i\gamma z\int_0^t q^2(t')dt'\right] \tag{1.41}$$

where

$$q(t') = \int_0^{t'} q^2(t'')dt'' \tag{1.42}$$

This is only an attenuation factor and for its observation, the isochromats must be refocused in the xy-plane to form an FID or echo.

1.4 The Basic Spin-echo Experiment

In the basic spin-echo experiment, the macroscopic magnetization vector along the z axis of the laboratory system, is deflected 90° in to xy plane, and lies along the y axis (Figure 1.15). As a result of of the inhomogeneity of the $\mathbf{B_0}$ field the individual nuclear spins begin to fan out and the magnitude of transverse magnetization decreases, some nuclei with higher Larmor frequency are moving ahead while those with lower Larmor frequency lag behind. After a certain time τ a 180° pulse is applied so that all vectors are turned around into the other side of the xy plane, and continue precessing about the same z axis [40, 41]. Now because of "turning" the phases of spins with higher Larmor frequency now lag, whereas those with lower Larmor frequency now lead. After a time 2τ all the spins become in-phase again. The resultant transverse magnetization can now be detected in the receiver coil as a signal. This phenomenon is called spin-echo or Hahn echo. The experiment is conveniently formulated as a pulse sequence

$(\pi/2)_x$ ..... τ ..... $(\pi)_x$ ..... τ ..... FID

The intensity of the spin-echo depend on the transverse relaxation rate. The echo's shape is determined by the shape of the free induction decay curve. Carr and Purcell simplified the spin-echo pulse sequence by using a π pulse for refocusing and this has now become the standard procedure. A train of echo may be obtained by repeating π pulses at appropriate intervals, to produce several echoes after the initial $\pi/2$ pulse. Each new π pulse has the effect of reversing the dephasing that occurred since the previous pulse. The loss of transverse magnetization during the period 2τ has been eliminated by the refocusing process and the echo amplitude is proportional to $\exp(-2\tau/T_2)$. In multiple echo sequences, the height of successive echo decreases exponentially with a time constant T_2.

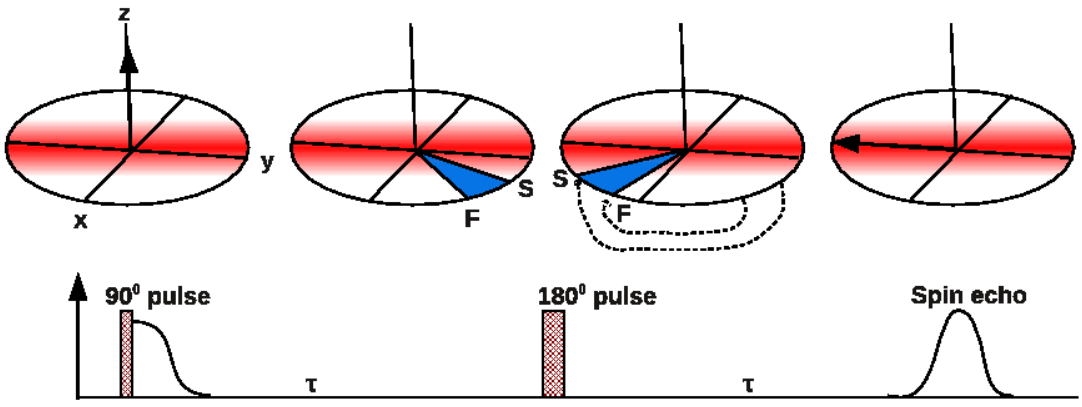

Figure 1.15: Schematics of spin-echo formation. A $(\pi/2)_x$ pulse rotates the magnetization vectors to the +y axis. Representative fast (F) and slow (S) vectors fan out in the xy plane. At time τ a $(\pi)_x$ pulse rotates them in to mirror positions. After time 2τ free precession brings to focus along the -y axis.

1.5 The 2D DOSY Experiment

Diffusion-ordered spectroscopy (DOSY) seeks to separate the NMR signals of different species according to their diffusion coefficient. It is based on a pulsed field gradient spin-echo NMR experiment in which components experience diffusion and the signal of each component decays exponentially according to self diffusion behavior of individual

molecules [28]. DOSY is a powerful tool for the study of mixtures analysis, separating the signals in a conventional spectrum according to their diffusion coefficient. In this two dimensional NMR technique, one dimension accounts for conventional chemical shift information and the second dimension distinguishes species by diffusion coefficients. While the chemical shift information is obtained by fast Fourier transformation (FFT) of the time domain data, the diffusion information is obtained by an inverse Laplace transformation (ILT) of the signal decay data [42] (Figure 1.16). Mixture analysis is based on diffusion differentiation according to:

$$E(q,\nu_m) = \sum_n A_n(\nu_m) exp[-D_n q^2(\Delta - \delta/3)] \tag{1.43}$$

where $A_n(\nu_m)$ is the amplitude of the 1D-NMR spectrum of the nth diffusing species having a diffusion coefficient of D_n [41].

Each frequency value in the PGSE NMR data set can be represented in terms of a sum of discrete exponentials with q^2 as the independent variable. The 1D data set with peak attenuation is described by

$$E(q,\nu_m) = \int_0^\infty g(D,\nu_m) exp[-D_n q^2(\Delta - \delta/3)] dD \tag{1.44}$$

where $g(D,\nu_m)$ represents a spectrum of diffusion coefficients for each spectrum, and $E(q,\nu_m)$ is the Laplace transform of the $g(D,\nu_m)$. If $g(D,\nu_m)$ is represented as a sum of Dirac delta functions

$$g(D,\nu_m) = \sum_n A_n(\nu_m)\delta(D - D_n) \tag{1.45}$$

In the 2D DOSY experiment ^{1}H spectra with increasing diffusional attenuation are recorded and diffusion coefficient for the resonances calculated from the signal decays. Diffusion coefficients are correlated theoretically by the Stokes-Einstein relation. The Stokes-Einstein equation only holds for free diffusion. DOSY spectra also include artifacts generated by temperature fluctuation, convection, and viscosity changes. The accuracy of diffusion measurements can be improved by eliminating sources of error such as eddy currents and convection currents caused by gradient pulses.

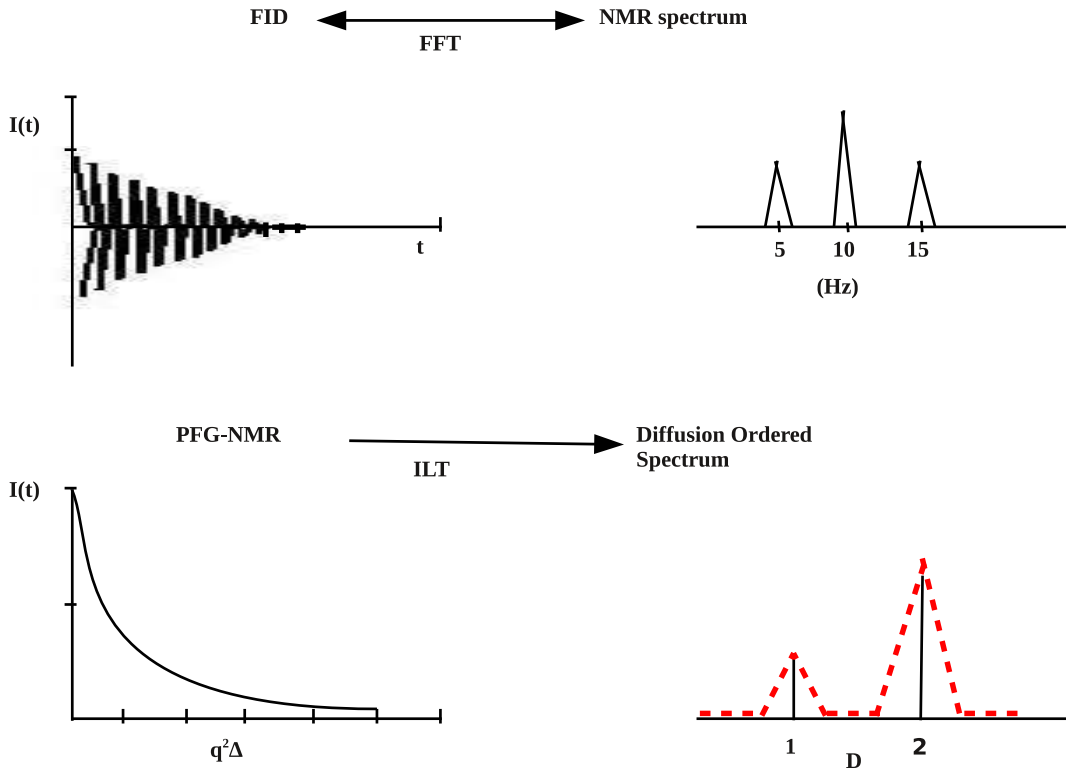

Figure 1.16: Schematic of FFT and ILT transformations. At the top an FFT converts the FID to a NMR spectrum with the line shapes. At the bottom the decay curve contains two components of diffusion coefficients and amplitudes differing by a multiple of two. The dotted red curves in the diffusion spectrum indicate broadening associated with errors.

1.6 Diffusion Experimental Details

Most of the diffusion experiments in this thesis were performed on a Bruker Avance-III 600 MHz spectrometer equipped with a 5-mm QXI probe and pulsed field gradients. Some of the experiments in Chapter 6 were performed on a Bruker Avance-III 600 MHz spectrometer equipped with a 5-mm Diff30 diffusion probe, capable of generating a maximum gradient strength of 1200 G/cm. All spectra were processed using Bruker Topspin 2.1 software. All diffusion experiments were performed at ambient temperature to reduce the effects of convection currents.

2D DOSY Experimental Parameters: Unless otherwise stated, 2D DOSY NMR spectra were acquired using the stimulated echo bipolar gradient pulse sequence with an eddy current delay [43]. The duration of the diffusion delay was kept as short as possible to minimize signal loss due to relaxation. The experimental parameters included 16 gradient amplitude steps ranging from 2 to 95% (in equal steps of gradient squared) using 32 transients, 16K complex data points, an eddy current delay 5 ms and diffusion time intervals between 100-200 ms. The gradient pulses ranged from 1-3 ms in duration.

The signal attenuation was fit to the previously described Stejskal-Tanner equation. The proton DOSY data were obtained with a spectral window of 8000 Hz by coaddition of 32 transients for the diffusion measurements, using an acquisition time of 0.772 s and a relaxation time of 1.5 s. The FIDs were apodized by multiplication by an exponential decay function equivalent to 1 Hz line broadening and zero-filled prior to Fourier transformation to form a 8K $\times$ 1K data matrix. The standard 2D DOSY processing protocol was applied in Topspin software with logarithmic scaling in the diffusion coefficient dimension. Numerical fitting was performed using the freeware Gnuplot. Errors of the diffusion coefficient were calculated by multiplying the standard fitting error calculated within Gnuplot by the *t* value for the 95% confidence level.

1.7 Applications of PFG NMR

This thesis focuses on using diffusion NMR experiments to resolve the diffusion coefficients of individual components of a mixture. Mixtures of organic compounds can be

assayed by NMR spectroscopy if distinguishable signals from each component can be integrated separately. PFG techniques are widely used in NMR spectroscopy to obtain DOSY spectra containing information about the translational diffusion coefficients of the diffusing molecules. DOSY is a versatile technique which can be used for mixture analysis, without prior physical separation of the mixture components, wherein signals from the components are ordered along a second dimension based on differences in their diffusion coefficients. The DOSY experiment has limited potential to differentiate between severely overlapped signals in a mixture, which can lead to inaccurate estimates of diffusion coefficients or ambiguities in identification of the mixture components. Several 3D DOSY experiments have been designed that achieve resolution of overlaps by concatenating a diffusion pulse sequence with common 2D pulse sequences. Proton 3D DOSY experiments suffer from signal overlap while carbon 3D DOSY experiments offer better resolution but suffer from poor signal-to-noise ratios and very long experimental times.

Diffusion NMR measurements are used in many different fields ranging from the medical sciences to material sciences [44, 45, 46, 26, 47, 48, 24]. Diffusion measurements have been used to study surfactants due to their sensitivity to molecular organization and consequently for determining parameters such as the critical micellar concentration [49]. PGSE NMR plays an important role in clarifying the mechanism of ionic liquids which have application to devices such as solar cells, fuel cells, double layer capacitors and batteries [50]. Pulsed-field gradient NMR is used for the characterization of ligand-protein interactions which is important for the binding of a small molecule to an enzyme or cell-surface receptor. NMR diffusion measurements have also been applied to the study of the interaction between drug and proteins and to study drug delivery systems [51]. Diffusion ordered spectroscopy is also used in the analysis of decontamination reaction products of chemical warfare agents especially for the development of new generation decontamination agents [52, 42, 38, 23].

CHAPTER 2

Separating Diffusion Coefficients in Mixtures Using a Novel 3D BEST-HMQC-DOSY Experiment

2.1 Background and Motivation

Applications of the DOSY technique are plentiful [29, 28, 37, 53, 54, 55, 56] and range from the analysis of polymer blends [57], residue-specific NH rates and intermolecular interactions [58, 59], stacking and nanorod formation [60], molecular diffusion in cells [61], compositional analysis of block copolymers and host-guest complexes [62, 63], DNA secondary structural elements [64] and mapping ligand-protein interactions [65, 66, 67, 68]. ^{1}H DOSY spectra of molecular mixtures suffer from problems of severe signal overlap, because of the relatively narrow range of proton chemical shifts and hence a number of 3D DOSY techniques have been developed to overcome this problem, wherein additional resolution is obtained by dispersing signals in the third dimension by appending a standard 2D pulse sequence to a DOSY experiment [69, 70, 71]. Yet another route to resolve spectral overlap is to perform heteronuclear DOSY experiments using nuclei such as carbon-13 which have high chemical shift dispersion [72, 73, 74, 75]. The experiment time is however a crucial limitation in 3D heteronuclear DOSY schemes due to the requirement of sampling in the indirect frequency dimension, with only a few increments allowed in the diffusion dimension. The overlap of spectral peaks in multi-component mixtures can severely compromise the quantitative estimation of diffusion coefficients of each component. A number of sophisticated data analysis methods have been evolved to circumvent this problem which use multi-exponential or continuous distribution fitting, which are successful only to a limited extent [76, 77, 41, 78]. Recently, sensitivity-enhanced BEST-HMQC methods [79, 80, 81] and SOFAST-HMQC methods [82, 83, 84, 85] were described that achieve a substantial improvement in resolution and can be used to record two-dimensional heteronuclear correlation spectra of biomolecules in very short times

ranging from a few minutes to only a few seconds. The BEST type of experiments benefit from longitudinal relaxation enhancement by using shaped RF pulses while the SOFAST type of sequences have the added advantage of using Ernst-angle excitation.

The standard HMQC experiment provides correlation between protons and scalar coupled heteronuclei through the creation of heteronuclear multiple-quantum (MQ) coherence. The HMQC is one example of the aptly named inverse spectroscopy schemes, wherein the excited and the observed nucleus are the same and the heteronucleus is detected indirectly via evolution during an incremented delay. The advantage of the inverse spectroscopy is that the nucleus with the highest γ is detected, and so it is possible to obtain good sensitivity. The pulse sequence for the basic HMQC scheme is shown in Figure 2.3. The sequence is analyzed here for a coupled carbon- proton pair, with the carbon-13 labeled as spin 1 and proton labeled as spin 2. The basic idea behind the HMQC experiment is related to the echo difference technique, which is used to eliminate protons signals not coupled to the heteronuclei. A proton pulse is followed by a delay τ = *1/2*J_{XH}. As a result, the proton magnetization is converted into antiphase ($2I_{1y}I_{2z}$) magnetization. A 90° pulse applied to the X nuclei converts this antiphase term into a combination of zero and double quantum coherence ($2I_{1y}I_{2x}$). The proton chemical shift and heteronuclear coupling are refocused by using a 180° pulse at mid-evolution time. In the absence of the 180° proton pulse in the center of t_1 period, the $I_{1y}I_{2x}$ term would have evolved with the sum ($\Omega_1 + \Omega_2$) and difference ($\Omega_1 - \Omega_2$) frequencies of the two spins. The last 90° heteronuclei pulse returns the multiple quantum coherence to observable antiphase proton magnetization. The second delay τ converts the antiphase term into an in-phase term. The linewidth in the F_1 dimension of an HMQC spectrum is determined by the relaxation rate constant of the heteronuclear MQ coherence. Steps (A-D) can be described by using a product operator analysis as follows:

$$(A \rightarrow B) \qquad I_{1z} \xrightarrow{(90^\circ)I_{1x}} -I_{1y} \xrightarrow[\tau=1/(2J_{XH})]{2J_{XH}I_{1z}I_{2z}} 2I_{1x}I_{2z}$$

It will be assumed that τ = *1/2*J_{XH}, so only the anti-phase term is present. The second 90° pulse is applied to carbon-13 only.

$$2I_{1x}I_{2y} \xrightarrow{(90^\circ)I_{2x}} -2I_{1x}I_{2y}$$

This anti-phase magnetization is converted in to multiple-quantum coherence by the 90° pulse and evolves chemical shift during t_1

$$(B \rightarrow C) \quad -2I_{1x}I_{2z} \xrightarrow{\Omega_2 t_1 I_{2z}} -cos\Omega_2 t_1\ 2I_{1x}I_{2y} + sin\Omega_2 t_1\ 2I_{1x}I_{2y}$$

The second 90° heteronuclei pulse with the receiver phase provides cancellation of the unwanted proton not coupled to the ^{13}C nuclei.

$$(C \rightarrow D) \quad -cos\Omega_2 t_1\ 2I_{1x}I_{2y} \xrightarrow{(90^\circ)I_{2x}} -cos\Omega_2 t_1\ 2I_{1x}I_{2z}$$

This term then evolves under the coupling

$$-cos\Omega_2 t_1\ 2I_{1x}I_{2z} \xrightarrow{(180^\circ)J_{XH}\ \tau\ I_{1z}I_{2z},\ \tau=1/2J_{XH}} -cos\Omega_2 t_1\ 2I_{1y}$$

This chapter focuses on exploiting the sensitivity-enhanced BEST-HMQC technique to achieve resolution of overlaps in a novel 3D heteronuclear $^{13}C - {}^1H$ diffusion ordered experiment with good sensitivity and a substantial reduction in experiment time. The method is demonstrated on a mixture of molecules with similar translational diffusion coefficients, a mixture of amino acids which are also very close in their molecular weights and hence their diffusion coefficients, and a mixture of commercial gasoline. The main advantage in using a BEST-HMQC instead of the standard HMQC in a 3D DOSY scheme is the significant reduction in experimental time without a corresponding loss of sensitivity (we found that typical 3D BEST-DOSY experiments are around four times faster than standard 3D HMQC-DOSY experiments). Several PFG sequences have been proposed to overcome problems of solvent suppression and thermal convection in proteins [86, 87]. We also used band-selective pulses in the diffusion sequence in conjunction with water suppression, and implemented a selective analog of the BEST-DOSY experiment to obtain the diffusion coefficient of a model protein.

2.2 Experimental Section

Model Systems & Spectrometer Details: All the amino acids, small molecules and proteins were purchased from Sigma Aldrich and used without further purification. The mixture of geraniol (20 μl), camphene (10 mg) and quinine (15 mg) in deuterated methanol is referred to as Mixture 1, the model mixture of amino acids L-Tryptophan (8 mg), DL-Valine (15 mg), and L-Phenylalanine (10 mg) in D_2O is referred to as Mixture 2 and the complex mixture of commercial gasoline (100 μl in deuterated methanol) is referred to as Mixture 3 throughout.

2D DOSY Experiments: The signal attenuation in the 2D DOSY experiment were fitted to the Stejskal-Tanner equation as previously described in Chapter 1. The gradient pulses ranged from 1-3 ms in duration. The gradient field strength was varied between 2 and 34.5 Gcm^{-1}. The DOSY data were obtained with a spectral window of 8000 Hz by Co-addition of 32 transients for the diffusion measurements, using an acquisition time of 0.772 s and a relaxation time of 1.5 s. The FIDs were were apodized by multiplication by an exponential decay function equivalent to 1-Hz line broadening and zero-filled prior to Fourier transformation to form a 8K $\times$ 1K data matrix.

Gradient field strength calibration: For calibration of the maximum value of the gradient strength, we have used a dilute solution of 500 μl H_2O in D_2O (doped water), in order to avoid radiation damping effects [88]. The apparent diffusion coefficient (D_{app}) was measured using the standard diffusion pulse sequence. The value of gradient strength g is calculated from the equation

$$g_{new} = \sqrt{\frac{D_{app}}{D_{known}}} \times g_{known} \tag{2.1}$$

where g_{known} and D_{known} are the known values for g at the center of the coil and the diffusion coefficient of water within the doped sample, respectively. The standard diffusion coefficient value of H_2O is 2.031×10^{-9} m^2/s measured at room temperature (293K) [88]. Full details of the calibration procedure are given in the Appendix.

3D BEST-DOSY Sequence: The 3D BEST-DOSY pulse sequence (Figure 2.1) concatenates a BEST-HMQC experiment with a stimulated-echo diffusion sequence (STE-

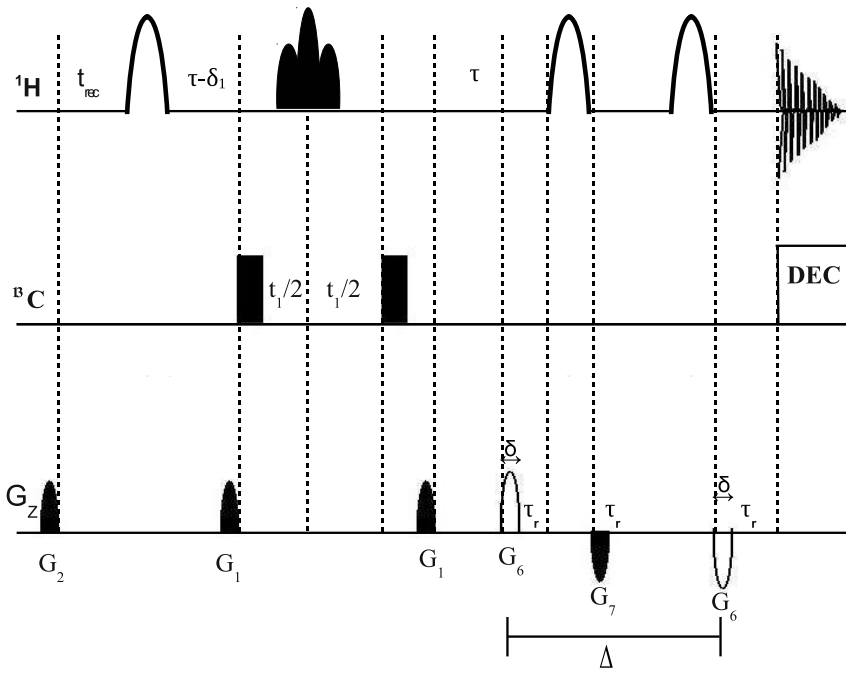

Figure 2.1: Pulse sequence for the 3D BEST-DOSY experiment. τ denotes the magnetization transfer delay $1/2J_{CH}$ in the BEST-HMQC sequence and t_{rec} is the recycle delay between scans. The delay δ_1 accounts for spin evolution during the band-selective pulse and is adjusted to yield pure phase spectra in the ^{1}H dimension. The unfilled shaped pulses denote the band-selective pulses that were used for proton excitation in the desired region. Refocusing of the protons in the t_1 evolution period is achieved by the band-selective pulse denoted by the filled shape. Δ denotes the diffusion interval and the G_6 gradients are used for dephasing/rephasing magnetization during the diffusion interval. The gradient pulse lengths are denoted by δ and τ_r is the gradient recovery delay. ^{13}C decoupling during acquisition was achieved using an adiabatic decoupling sequence. For phase sensitive detection the phase of the second proton pulse is incremented according to the States-TPPI method. If no phase cycling is indicated, pulses were applied along the x-axis.

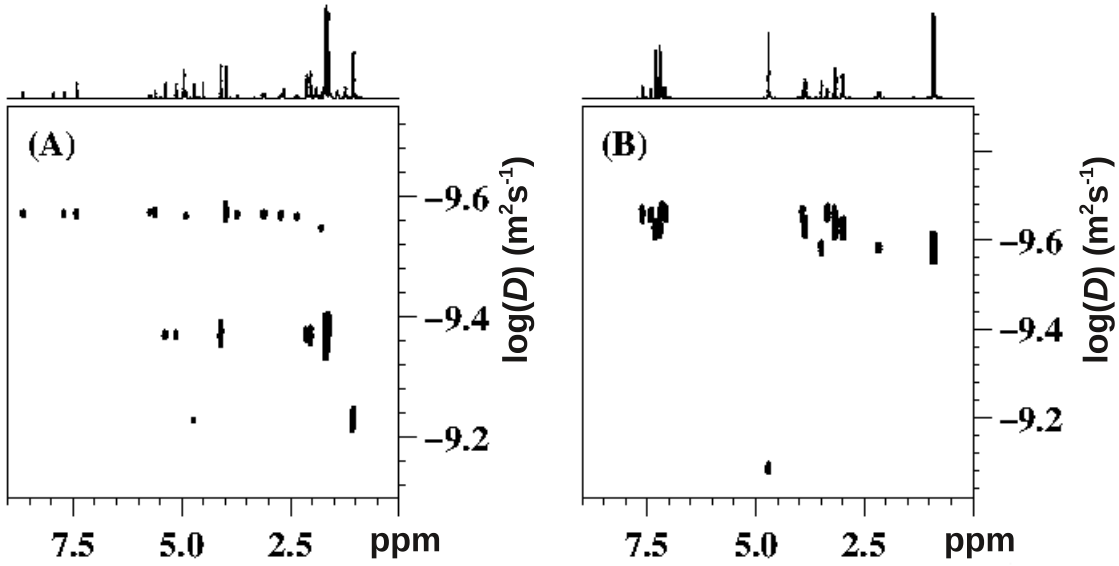

Figure 2.2: 2D ^{1}H DOSY NMR spectra of (A) Mixture 1 (geraniol, camphene, and quinine) and (B) Mixture 2 (L-phenylalanine, DL-valine and L-tryptophan). Proton chemical shifts (ppm) are indicated along the x axis and diffusion units $(\log(D/\mathrm{m^2 s^{-1}}))$ on the y axis.

DOSY) yielding a 3D data matrix. The ^{1}H band-selective excitation pulses used for the different samples were either of a polychromatic PC9 [89], Q5 Gaussian excitation [2] or Seduce shape [90] with the excitation angle set to 90°. Band-selective ^{1}H refocusing is achieved using an RSNOB refocusing pulse in the middle of the t_1 evolution period. The transfer delay τ is set to $1/(2J_{CH})$. The gradient ratios $G_1 : G_2$ in the BEST sequence are set to $11 : 7\%$ of the maximum gradient field strength. Δ denotes the diffusion interval and G_6 is the diffusion encoding/decoding gradient. Gradient pulse durations varied between 1.0 and 2.0 ms and the relaxation delay between scans was set to 200-500 ms. The BEST sequence excited only a selected region of protons using a band-selective pulse centered in the middle of the desired region. The spectra were zero-filled to 8192 points in the t_3 dimension and 2048 points in the t_1 dimension. After a 2D Fourier transform using the States-TPPI method, the DOSY dimension was reconstructed on a logarithmic scale and the peaks were represented in the diffusion constant dimension on a grid of 32 data points. The HMQC subspectra were obtained by averaging slices centered at the respective diffusion coefficients. Diffusion constants were obtained by using a monoexponential fit to three resonances in each subspectrum and taking the average. Broadband adiabatic ^{13}C decoupling was achieved with a smoothed 1.5 ms chirp pulse Crp60,0.5,20.1 for inversion and a decoupling supercycle given in

the Bruker library: P5m4sp180. The number of diffusion encoding steps in all the 3D BEST-DOSY experiments is 16, and 16 scans were recorded for a gradient pulse length $\delta = 2$ ms and a gradient recovery time of 200 μs. Band-selective refocusing RSNOB pulse shapes [3] were used for refocusing in the BEST part of the sequence for all the mixtures. Band-selective pulses of Gaussian cascade (Q5) shape were used for Mixture 1 and Mixture 2, respectively while band-selective pulse of Seduce shape was used for Mixture 3. Diffusion (Δ) interval times of 43 ms, 50 ms and 200 ms were used for Mixture 1, Mixture 2 and Mixture 3, respectively.

2.3 Results and Discussion

We have designed a novel fast-pulsing 3D heteronuclear diffusion experiment by concatenating a BEST-HMQC scheme with a STE-DOSY sequence (Figure 2.1). A substantial speedup in data acquisition and high sensitivity are the hallmarks of this 3D heteronuclear diffusion experiment, and are achieved by reducing the recycle delay between scans. The STE pulse sequence retains the magnetization along the z-axis during the diffusion interval, thereby minimizing losses due to fast relaxation of transverse magnetization.

The 1D ^{1}H spectra of the mixture of quinine, camphene and geraniol in methanol-d4, (Mixture 1), and the mixture of amino acids L-phenylalanine, DL-valine and L-tryptophan (Mixture 2) are shown in Figure 2.4. The spectra of the mixtures show considerable overlap in resonances. The standard 2D DOSY spectra of Mixture 1 and Mixture 2 are shown in Figure 2.2, which show a set of overlapping peaks. While it is clear from the DOSY spectrum of Mixture 1 (Figure 2.2(a)) that there are at least three components in this mixture, a closer inspection and comparison with the ^{1}H spectrum of Figure 2.4(a) reveals overlaps between quinine and geraniol and between camphene and geraniol along the DOSY dimension, which would lead to inaccuracies in the estimation of their respective diffusion coefficients. While the solvent peak in the amino acid mixture (Figure 2.2(b)) is separated along the diffusion dimension, none of the three amino acids could be resolved along the DOSY dimension. These overlaps could not be separated with the processing methods available with TopSpin software, leading to

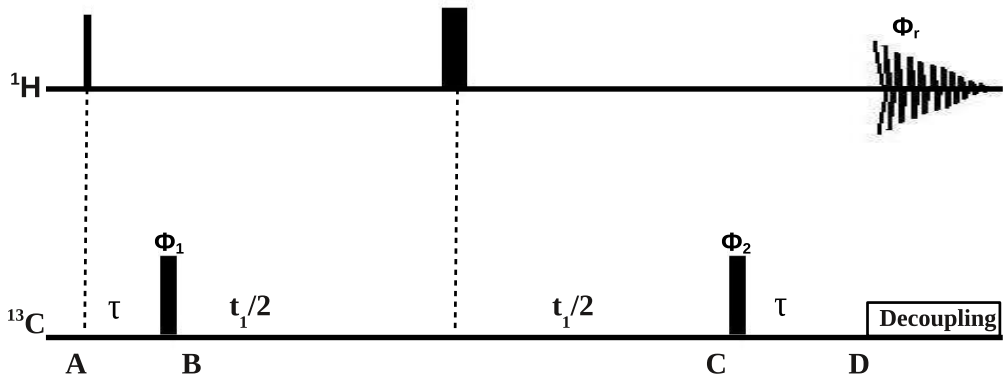

Figure 2.3: The pulse sequence for the 2D HMQC experiment. The filled rectangles represent 90° and 180° pulses. Phase of the 90° pulses on ^{13}C and the receiver are ϕ_1(x, -x, x, -x), ϕ_2(x, x, -x, -x), and ϕ_r(x, -x, -x, x), respectively. Points (A-D) describe magnetization at each point in the pulse sequence.

the conclusion that a 3D extension of the DOSY method would be required to obtain accurate diffusion coefficients for each of the individual components of these mixtures.

The BEST/SOFAST-HMQC sequence is a fast-pulsing technique wherein reduced acquisition times are achieved by Ernst-angle excitation, smaller number of rf pulses and longitudinal relaxation optimization [82]. The spin states of all other unexcited protons that are not directly involved in the coherence transfer pathways remain unperturbed leading to efficiency of spin-lattice relaxation and hence reduced relaxation delays between experimental scans. The Ernst angle is the flip angle for a particular spin that gives the maximal signal in the least amount of time, when signal averaging over many transients. If only one pulse were applied, the best experiment would use a 90° pulse, which would achieve a maximum transfer of z-magnetization to the x, y plane. During the relaxation delay between pulses (to account for recovery of magnetization to equilibrium), the relation between the pulse angle α and the ratio $t/T1$ becomes important. The induced transverse magnetization along the y-axis is equal to $M_0 \sin\alpha$. Concomittantly, the z-magnetization is reduced to a value of $M_0 - M_0 \cos\alpha$. For small

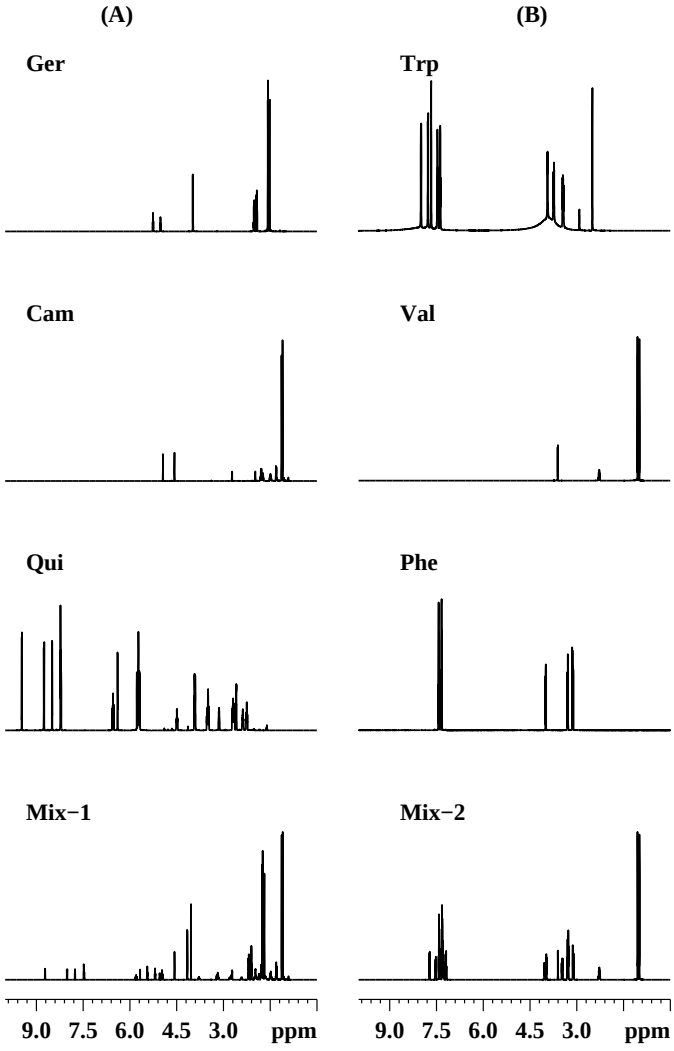

Figure 2.4: The 1D ^{1}H spectra of (A) Mixture 1 with its individual components of quinine, camphene and geraniol. and (B) Mixture 2 and its individual amino acid components L-phenylalanine, DL-valine and L-tryptophan. Sixteen scans were collected with 8192 complex points for each scan. Spectra were apodized with a 1 Hz exponential line-broadening function, baseline-corrected and zero-filled to minimize digitization errors. The vertical scaling factor has been adjusted so that the noise level in all spectra is the same.

flip angles of the pulse ($\alpha < 30^\circ - 50^\circ$), $\sin\alpha > 1 - \cos\alpha$ and the detected signal is larger than the loss of longitudinal magnetization. For the optimal pulse angle (Ernst angle), $\cos\alpha = \exp(-t/T_1)$. The BEST-HMQC abbreviates Band-selective Excitation Short-Transient HMQC. The BEST experiments are optimized for minimal perturbation of aliphatic and water protons. This is realized by applying exclusively band-selective pulses, PC9 [89], E-BURP2, and RE-BURP and pairs of broadband inversion pulses on the proton channel. The large amount of aliphatic and water proton spin polarization at the end of the BEST pulse sequence then enhances longitudinal relaxation of amide hydrogen spins via dipole-dipole interactions and hydrogen exchange [80].

The standard HMQC pulse sequence using gradients and the 2D BEST-HMQC sequence are implemented on quinine in methanol-d4 and compared in Figure 2.5(a) and (b), respectively. The standard HMQC spectra of all the mixtures are shown in Figure 2.6. The ^{1}H excitation pulse is applied using a Gaussian cascade (Q5) excitation shape [2]. Band-selective ^{1}H refocusing is realized using an RSNOB pulse [3]. The pulses are centered at 3.0 ppm and cover a bandwidth of 3756 Hz and 3901 Hz corresponding to pulse lengths of 2 ms and 1.2 ms respectively, for the Q5 and RSNOB shapes at 600 MHz. The transfer delay is set to $1/(2J_{CH})$ with J_{CH}=145 Hz. Peaks in the range 1.78 ppm to 4.0 ppm were excited.

The signal-to-noise (S/N) ratios of individual peaks in the 2D experiments were calculated using the SINO command in Topspin. The S/N ratio for the peaks at 2.33 ppm/40.2 ppm, 2.68 ppm/56.2 ppm and 3.10 ppm/60.4 ppm is 59.87, 94.21 and 107.46, respectively in the standard HMQC experiment. The S/N ratio for the peaks at 2.33 ppm/40.2 ppm, 2.68 ppm/56.2 ppm and 3.10 ppm/60.4 ppm is 65.98, 126.29 and 166.52, respectively in the BEST-HMQC experiment. The BEST-HMQC spectrum shows a gain in signal to noise ratio as compared to the standard HMQC spectrum for quinine, all other experimental parameters including the decoupling sequence being kept the same.

For both 2D experiments, 256 t_1 increments of 2K data points and 16 scans were recorded, with relaxation times of $d_1 = 1$ s and 200 ms for the standard HMQC and BEST experiments, respectively. Phase cycling followed the States-TPPI method and processing consisted of apodization using a squared cosine bell, followed by zero-filling

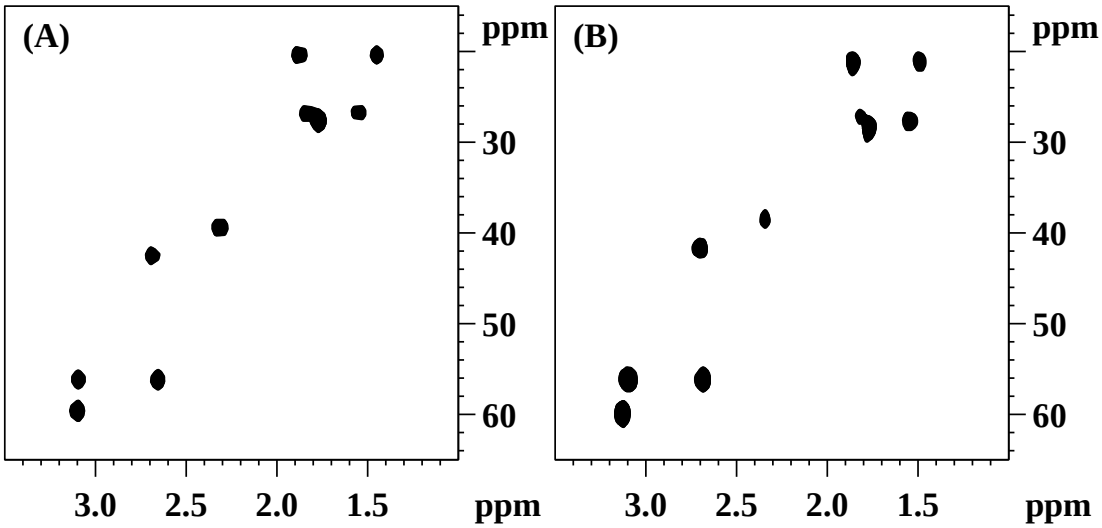

Figure 2.5: Comparison of 2D ^{1}H-^{13}C spectra of quinine in deuterated methanol recorded at 600 MHz using (A) standard HMQC pulse sequence with gradients and (B) BEST-HMQC pulse sequence. ^{1}H excitation and refocusing covering the frequency range from 1.78 ppm to 4.0 ppm in the BEST-HMQC experiment was achieved using a Gaussian cascade (Q5) excitation [2] pulse of 2 ms and an RSNOB pulse [3] of 1.2 ms, respectively. The flip angle of the excitation pulse was set at $90°$. The selective pulses were centered at 3.0 ppm and had a bandwidth of 3756 Hz and 3901 Hz, respectively. The relaxation delay in the BEST-HMQC experiment was set at 200 ms and at 1 s in the HMQC experiment. ^{13}C decoupling during t_2 was realized for the standard HMQC and for the BEST-HMQC using an adiabatic decoupling sequence in both experiments.

Experiment	Mixture 1	Mixture 2	Mixture 3
HMQC	62.46 (2.39 ppm)	44.48 (2.19 ppm)	48.6 (1.6 ppm)
	103.0 (2.67 ppm)	27.38 (3.05 ppm)	66.24 (3.21 ppm)
PC9	68.38 (2.39 ppm)	33.24 (2.19 ppm)	25.44 (1.6 ppm)
	117.0 (2.67 ppm)	48.3 (3.05 ppm)	148.46 (3.21 ppm)
Q5	47.01 (2.39 ppm)	25.78 (2.19 ppm)	15.96 (1.6 ppm)
	113.42 (2.67 ppm)	46.58 (3.05 ppm)	94.42 (3.21 ppm)
Seduce	103.77 (2.39 ppm)	36.58 (2.19 ppm)	22.48 (1.6 ppm)
	137.1 (2.67 ppm)	30.27 (3.05 ppm)	122.04 (3.21 ppm)

Table 2.1: Comparison of S/N ratios for the standard HMQC experiment and for the BEST experiment using different shaped pulses for the three different mixtures. The chemical shift in ppm of each peak is given in brackets.

and Fourier transformation to a 2K $\times$ 2K data matrix. In order to explore the efficacy of the BEST sequence in obtaining good 2D correlations we have carried out a comprehensive analysis of the S/N ratios for all the three Mixtures. The data is collated in Table 2.1.

The S/N ratios for different signals in each BEST spectrum were computed and compared with the S/N of the same signal in the standard HMQC experiment. The BEST experiment was repeated for three different pulse shapes: a polychromatic PC9 excitation [89], a Gaussian (Q5) wideband excitation cascade [2] and a broadband Seduce excitation shape [90]. In general we found that all three shapes gave good results. The band-selective pulses of the different shapes considered are centered at 3.0 ppm, 3.0 ppm and 4.0 ppm corresponding to a pulse length of 2.0 ms for Mixture 1, Mixture 2 and Mixture 3, respectively. Phase cycling followed the States-TPPI method and processing consisted of apodization using a squared cosine bell, followed by zero-filling and Fourier transformation to a 2K $\times$ 2K data matrix.

A diffusion coefficient is computed for each correlation in the 3D BEST-DOSY experiment by varying the gradient strengths in a number of experiments, concatenated into a single 3D experiment. Identical diffusion coefficients are identified as belonging to the same individual component and the BEST-HMQC correlations become "diffusion-tagged". Figures 2.7 and 2.8 show the 2D subspectra extracted from the 3D BEST-HMQC DOSY experiments on Mixture 1 and Mixture 2. For both experiments, three slices from the transformed 3D DOSY spectra are shown at the diffusion coefficients corresponding to the individual components. Despite spectral crowding and

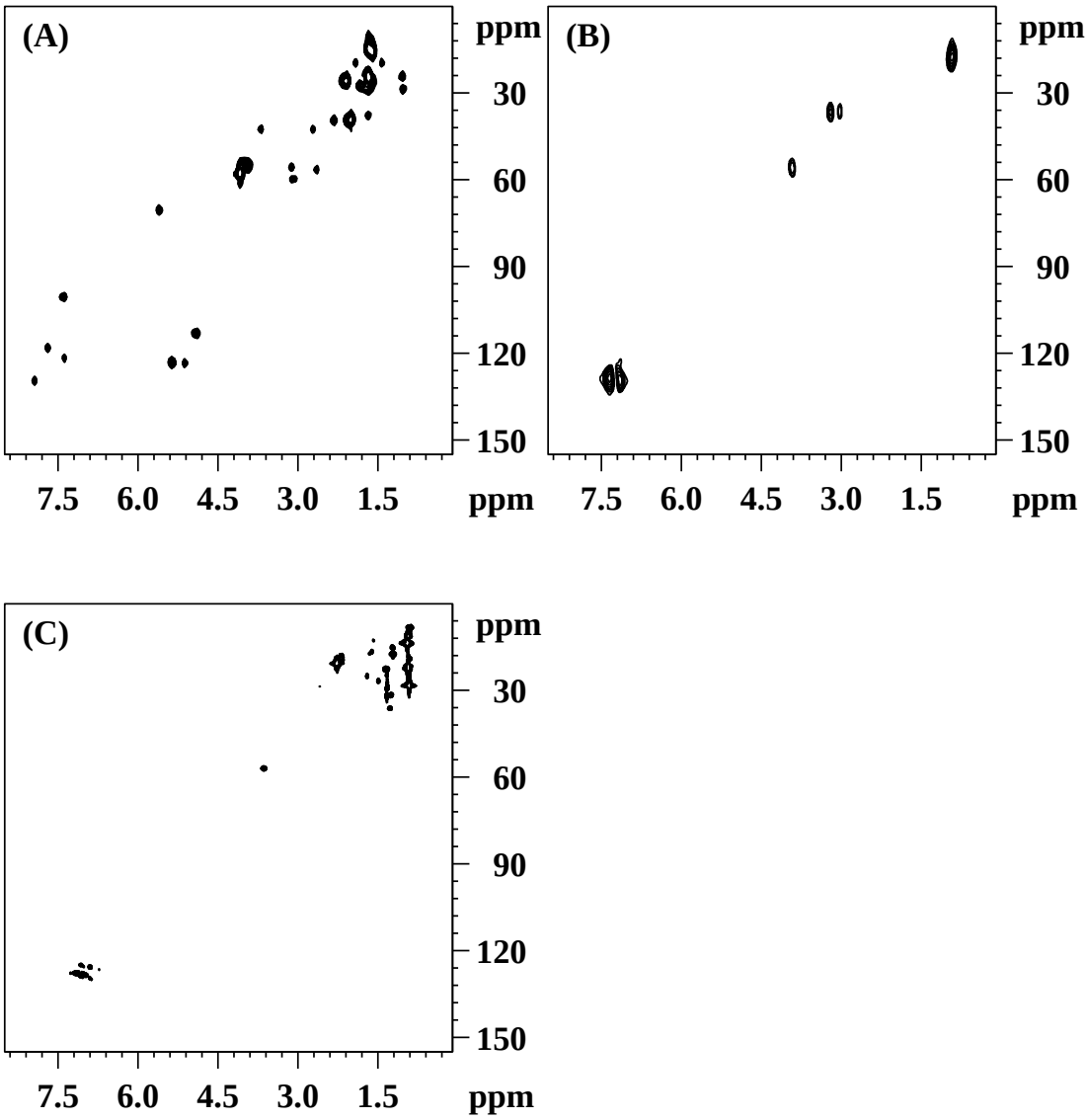

Figure 2.6: 2D ^{1}H-^{13}C HMQC spectra of (A) mixture of quinine, camphene and geraniol in deuterated methanol (B) mixture of L-tryptophan, L-phenylalanine and DL-valine in D_2O. (C) commercial gasoline in deuterated methanol. The relaxation delay in the HMQC experiment was set at 1 s resulting in an experimental of 1 hour 10 sec.

similarity of diffusion coefficients, the resolution in the DOSY dimension is sufficient to clearly separate the individual diffusing components. The results of the 3D heteronuclear DOSY experiments are displayed as a series of projected 2D spectra which are the integrals between given diffusion limits of the 3D spectrum with axes (ω_H, ω_C, D). At higher gradient strengths, faster diffusing components are suppressed and each spectrum is simplified. Figures 2.7(a), (b) and (c) show projections of the BEST-HMQC

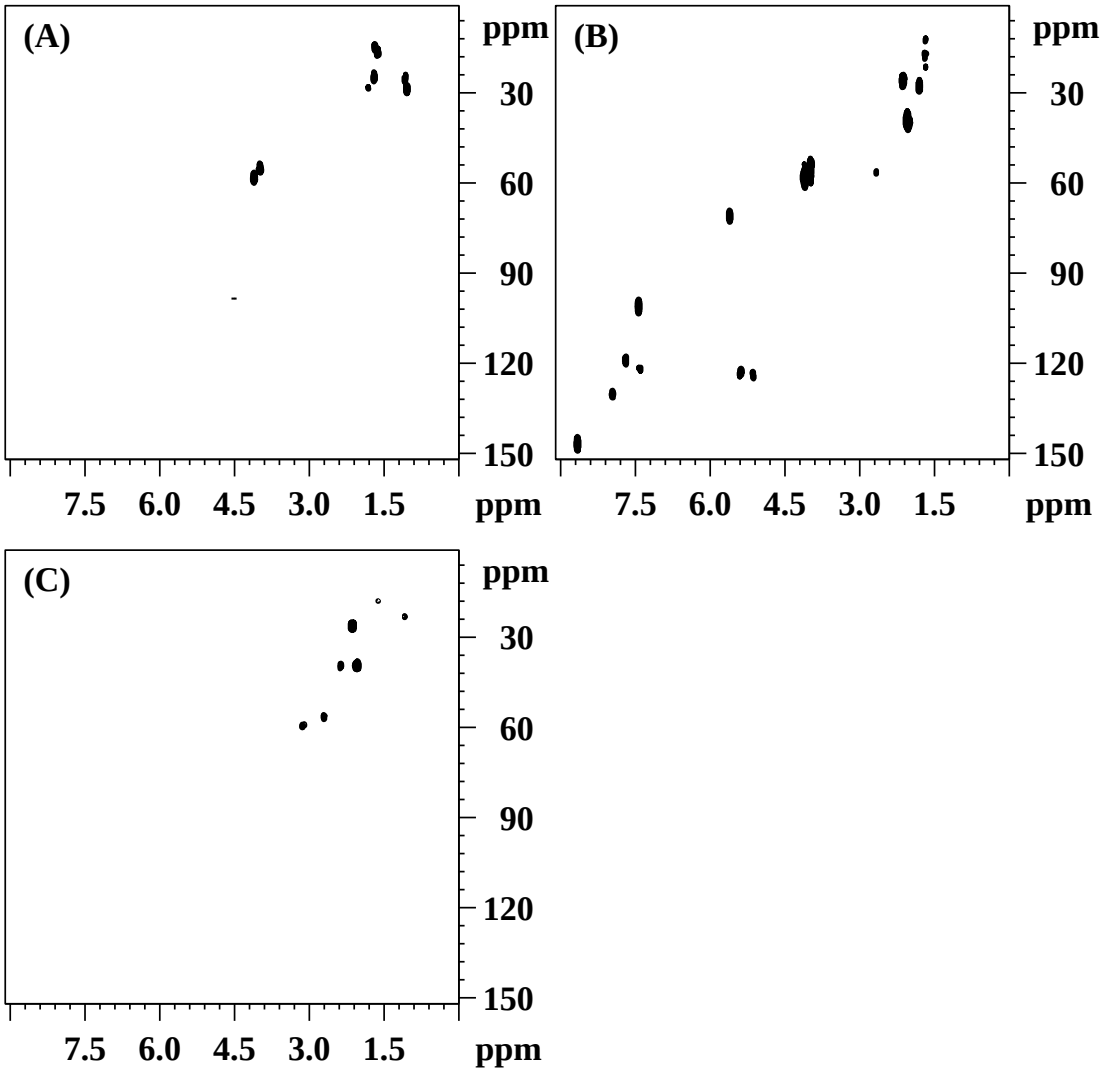

Figure 2.7: BEST-HMQC planes extracted from the 3D BEST-DOSY experiment for each subspectrum in Mixture 1. BEST-HMQC subspectra of (A) geraniol, (B) quinine and (C) camphene extracted from the respective 3D experiments for diffusion coefficient ranges of $9.0-10.0\times10^{-10}$ m^2/s, $6.2-7.2\times10^{-10}$ m^2/s and $12.2-13.2\times10^{-10}$ m^2/s, respectively.

subspectra from the 3D BEST-DOSY experiment on Mixture 1 corresponding to geraniol, quinine and camphene respectively onto the $\omega_H - \omega_C$ plane. The diffusion coefficients D computed from the 2D subspectra turn out to be 9.0×10^{-10} m^{2}s^{-1}, 6.4×10^{-10}

m^2s^{-1}, and 12.2×10^{-10} m^2s^{-1} for geraniol, quinine and camphene, respectively. The relaxation delay was set to 200 ms and the experimental time was around 2 hours. This is a substantial time savings over the previous study which performed a 3D standard HMQC-DOSY experiment on the same mixture [72] and used a total experimental time of 17 hours for a total of 5 diffusion points. Figures 2.8(a), (b) and (c) show projections

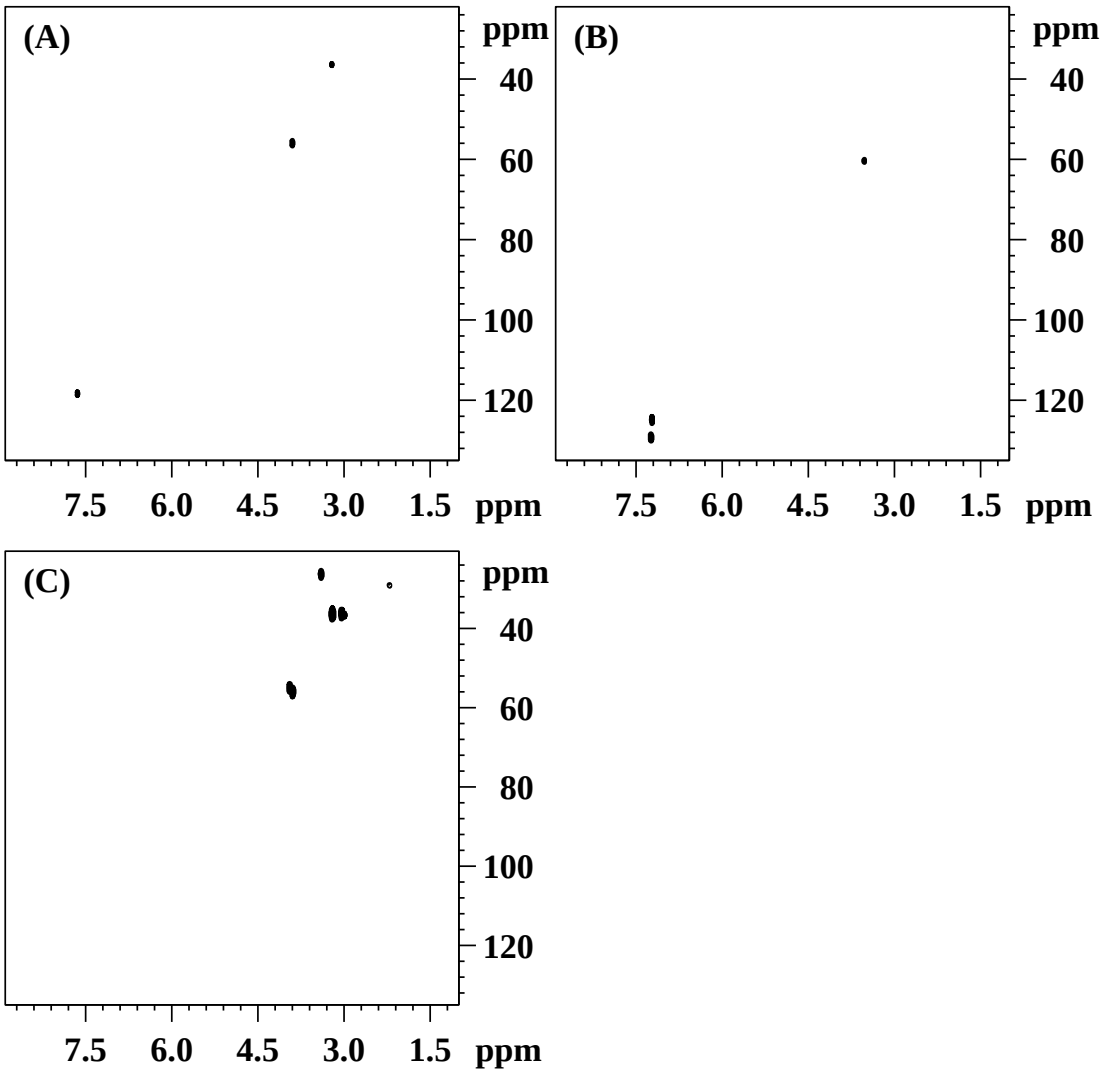

Figure 2.8: BEST-HMQC planes extracted from the 3D BEST-DOSY experiment for each subspectrum in Mixture 2. BEST-HMQC subspectra of (A) L-tryptophan (B) L-phenylalanine and (C) DL-valine extracted from the respective 3D experiments for diffusion coefficient ranges of $1.5-2.5\times10^{-10}$ m^2/s, $5.0-6.0\times10^{-10}$ m^2/s and $6.0-7.0\times10^{-10}$ m^2/s, respectively.

of the BEST-HMQC subspectra from the 3D BEST-DOSY experiment on Mixture 2 corresponding to L-tryptophan, L-phenylalanine and DL-valine, respectively. The diffusion coefficients D computed from the 2D subspectra turn out to be 1.5×10^{-10} m^2s^{-1}, 5.2×10^{-10} m^2s^{-1}, and 6.2×10^{-10} m^2s^{-1} for phenylalanine, tryptophan and valine,

respectively. The relaxation delay was set to 500 ms for a total experiment time of 4 hours.

In both Figures 2.7 and 2.8, almost complete resolution of the diffusion encoded spectrum is obtained and each subspectrum contains signals only from the particular individual mixture component. A good match was observed between the peaks in the 2D slice through the diffusion domain of the 3D BEST-DOSY spectrum and the 2D BEST-HMQC spectrum of the individual mixture components. In order to reduce convection due to possible sample heating during the 3D experiments, a "cool" adiabatic decoupling sequence using smoothed chirp inversion pulses was used during acquisition. Using adiabatic ^{13}C decoupling enables lower powers than standard decoupling sequences such as GARP and hence less heating over a broader spectral width.

In order to demonstrate the efficacy of the BEST-DOSY technique on a "real" complex mixture, we performed the experiment on a sample of commercial gasoline. The components of gasoline can be separated into paraffins, olefins, naphthenes and aromatics and has been analyzed previously using routine ^{1}H NMR spectroscopy [91, 92].

The 1D proton spectrum of gasoline is shown in Figure 2.9(a). The spectrum can be subdivided into aromatic (6.7 ppm to 8.0 ppm), olefinic (4.6 ppm to 6.0 ppm) and aliphatic (0.5 ppm to 3.3 ppm) chemical shift regions. Figure 2.9(b) shows the proton DOSY spectrum recorded on gasoline, showing considerable overlap in the diffusion coefficients. Figures 2.9(c), (d) and (e) show projections of the BEST-HMQC subspectra from the 3D BEST-DOSY experiment on Mixture 3 corresponding to aromatics, olefins and aliphatics, respectively. The diffusion coefficients D computed from the 2D BEST-HMQC subspectra for commercial gasoline turn out to be 3.3 $\times 10^{-10}$ m^{2}s^{-1}, 5.1 $\times 10^{-10}$ m^2 s^{-1}, and 8.9 $\times 10^{-10}$ m^{2}s^{-1} for aromatics, olefins and aliphatics, respectively. The relaxation delay was set to 200 ms for a total experiment time of 2 hours. The different regions are well separated in Figure 2.9 according to differences in their diffusion coefficients, indicating that the 3D BEST-DOSY experiment could be of use for high-throughput purposes and in developing quality control NMR based protocols for commercial gasoline.

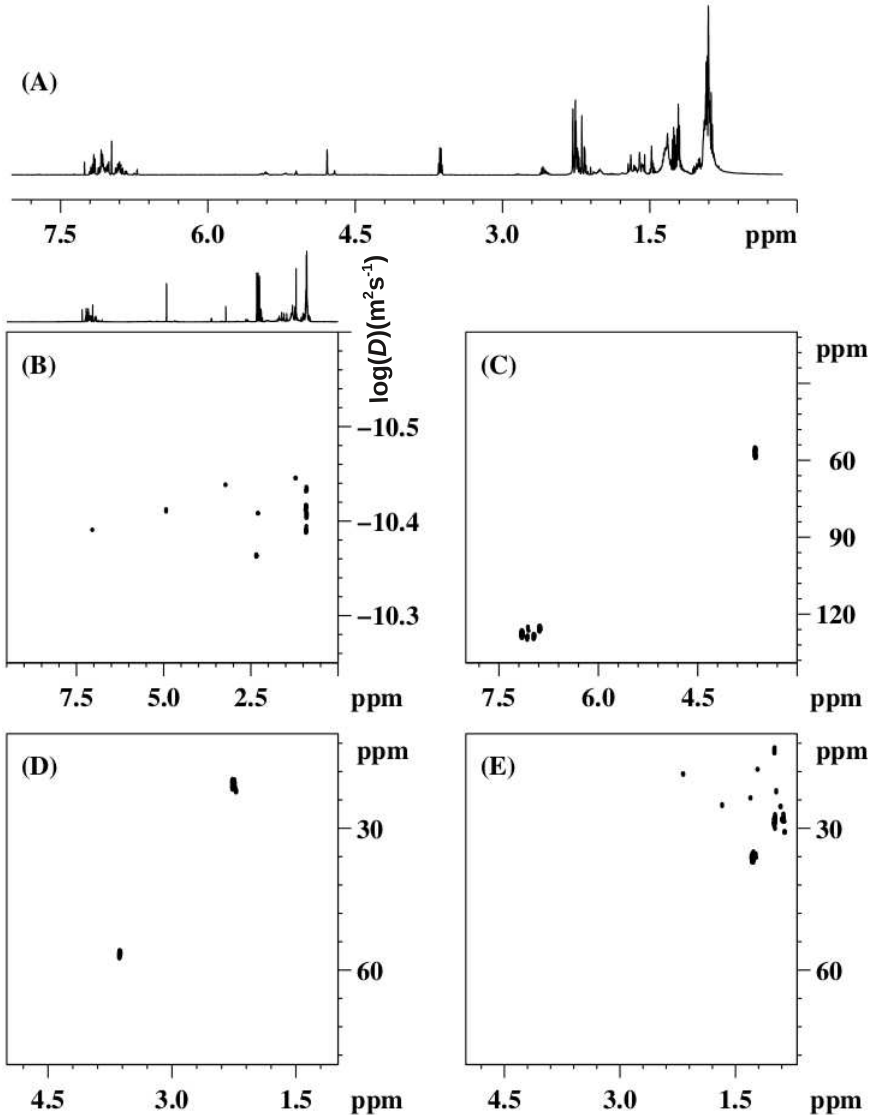

Figure 2.9: (A) The 1D ^{1}H spectrum of Mixture 3 (commercial gasoline) and (B) 2D ^{1}H DOSY NMR spectrum with proton chemical shifts (ppm) indicated along the x axis and diffusion units $(\log(D/\mathrm{m^2s^{-1}}))$ on the y axis. BEST-HMQC planes extracted from the 3D BEST-DOSY experiment for each individual component in Mixture 3 of commercial gasoline are shown in (C), (D) and (E). BEST-HMQC subspectra of (C) Aromatics (D) Olefins and (E) Aliphatics extracted from the respective 3D experiments for diffusion coefficient ranges of $3.0 - 4.0 \times 10^{-10}$ m^2/s, $4.5 - 5.5 \times 10^{-10}$ m^2/s and $8.0 - 9.0 \times 10^{-10}$ m^2/s, respectively.

Molecule	D (from 2D in 10^{-10} m^{2}s^{-1})	D (from 3D in 10^{-10} m^{2}s^{-1})
Geraniol	9.2 ± 0.5	9.0 ± 0.4
Quinine	6.6 ± 0.3	6.4 ± 0.3
Camphene	12.5 ± 0.5	12.2 ± 0.5
Tryptophan	1.7 ± 0.5	1.5 ± 0.5
Phenylalanine	5.2 ± 0.3	5.2 ± 0.3
DL-Valine	6.0 ± 0.4	6.2 ± 0.3
Gasoline (Aromatic)	–	3.3 ± 0.1
Gasoline (Olefin)	–	5.1 ± 0.1
Gasoline (Aliphatic)	–	8.9 ± 0.1

Table 2.2: Average diffusion coefficients of the individual components of various mixtures obtained from 2D DOSY ^{1}H NMR experiments and 3D BEST-DOSY experiments.

Average diffusion coefficients determined for the individual components of Mixture 1, Mixture 2 and Mixture 3 determined by analysis of different signals in the mixtures for the 2D DOSY and the 3D BEST-HMQC experiments are given in Table 2.2. The Stejskal-Tanner equation was fit to each data set using a nonlinear least squares algorithm as described in Chapter 1. The second column in Table 2.2 has diffusion coefficient values (D in m^{2}s^{-1}) measured by performing a separate 2D DOSY experiment on each individual component of both Mixture 1 and Mixture 2. Since we did not physically separate the components of Mixture 3, the 2D DOSY experiment on each individual component was not performed on Mixture 3. The third column in Table 2.2 has D values computed for each individual component by extracting its 2D subspectrum from the 3D BEST-DOSY experiment. In general, there is a good agreement between the D values of components measured separately and obtained from the 3D BEST-DOSY experiment on the corresponding mixture. Recently a double echo PGSTE-WATERGATE sequence was developed that provides convection compensation and good solvent suppression for diffusion experiments on biomolecules [86, 87]. The implementation of this pulse sequence on a small protein lysozyme (90% H_2O and 10% D_2O at a concentration of 2 mM) is shown in Figure 2.10(a). We have designed a selective analog of the PGSTE-WATERGATE diffusion sequence that provides good convection compensation and solvent suppression, whilst exciting only a desired spectral region. The 90° preparation hard pulse in the diffusion part of the pulse sequence is replaced with a band-selective Gaussian cascade (Q5) shaped pulse [2] centered at 2.5 ppm that excites resonances in the 1.0 to 4.0 ppm region. As seen in Figure 2.10(b),

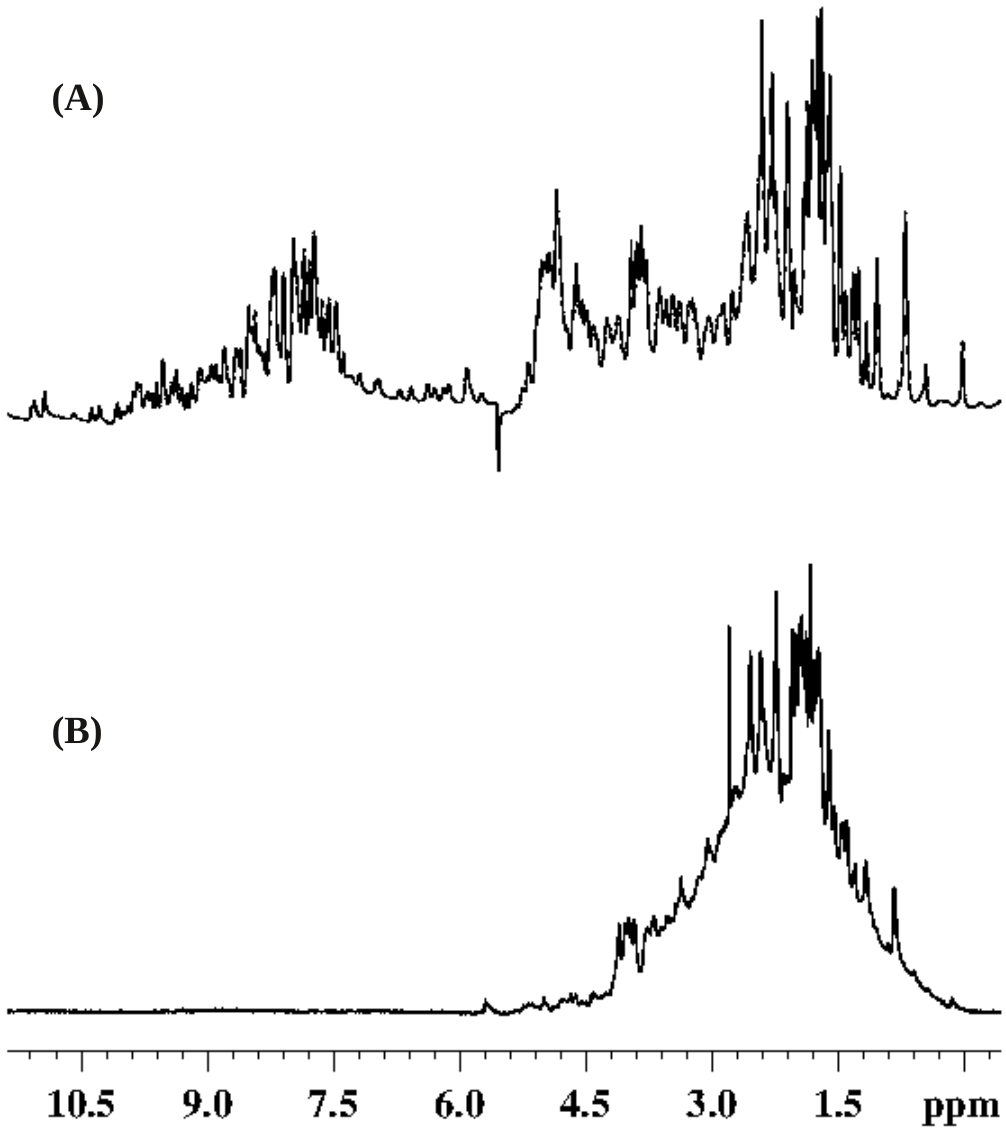

Figure 2.10: 600 MHz ^{1}H spectra of protein lysozyme in water (10:90 D_2O/H_2O) acquired at ambient temperature and a low gradient strength (5%) using (A) standard WATERGATE DOSY sequence and (B) Selective DOSY sequence with water suppression and a Gaussian cascade (Q5) excitation pulse centered at 2.5 ppm. The number of scans = 32, $\Delta = 100$ ms and $\delta = 4$ ms. The inter-pulse delay in the binomial pulses was set to 250 μs.

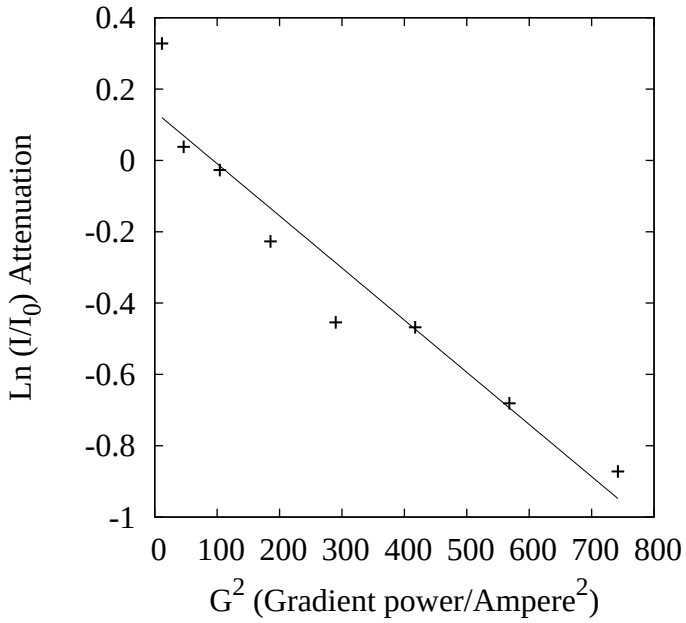

Figure 2.11: The diffusion plot of lysozyme in water (10:90 D_2O/H_2O). The log of the normalized intensity is plotted with increasing gradient strength. The data was fitted to the Stejskal-Tanner equation. The diffusion coefficient is computed to be $1.002 \pm 0.012 \times 10^{-10}$ m^2/s.

aliphatic proton peaks in this region are excited, with a fairly good solvent suppression. The 2D selective DOSY sequence with water suppression was concatenated with a BEST-HMQC sequence in a 3D DOSY fashion and applied on the lysozyme sample. The fit of the Stejskal-Tanner equation and the computation of the diffusion coefficient is shown in Figure 2.11. The diffusion coefficient of lysozyme is determined to be $1.002 \pm 0.012 \times 10^{-10}$ m^2/s. As seen from the data in Figure 2.11, there is a fair amount of scatter and the 3D sequence on the protein (unlike for the small molecules described previously) did not yield accurate values of the diffusion coefficient. The 2D BEST-HMQC spectrum of lysozyme protein is shown for comparison in Figure 12, with excitation in the range 0-2 ppm. The 3D selective-DOSY experiment needs to be refined in order to work well for protein samples, however the method offers fairly good sensitivity and once optimized, would find useful application in obtaining accurate diffusion coefficients of proteins and macromolecular complexes.

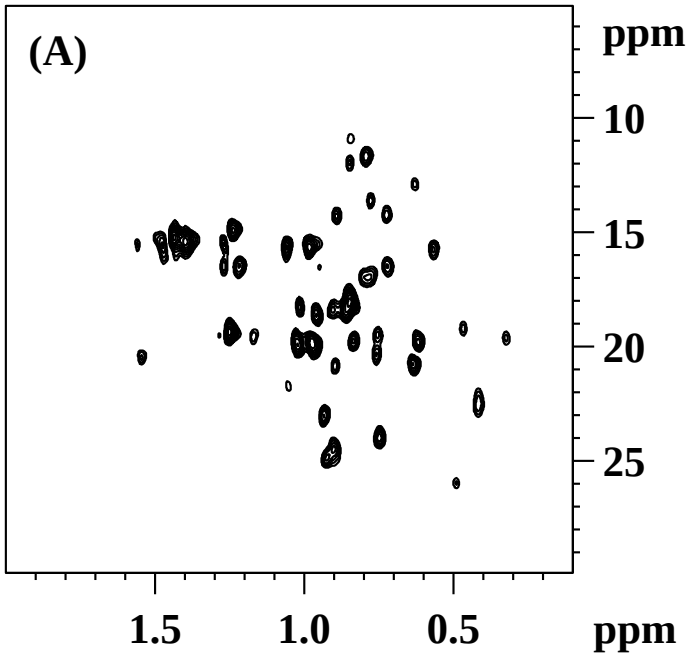

Figure 2.12: (A) 2D BEST-HMQC spectrum of lysozyme in water recorded at 600MHz (10:90 D_2O/H_2O). ^1H excitation and refocusing covering the frequency range from 0.0 ppm to 2.0 ppm in the BEST-HMQC experiment was achieved using a Seduce.100 excitation pulse of 1.5 ms and an RSNOB pulse of 1.0 ms, respectively. The relaxation delay was set at 100 ms with number of scan = 32.

2.4 Conclusions

A novel diffusion-edited 3D NMR experiment that incorporates a BEST-HMQC pulse sequence in its implementation is presented. Heteronuclear 3D DOSY NMR experiments are useful in elucidating the diffusion coefficients of individual constituents of a mixture, especially in cases where the proton NMR 2D DOSY spectra show considerable overlap. The present 3D BEST-DOSY pulse sequence provides a more sensitive and less time-consuming alternative to standard 3D HMQC-DOSY experiments. Cleanly separated subspectra of individual mixture components are obtained, leading to the determination of diffusion coefficients with better accuracy. The feasibility of the technique is demonstrated on a mixture of amino acids, on a mixture of small molecules with similar diffusion coefficients, and on a complex mixture with large dynamic range (commercial gasoline). An efficient and "cold" heteronuclear decoupling scheme is used which avoids problems in quantitative analysis of diffusion due to slow convection currents arising in the sample. The implications of using adiabatic decoupling schemes

and band-selective shaped pulses for selective BEST-DOSY experiments on proteins were also discussed in this chapter. The model mixtures used in this work form a good testbed to check the accuracy of the experimental methods proposed. Such experiments would be useful in structure elucidation studies of mixtures, in natural product drug discovery protocols and in ligand-protein binding studies.

CHAPTER 3

Disentangling Diffusion Information of Individual Components in a Mixture With a 3D COMPACT-IDOSY NMR Experiment

3.1 Background and Motivation

Several variants of the 3D DOSY technique have been suggested to overcome the limitation of long experimental times, such as internally encoded (I-DOSY) schemes [69, 70, 71, 93], spectral aliasing in the indirect dimension [74], and Hadamard-encoded diffusion measurements [94, 33]. In I-DOSY experiments, the diffusion encoding gradients are intertwined with the main 2D correlation pulse sequence, leading to a substantial reduction in experimental time. While I-DOSY schemes have the advantage of taking less time, they have the limitation that the diffusion-encoding gradient pulses need to be fitted into the polarization transfer intervals. This is the reason why heteronuclear I-DOSY schemes like the HMQC-IDOSY sequence have hitherto been implemented on systems which have small H-X scalar couplings [73]. Since the 2D heteronuclear multiple bond correlation (HMBC) pulse sequence [95, 96, 97, 98, 99, 100] correlates long-range ^{1}H-^{13}C scalar couplings and uses small (approximately 6-8 Hz) couplings, it is a good candidate for incorporation into an I-DOSY experiment. However, the HMBC experiment is also the least sensitive of the 2D heteronuclear correlation schemes, which is a major stumbling block in using it in a 3D DOSY pulse sequence.

This chapter describes a novel 3D I-DOSY experiment that we have designed, which allows diffusion weighting to be folded into an HMBC sequence. The pulse sequence utilizes a recent innovation in the HMBC family of experiments [101, 102, 103] wherein a cross-polarization acceleration by sharing adjacent polarization (ASAP) mixing period [104] transfers polarization of nearby spins and enhances sensitivity by using short recovery times. This work combines the advantages of superb resolution of

heteronuclear ^{13}C DOSY experiments with the time advantage of I-DOSY pulse sequences using a sensitivity-enhanced HMBC-type pulse sequence. We have given this pulse sequence the acronym COMPACT-IDOSY (**c**ross polarization **o**ptimized **m**ulti-site **p**olarized **ac**celerated **t**ime IDOSY). The 3D COMPACT-IDOSY sequence is experimentally tested on a mixture of flavonoids rutin and quercetin which have similar diffusion coefficients and show overlaps in their 1D and 2D NMR spectra. The diffusion coefficient values obtained from the 3D COMPACT-IDOSY experiment are compared with fits obtained from 2D DOSY experiments on each individual component of the mixture. The proposed experimental scheme is easily implemented with existing spectrometer software and achieves significant reduction in experimental time and concomitantly in sensitivity gain and resolution of signal overlap. This extends the scope of its application to a wider range of complex mixtures, ligand-binding studies and drug development protocols.

3.2 HMBC and Variants

The HMBC experiment detects chemical shift (usually ^{13}C-^{1}H) correlations for long-range couplings of about two or three bonds by using an inverse detection [105]. Single-bond coupling constants tend to lie in a narrow range while multiple-bond coupling constants lie in a wider range and cannot measured in a single HSQC or HMQC experiment. The basic 2D HMBC pulse sequence is closely related to the HMQC pulse sequence and contains a specific delay time between pulses which allows detection only of a range around a specific coupling constant (Figure 3.1). In HMBC, this difficulty is overcome by reducing these delays from an HMQC sequence, so that direct one-bond cross-peaks are suppressed and leaving only cross peaks between protons and carbons that are two or three bonds apart. The HMBC pulse sequence has a ^{13}C 90° pulse which occurs $1/(2^1J_{XH})$ after the first ^{1}H 90° pulse and serves as a low-pass J-filter to suppress one-bond correlations in the 2D spectrum. After the interval Δ_2 the second ^{13}C 90° pulse creates the desired heteronuclear multiple quantum coherence for ^{1}H *J*-coupled to a ^{13}C two or three bonds followed by the evolution time t_1. A ^{1}H 180° pulsed placed after $t_1/2$ removes the effect of ^{1}H chemical shift from the t_1 modulation

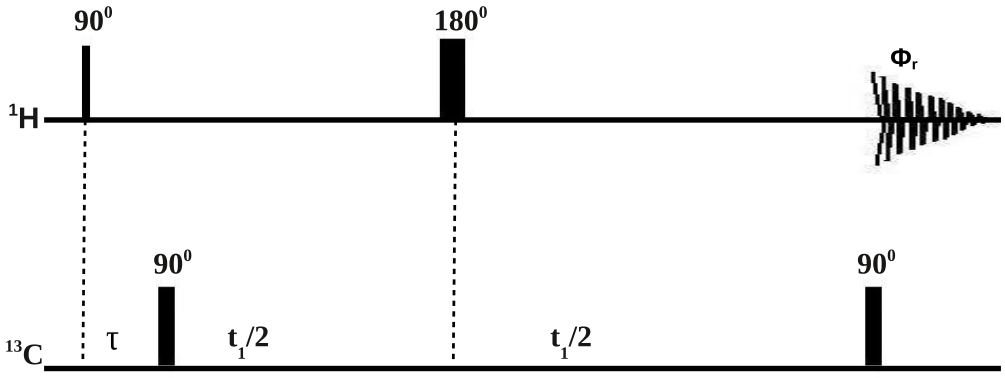

Figure 3.1: The basic sequence for long range C-H correlation spectroscopy (HMBC). The value of $\tau = 1/2^n J_{XH}$.

frequency. The final ^{13}C 90° pulse occurs after the evolution period followed by the detection period t_2. The signal detected during t_2 is phase modulated by the homonuclear ^{1}H *J*-couplings. The 2D spectrum is generated by a Fourier transform with respect to t_1 and t_2. HMBC and its variants are some of the most powerful 2D NMR experiments for structure determination of small and medium size molecules at natural abundance isotope levels. Some of the variations of HMBC are described below.

3.2.1 ge-2D HMBC Experiments

The ge-2D HMBC experiment is the gradient-enhanced version of the conventional 2D HMBC experiment in which coherence selection is gained by using pulsed field gradients (Figure 3.2). Gradient versions are preferred as they give clean results in a single scan per t_1 increment without need for phase cycling (when sample concentration is high). Other advantages are the improved water and artefact suppression, allowing for maximum gain.

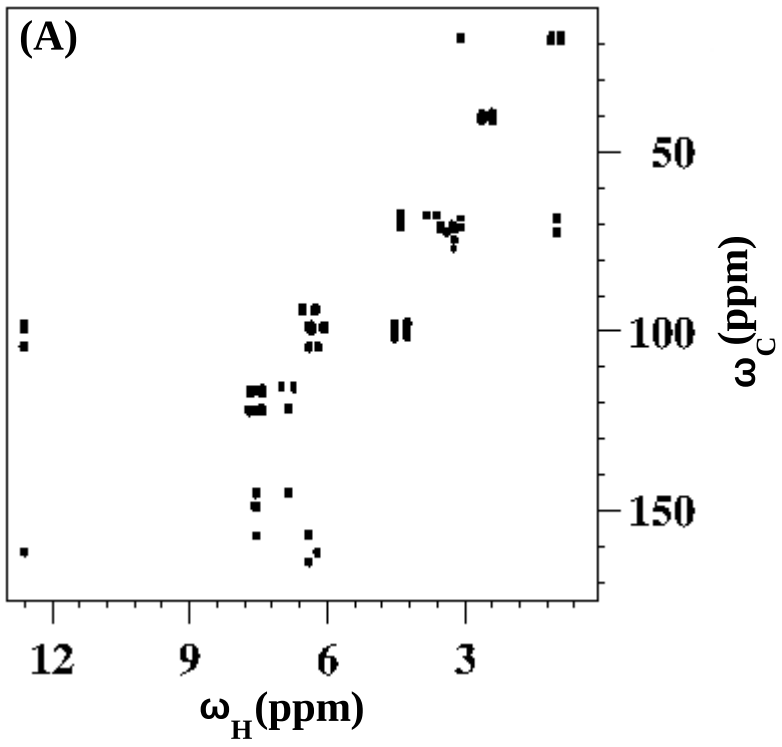

Figure 3.2: (A) ge-2DHMBC spectrum using sensitivity enhanced scheme, recorded at 600 MHz on a sample of rutin trihydrate dissolved in DMSO-D6. The relaxation delay was set at 100 ms with number of scans = 32.

3.2.2 Decoupled HMBC (D-HMBC)

The sensitivity of the HMBC signal is high when the ^{1}H signals to be observed appear as sharp lines. If the proton signal has broad lines due to complicated splitting, the corresponding HMBC spectrum suffers from a considerable decrease of the sensitivity. Due to this problem the detection of cross peaks becomes difficult. The decoupled HMBC (D-HMBC) reduces such problems and gives a spectrum with improved signal to noise ratio [106].

3.2.3 HAT HMBC

The HMBC experiment yields long range correlation between the proton and carbon or heteroatoms separated by two or three bonds but occasionally also over four or more rarely even five bonds. A HAT HMBC spectrum shows predominantly two-bond correlations [107].

3.2.4 Constant Time HMBC (CT-HMBC)

The ^{1}H-^{1}H homonuclear spin coupling plays an important role and remains active throughout the HMBC pulse sequence for detection of ^{13}C-^{1}H couplings with high sensitivity. One problem of HMBC is that J modulation due to ^{1}H-^{1}H coupling during the t_1 evolution period causes line broadening of the ^{13}C signals in the F_1 dimension. This undesirable effect sometimes results in difficulty in analyzing ^{13}C-^{1}H cross peaks of complicated molecules with poorly separated carbon signals. In order to overcome this problem, a new technique CT-HMBC has been developed [108]. The pulse sequence of CT-HMBC is analogous to HMBC, except for the introduction of a constant time evolution period [(Δ_3- t_1/2) + t_1/2] before and after the 180° pulse. The aim of incorporating the constant time period is to keep unchanged the effect of ^{1}H-^{1}H J-modulation and furthermore, the splitting of the cross peaks by ^{1}H-^{1}H coupling in the F_1 dimension is also suppressed.

3.2.5 Clean HMBC

Clean HMBC (Figure 3.3) is used for suppression of strong coupling induced artifacts in HMBC spectra [95]. Artifact suppression is extremely important in HMBC spectra as key peaks can be of very low intensity. Low pass J filters have been designed to suppress unwanted one-bond correlations. Clean HMBC provides good suppression of undesired one bond correlation peaks which is achieved even in case of strong coupling.

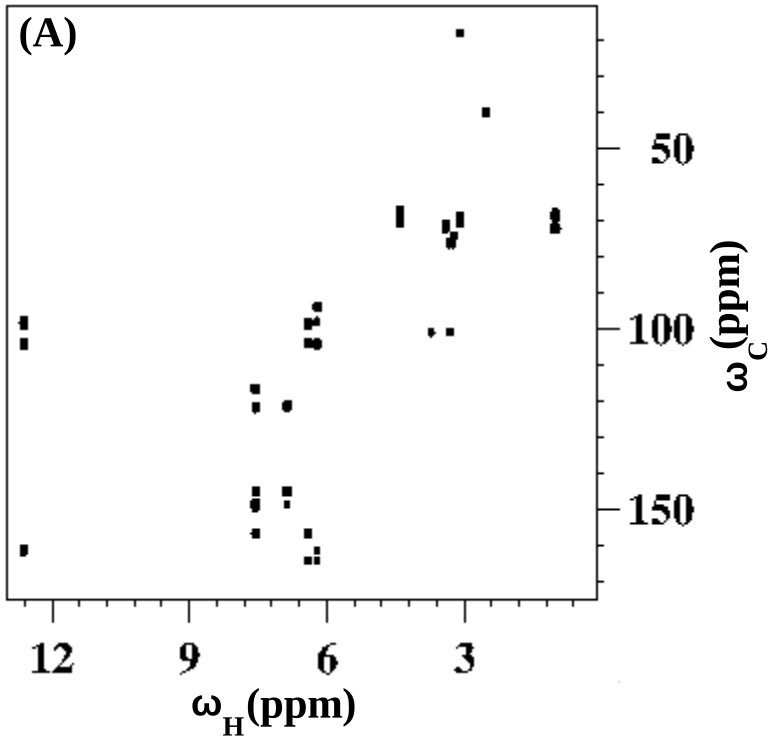

Figure 3.3: (A) 2D Clean HMBC spectrum recorded with 256 t1 increments. The number of complex points in the acquisition dimension was 1024 the relaxation delay was 1 s, ${}^{n}J_{CH}$ transfer delay Δ= 62 ms, and the range for the overall 3rd order low pass J filter delay settings was 125 Hz$<{}^{1}J_{CH}<$ 175 Hz. The data matrices cover 2K$\times$2K in F_1 and F_2 dimensions.

3.2.6 IMPACT-HMBC

The IMPACT-HMBC (improved and accelerated constant-time heteronuclear multiple-bond correlation) is a variation of 2D HMBC pulse sequence (Figure 3.4) [109]. By using this technique it is possible to obtain a high quality 2D spectrum with less arti-

facts, enhanced sensitivity in lesser time. The pulse sequence has a three fold low pass J filter for a better suppression of $^{1}J_{CH}$ with constant time interval to improve signal shape and uses the ASAP method for quick recovery delay.

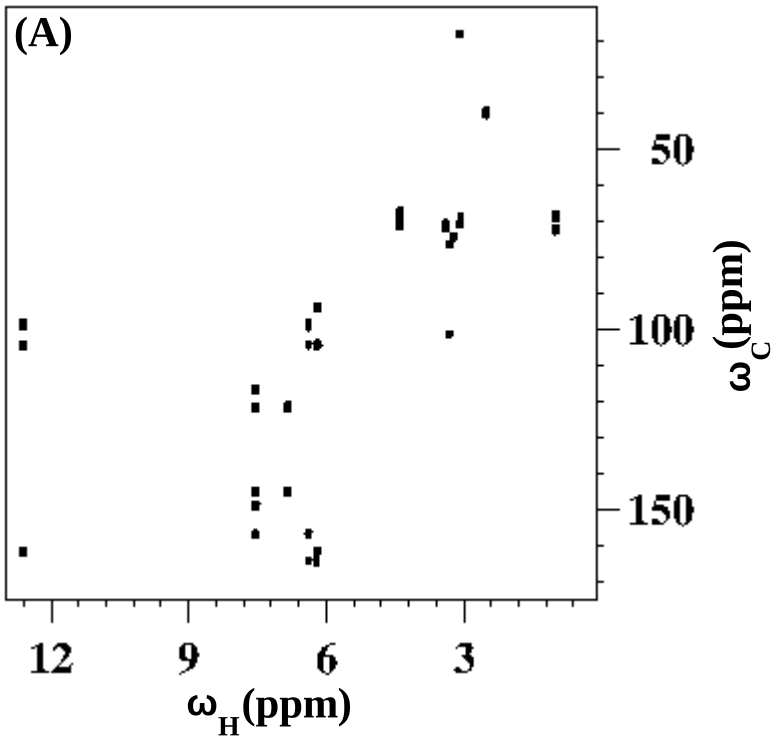

Figure 3.4: (A) Two-dimensional HMBC spectrum of rutin trihydrate recorded at 600 MHz with the IMPACT-HMBC sequence. The spectrum was recorded using 128 increments and a recovery delay of 0.5 s. Ernst angle α= 120° was used. The Ernst angle was calibrated with a one-dimensional version of the pulse sequence. The measurement duration of the experiment was 27 min.

3.3 3D HMBC-DOSY NMR

For structural studies of small and medium size of molecule by NMR spectroscopy, it is very important to detect the ^{13}C-^{1}H long-range correlations. For getting good HMBC spectra, it is important to properly set several parameters such as the magnitude of long-range ^{13}C-^{1}H coupling constants. These parameters are variable and depend on the relationship between a given proton and its long range coupled carbon. It is impossible to select the absolute delay time value which will give satisfactory results for all ^{13}C-

^{1}H long range couplings present. In our experiment we have used the delta value Δ = 60 ms for the ordinary HMBC experiment. This gives decrease of the sensitivity for detection of some ^{13}C-^{1}H long range correlations. To overcome these problems a NMR experiment 3D-HMBC was performed by modifying the conventional 2D-HMBC pulse sequence. The delay time Δ_2 and t_1 in the 2D-HMBC have been replaced by t_1 and t_2 respectively, in the 3D-HMBC experiment.

3.4 3D IDOSY Experiments

There are three strategies for creating a DOSY pulse sequence: prepending the diffusion encoding (DOSY-X), appending it (X-DOSY), and incorporating it internally (X-IDOSY). The IDOSY approach can be simpler, quicker and more sensitive. A number of IDOSY techniques have been developed such as TOCSY-IDOSY [110], a convection-compensated HMQC-IDOSY [73] and a 2DJ-IDOSY pulse sequence [**?**] which improves the signal to noise ratio by approximately a factor of 2 and reduces minimum experimental time at least 4-fold. The COSY-IDOSY experiment is derived from the basic gradient enhanced COSY experiment by adding two short extra delays $\Delta/2$ and using the same field gradient pulses for coherence transfer pathway selection and for diffusion encoding [70]. The COSY-IDOSY pulse sequence may be used as either p-type or n-type. The p-type version has lower t_1 noise while the first gradient pulse in the n-type pulse sequence helps to minimize field and field frequency lock disturbances.

3.5 Experimental Methods

Materials: The experiments were performed on a Bruker Avance-III NMR spectrometer operating at 600.13 MHz for ^{1}H equipped with a 5-mm QXI probe and an actively shielded Z-gradient coil. All experiments were performed at ambient temperature (in an air-conditioned room at $22\,^{\circ}\mathrm{C}$ to avoid errors due to convection gradients. The spectra were processed using Bruker Topspin 2.1 software. The samples of quercetin dihydrate and rutin trihydrate were obtained from Sigma Aldrich and used without further purifi-

cation. The mixture was prepared by dissolving 15 mg of quercetin dihydrate and 20 mg of rutin trihydrate in 400 μl of DMSO-D6, at a concentration of 50 mM.

^{1}H and ^{13}C 2D DOSY: ^{1}H 2D DOSY NMR spectra were acquired using the stimulated echo bipolar gradient pulse sequence with an eddy current delay [43, 28]. The duration of the diffusion delay was kept as short as possible to minimize signal loss due to relaxation. The experimental parameters included 16 gradient amplitude steps ranging from 2 to 95% (in equal steps of gradient squared) using 32 transients, 16K complex data points, a gradient duration of 1 ms, eddy current delay 5 ms and diffusion time 200 ms leading to an experiment time of 9 minutes. The gradient system was calibrated to 54.5 Gcm^{-1} at maximum intensity. The experimental conditions for the ^{13}C 2D DOSY measurements were: diffusion time 200 ms; gradient pulse width 3 ms; 512 transients and the gradient amplitude was changed from 2 to 95% in 16 equal steps of gradient squared taking an experimental time of 8 hours. The data were fitted to the Stejskal-Tanner equation using the method described in Chapter 1.

2D HMBC & variants: 2D COMPACT-HMBC spectra were acquired with 128 t_1 increments and a spectral width of 13.93 ppm and 180 ppm in the ^{1}H and ^{13}C dimensions, respectively. A total of 48 transients were acquired for each increment, with an acquisition time of 122.5 ms and a recycle delay of 100 ms for a total experimental time of 40 minutes. Spectra were apodized in both dimensions with a sine-bell function shifted by 90° and zero-filled in the F_1 dimension to 2048 data points. Artifact removal was achieved with a three-fold low-pass J-filter to suppress one-bond correlations [111, 112, 113]. The ^{13}C 180° pulse was set as a band-selective refocusing pulse with length optimized to 2 ms. The delays $\Delta_1, \Delta_2, \Delta_3$ are pre-set to filter out the one-bond couplings as described previously [111, 112, 113], with the filter range set between 125-165 Hz. The length of the ASAP period [104] was optimized to 40 ms and the DIPSI-2 mixing sequence was used for cross-polarization. A period of 83.33 ms was used to generate the multiple-quantum coherence corresponding to a long-range scalar coupling of 6 Hz. Ernst angle optimization led to a flip angle $\alpha = 130^{\circ}$ for maximum sensitivity. The standard HMBC spectra were acquired with 16 transients and a recycle delay of 1 s, all other parameters and experimental time being the same. The 2D HSQC spectrum was recorded as a data matrix of 2048 (^{1}H) $\times$ 128 (^{13}C) complex

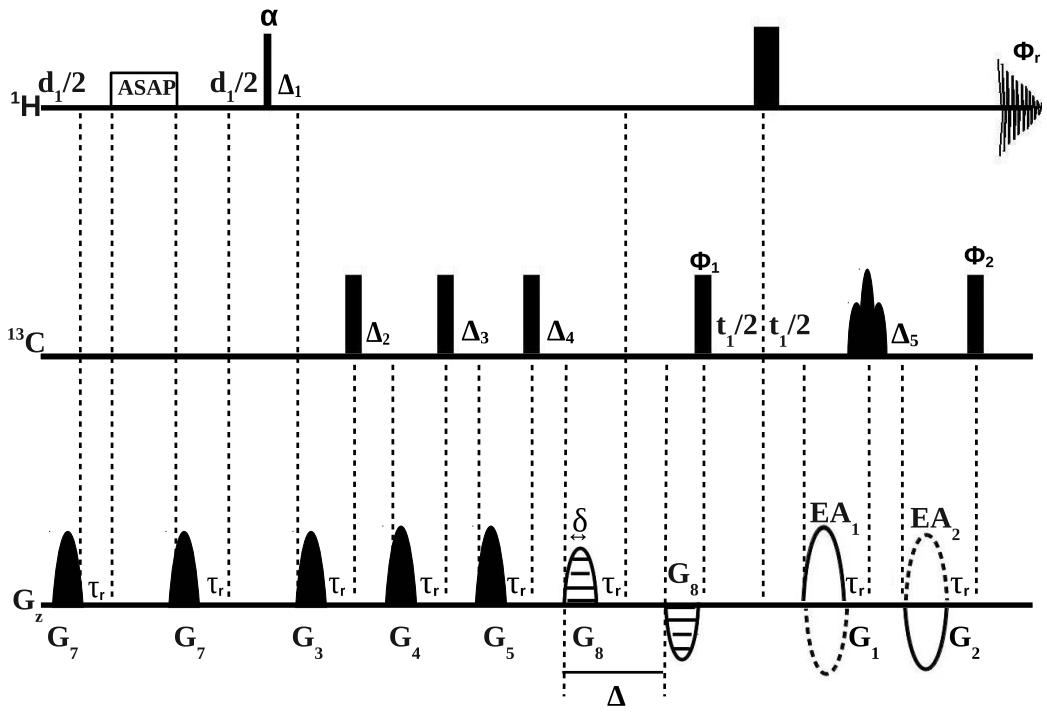

Figure 3.5: Pulse scheme for the 3D COMPACT-IDOSY experiment with internal diffusion encoding. Narrow and wide pulses correspond to pulse flip angles of 90° and 180°, respectively. Phase cycling is $\phi_1 = x, -x; \phi_2 = 4(x), 4(-x); \phi_r = 2(x, -x), 2(-x, x)$. Phases if not indicated otherwise are applied along the x axis. The α degree ^{1}H pulse is set to the Ernst angle, while the 180°, ^{13}C pulse is a band selective pulse. $^1J_{CH}$ couplings are suppressed with a three-step low pass J filter with pre-set delays $\Delta_1, \Delta_2, \Delta_3$ to filter out one-bond couplings. The delay Δ_4 is for the evolution under long-range correlations. $\Delta_5 = (t_1)_0 + p2$ where $(t_1)_0$ is the first t_1 value and $p2$ is the proton 180° pulse. The ASAP period with a DIPSI-2 mixing sequence is sandwiched between gradient pulses and relaxation intervals $d_1/2$. Gradients are applied in the ratios: $G_1 : G_2 : G_3 : G_4 : G_5 : G_6 : G_7 = 80 : 80 : 14 : -8 : -4 : -2 : -17$ with recovery times τ_r and EA refers to Echo-Antiecho phase cycling. The diffusion interval is Δ, gradient length δ and encoding/decoding gradient strength G_8.

data points, respectively.

3D COMPACT-IDOSY: 3D COMPACT-IDOSY experiments were performed using the pulse sequence described in Figure 3.5. In the HMBC dimension, 2048 $\times$ 128 data points were used with a spectral window of 13.93 ppm. A mixing time of 40 ms and the DIPSI-2 sequence were used for the ASAP period. The diffusion encoding gradients were varied in 08 gradient steps from 2 to 95%, with 54.5 G/cm maximum gradient intensity. Diffusion time was 83.33 ms, gradient pulse length 2 ms and recovery delay 100 ms for 32 transients, leading to a 3 h 42 min experiment. The spectrum was processed in the HMBC dimension with FT using echo-antiecho phase cycling before applying an inverse Laplace transform to obtain the DOSY dimension.

3.6 Results and Discussion

The HMBC experiment is based on long-range $^{n}J_{CH}$ couplings and can pick up two-bond and three-bond carbon-proton connectivities. However, standard HMBC spectra suffer from unwanted residual one-bond $^{1}J_{CH}$ signals which interfere with long-range signals and lead to confusion. Artifact suppression is very important in HMBC since the "real" peaks could be of low intensity. The pulse sequence to implement the sensitivity-enhanced and artefact suppressed 3D COMPACT-IDOSY scheme is shown in Figure 3.5. The 2D HMBC part of the pulse sequence is similar to the IMPACT-HMBC sequence [102] which introduces a constant time element in the HMBC sequence after the low-pass filters for sensitivity increase. Since the focus in our scheme is on obtaining a clean spectrum purged of all artefacts and in getting a uniform sensitivity enhancement across peaks, we did not retain the constant time sequence and instead used a different set of gradient ratios along the lines of the Clean-HMBC [95, 96]. The delays $\Delta_1, \Delta_2, \Delta_3$ in the sequence described in Figure 3.5 are pre-set to filter out one-bond artefacts in a coupling range J_{min} to J_{max}. The delay Δ_5 is set to $(t_1)_0 + p2$ to ensure there is no ^{13}C chemical shift evolution for the first t_1 increment, where $p2$ is the length of the proton 180° pulse. The COMPACT-HMBC experiment starts with an ASAP cross-polarization interval, which speeds the recovery of longitudinal proton magnetization by sharing polarization with nearby protons [104]. The homonu-

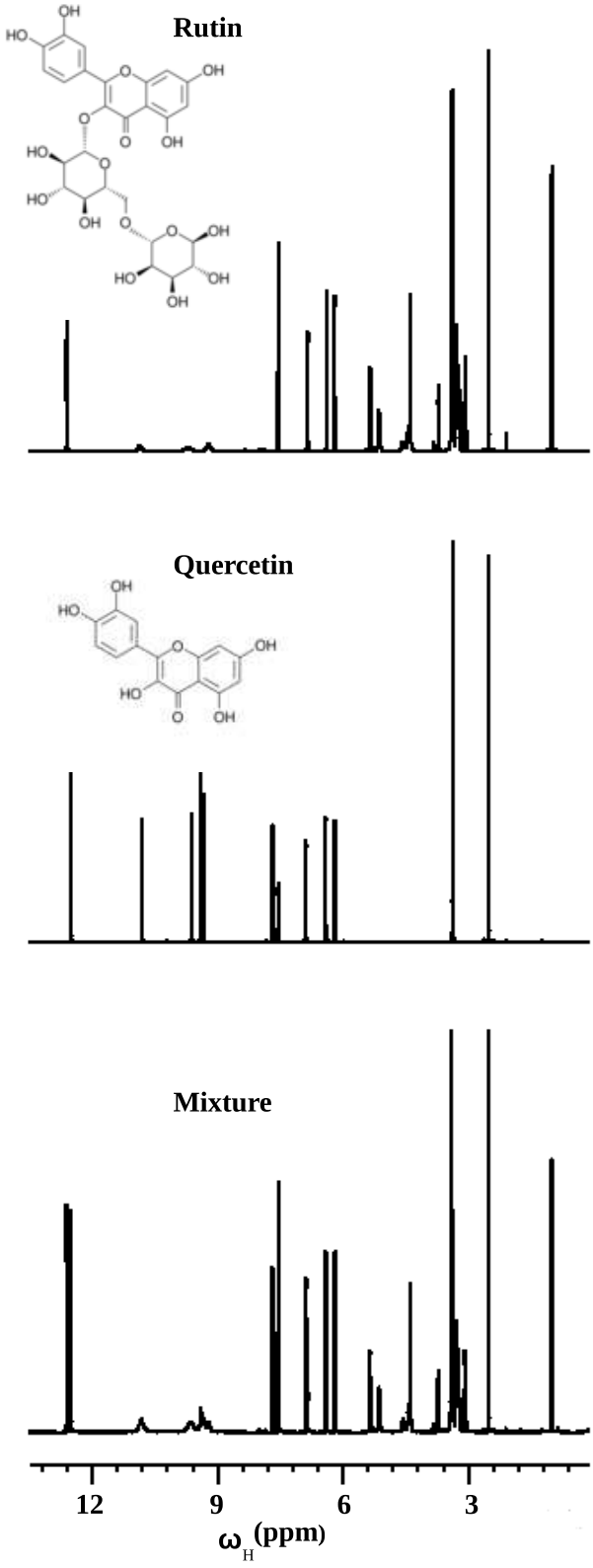

Figure 3.6: Structures of rutin and quercetin molecules and 1D ^{1}H NMR spectra of the mixture. ^{1}H spectra were acquired with 16 transients, 32K data points using a 8361 Hz spectral window and a relaxation delay of 1 s.

clear Hartmann-Hahn effect is the mechanism responsible for cross-polarization and the usual relaxation delay is replaced with a short cross-polarization interval which offers a significant reduction in recycle delay and an improvement in overall sensitivity. Since the ASAP method does not rely on spin-diffusion, it is applicable to small molecules as well. If a short relaxation delay is used with no cross-polarization, the recovery of longitudinal magnetization between scans is incomplete and the sensitivity is poor. An additional sensitivity improvement in the ASAP spectra can be obtained by using Ernst-angle excitation (denoted by the α flip angle pulse in Figure 3.5). The ASAP sequence is also effective in suppressing noisy F1 ridges that often occur in 2D spectra recorded with short relaxation delays. The interval between the encoding and decoding gradients is the diffusion interval Δ and the entire diffusion weighting (including the incremented/decremented diffusion gradients, gradient recovery times and diffusion time) is incorporated into the delay Δ_4 for the evolution of long-range ${}^nJ_{CH}$. F1 quadrature detection is implemented by combining datasets acquired with the solid and dotted gradient waveforms. The structures and ^{1}H NMR spectra of quercetin, rutin and their mixture are shown in Figure 3.6. Quercetin and its glycoside rutin are flavonoids widely found in plants and medicinal herbs and have important pharmacological activities. The 1D ^{1}H NMR spectrum of the rutin/quercetin mixture shows considerable overlap in the chemical shifts. The 2D ^{1}H DOSY and ^{13}C DOSY spectra of the rutin/quercetin mixture are shown in Figure 3.7, with the chemical shifts on the horizontal axis and the diffusion coefficients on the vertical axis expressed in m^2s^{-1}. Most ^{13}C diffusion experiments use either a stimulated echo such as in an INEPT-DOSY or a spin echo such as a DEPTSE sequence [114]. Since the gyromagnetic ratio of ^{13}C is four times lower than that of ^{1}H, a much larger gradient pulse area is required for ^{13}C DOSY as compared to ^{1}H DOSY for the same diffusion time (keeping in mind that the attenuation by diffusion scales as γ^2). A sharp peak in the F1 diffusion coefficient dimension represents one particular molecular species. The diffusion equation assumes that all molecules have the same overall shapes and relaxation properties. While both the ^{1}H DOSY and ^{13}C DOSY of individual molecules showed a mono-exponential behavior, the DOSY spectra of the mixture showed overlapping signals along the diffusion and chemical shifts dimensions. Signal overlap in a 2D DOSY experiment leads to inaccurate estimates of diffusion coefficients since the spurious diffusion peak actually represents the weighted average of

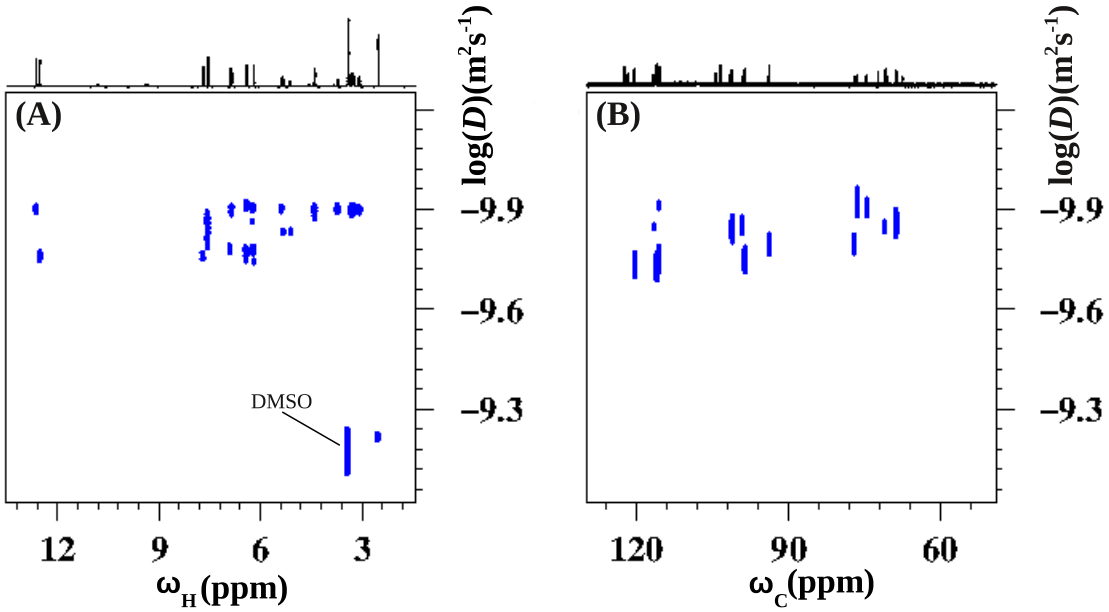

Figure 3.7: (A) 2D ^{1}H DOSY and (B) 2D ^{13}C DOSY spectrum of the rutin/quercetin mixture. Chemical shifts (ppm) are displayed on the x-axis and diffusion separation ($\log D/\mathrm{m^2 s^{-1}}$) is shown along the y-axis.

the two overlapping signals. While the resolution along the chemical shift dimension was better as compared to ^{1}H in the ^{13}C DOSY experiments, the low signal-to-noise ratio led to long experimental times (upto 8 hours for a single experiment on an individual component). Since the overlapped DOSY spectra did not allow for unraveling the diffusion coefficients of individual components and since the diffusion coefficients for the mixture were close enough that they could not be processed using advanced techniques, adding a third dimension to the diffusion experiment became necessary.

The standard gradient-selected HMBC and the COMPACT- HMBC spectra of the rutin/quercetin mixture are shown in Figures 3.8(A) and (B), respectively. The standard HMBC spectrum clearly shows residual one-bond artefacts which interfere with the true long-range correlations [97]. The COMPACT-HMBC experiment has been collected with the same experimental parameters except for a much shorter relaxation delay of 100 ms instead of 1 s and 48 transients instead of 16, keeping total measurement time identical for both experiments. The spectrum shows good $^{1}J_{CH}$ suppression, absence of F1 ridges and a good signal-to-noise ratio using a minimum experiment time. Ernst angle excitation gives optimized sensitivity for a given repetition rate. Since no decoupling is performed during acquisition in the HMBC experiment, somewhat longer acquisition times can be used without fear of decoupler heating problems. Both the HMBC and COMPACT-HMBC spectra in Figure 3.8 are overlaid with HSQC spectra recorded without ^{13}C decoupling during proton acquisition, in order to show the positions of one-bond artifacts. These artefacts are purged in the COMPACT-HMBC experiment.

In an I-DOSY experiment the diffusion encoding gradients are integrated into various delays in the pulse sequence when the parent 2D pulse sequence can accommodate an extra diffusion delay, which reduces the experiment time as compared to a sequential 3D DOSY sequence. Further, in the case of the sequential DOSY experiment a 50% signal loss occurs due to the stimulated echo sequence. Standard 3D HMQC-DOSY experiments correlate directly bonded carbon-proton pairs and hence use very short J-modulation delays (for one-bond couplings between 130-145 Hz). In an HMBC sequence the use of small two-bond and three-bond couplings allows diffusion weighting to be folded into the HMBC sequence in an I-DOSY experiment. The 3D COMPACT-

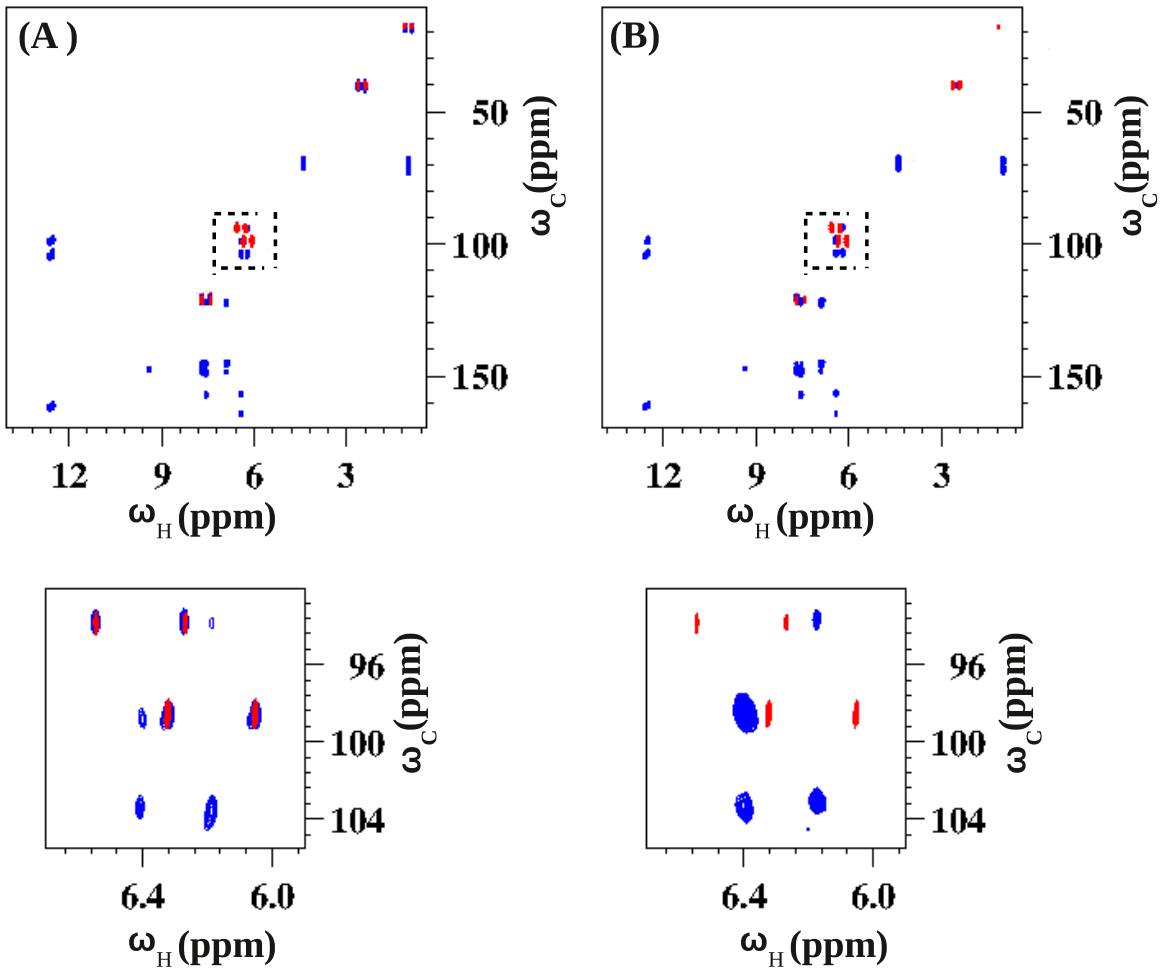

Figure 3.8: 2D HMBC NMR spectra of the rutin/quercetin mixture recorded on a 600 MHz NMR spectrometer using the (A) standard gradient enhanced HMBC and (B) COMPACT-HMBC pulse sequences. A total of 128 t_1 increments and 2048 complex points in the acquisition dimension were used. The recycle delays were 1 s and 100 ms and the number of transients per FID were 16 and 48 for the standard HMBC and COMPACT-HMBC experiments respectively, keeping total measurement time identical. The ${}^{n}J_{CH}$ transfer delay was set to 83.3 ms and the range for the overall low-pass J filter was 125 Hz < ${}^{1}J_{CH}$ < 165 Hz. Spectra are overlaid with HSQC spectra recorded without ^{13}C decoupling during acquisition, to indicate the positions of one-bond coupling artifacts. The expanded insets show the regions of crowded one-bond overlaps.

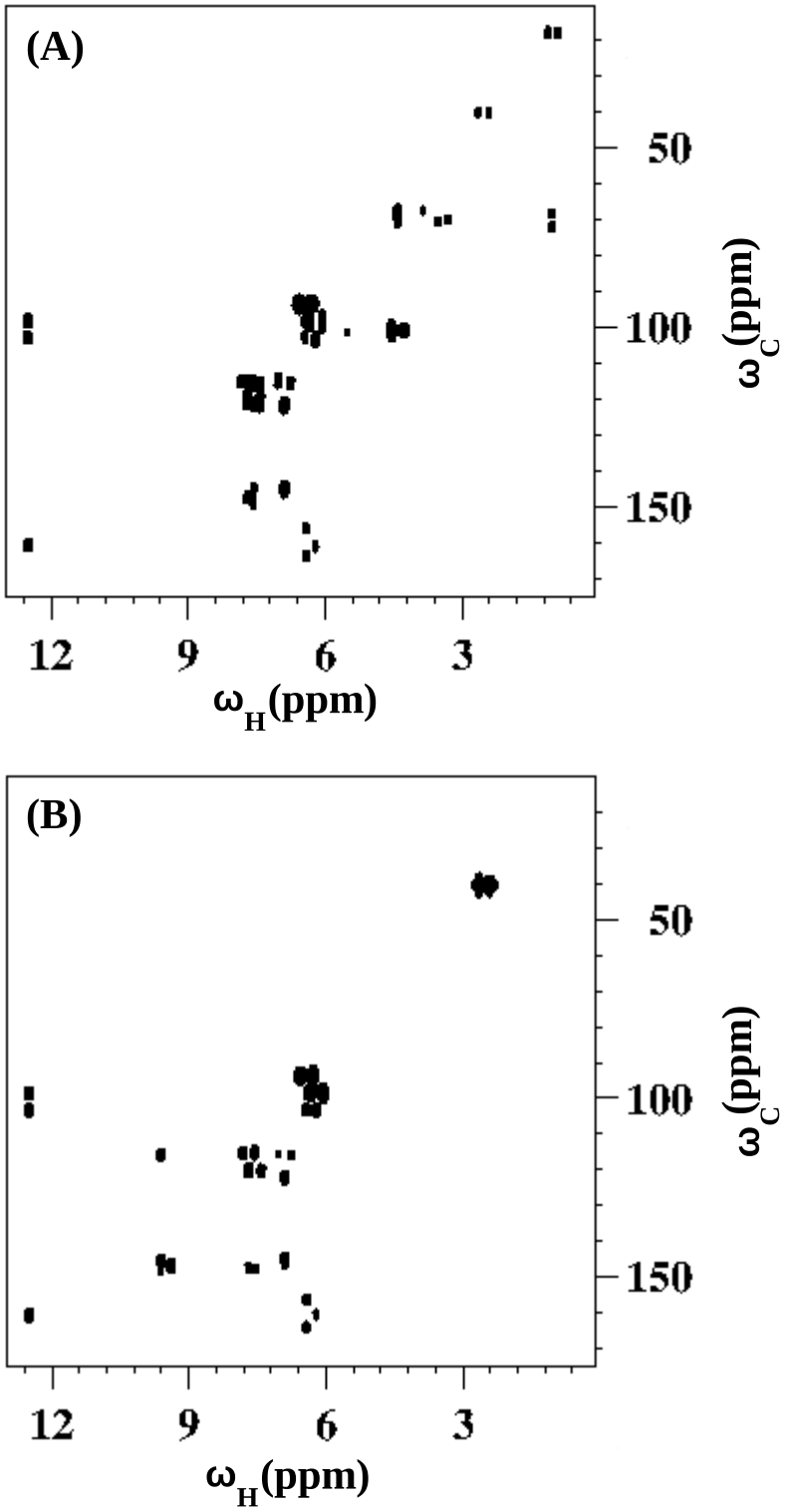

Figure 3.9: 2D HMBC subspectra of the rutin/quercetin mixture extracted from the 3D HMBC-DOSY experiment. Projections onto the $\omega_H - \omega_C$ plane of the 3D DOSY data set (a) for the diffusion coefficient range 0.68-0.79 $\times 10^{-10}$ m^2s^{-1} showing the signals of rutin and (b) for the diffusion coefficient range 0.89 - 1.04 $\times 10^{-10}$ m^2s^{-1} showing the signals of quercetin.

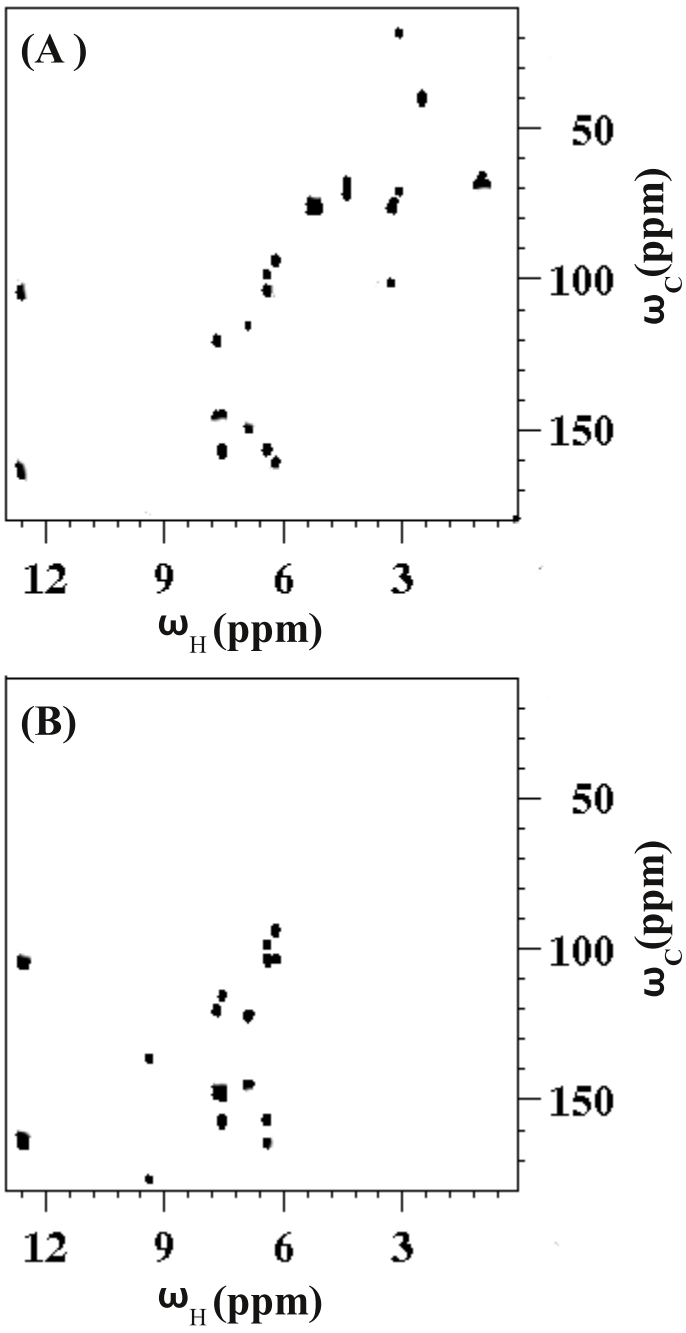

Figure 3.10: 2D HMBC subspectra of the rutin/quercetin mixture extracted from the 3D COMPACT-IDOSY experiment. Projections onto the $\omega_H - \omega_C$ plane of the 3D DOSY data set (a) for the diffusion coefficient range 0.68-0.79 $\times 10^{-10}$ $m^2 s^{-1}$ showing the signals of rutin and (b) for the diffusion coefficient range 0.89 - 1.04 $\times 10^{-10}$ $m^2 s^{-1}$ showing the signals of quercetin.

IDOSY experiment leads to a 3D data matrix and after double Fourier transformation, consists of a set of 2D COMPACT-HMBC spectra with different degrees of diffusion encoding. Measurements of the corresponding cross-peak volumes in successive spectra then enables diffusion coefficients to be extracted by least squares fitting of the cross-peak decays to the Stejskal-Tanner equation.

For purposes of comparison of signal enhancement and experimental time, the 2D projections obtained from the ordinary 3D HMBC-DOSY experiment on the rutin-quercetin mixture are shown in Figure 3.9. The experiment takes a very long time and the new 3D COMPACT-IDOSY experiment on the same mixture achieves much better sensitivity in correspondingly much shorter time. The two 2D projections of the 3D COMPACT-IDOSY spectrum of the rutin/quercetin mixture are shown in Figure 3.10 for different diffusion ranges. Figures 3.10(A) and (B) show projections onto the $\omega_C - \omega_H$ plane of the 3D COMPACT-IDOSY data for the diffusion coefficient ranges $0.68 - 0.79 \times 10^{-10}$ m^{2}s^{-1} and $0.89 - 1.04 \times 10^{-10}$ m^{2}s^{-1} for rutin and quercetin, respectively. The two projections obtained are cleanly separated into the subspectra of rutin and quercetin. The near-degenerate peaks in the 1D spectrum of the mixture are now resolved in the diffusion ordered spectra at 12.61 ppm for rutin (Figure 3.10(A)) and at 12.60 ppm for quercetin (Figure 3.10(B)), respectively. Two peaks at 2.52 ppm and 3.40 ppm in the ^{1}H 1D spectrum of quercetin are not picked up in its 2D subspectrum (Figure 3.10(B)). This however does not seriously impact the calculation of the diffusion coefficient since all the other peaks in the subspectrum are well-resolved and with adequate signal-to-noise ratio. The severe overlap in the 6-9 ppm region of the ^{1}H chemical shifts of rutin and quercetin is well resolved and is nicely illustrated by the clean diffusional separation of the corresponding signals in the 2D projections of the 3D COMPACT-IDOSY data (Figure 3.10). The benefit of the 3D COMPACT-IDOSY experiment in terms of experimental time reduction is significant as compared to times reported in the literature for the ordinary sequential 3D HMBC-DOSY experiment [115]. The mean diffusion coefficients determined by analysis of different subspectra in the rutin/quercetin mixture from the 3D COMPACT-IDOSY experiment are given in Table 3.1 alongwith the diffusion coefficients extracted from the 2D ^{1}H and ^{13}C DOSY experiments on the individual mixture components. The analysis from the 2D subspectra from the 3D experiment on the mixture and the 2D DOSY spectra on the

Table 3.1: Diffusion coefficients D ($\times 10^{-10}$ m^2s^{-1}) of rutin/quercetin mixture extracted from 3D COMPACT-IDOSY subspectra and compared with separate 2D ^{1}H DOSY and 2D ^{13}C DOSY measurements on individual components. Uncertainties in D values are the standard errors of the fits obtained from the regression analysis.

Molecule	D(^{1}H DOSY)	D(^{13}C DOSY)	D(3D COMPACT-IDOSY)
rutin	0.76 ± 0.03	0.72 ± 0.04	0.73 ± 0.01
quercetin	0.97 ± 0.04	0.95 ± 0.04	0.96 ± 0.01

individual components show comparable diffusion coefficients.

3.7 Conclusions

A new 3D diffusion-ordered heteronuclear NMR experiment COMPACT-IDOSY has been designed and experimentally implemented on a mixture of flavonoids rutin and quercetin. The pulse sequence uses a cross-polarization mixing period and diffusion encoding gradients internally incorporated into the coherence transfer interval of a long-range heteronuclear correlation experiment. Substantial reduction in experimental time, good sensitivity and excellent resolution of signal overlap lead to the accurate determination of translational diffusion coefficients of individual components in the mixture.

Usually the diffusion separation in 2D DOSY spectra of complex mixtures is not enough to resolve the diffusion coefficients completely and 3D DOSY sequences are required. 3D I-DOSY sequences save time by incorporating the diffusion weighting internally. We have designed a new 3D I-DOSY sequence called COMPACT-IDOSY, which includes a diffusion encoding sequence within a sensitivity enhanced HMBC-type pulse sequence. The direct incorporation of diffusion encoding into the heteronuclear coherence transfer sequence gives a substantial time and sensitivity advantage over standard 3D DOSY methods. The scheme has been experimentally demonstrated on a rutin/quercetin mixture wherein the diffusion coefficients of the two molecular species are very similar and there is considerable signal overlap in both ^{1}H and ^{13}C chemical shifts. Since the HMBC coherence transfer interval is large enough to fit the diffusion encoding pulses even for larger molecules, this experiment could in principle be applied

to larger molecules as well, though the efficiency of the ASAP sequence in competition with spin diffusion processes in such systems would have to be worked out. It is hoped this experimental scheme will find application in a wider range of mixtures that would require accurate determination of diffusion coefficients in optimal experimental times.

CHAPTER 4

A New Multiple-Quantum Correlation Scheme to Separate Components of a Mixture

4.1 Background and Motivation

2D DOSY spectra often are unable to resolve spectral overlap leading to inaccurate determination of diffusion coefficients, hence a large number of three-dimensional DOSY variants have been developed, that offer the added advantage of peak separation in an additional dimension [72, 116, 117, 71, 70, 74, 118, 119, 120, 114, 121]. Multiple-quantum (MQ) NMR was initially viewed as a theoretical curiosity, but later developed into a robust technique for the analysis of complex spectra such as those of molecules oriented in liquid crystals [122, 123, 124, 125]. The transfer of coherence in multi-dimensional NMR experiments through multiple-quantum pathways has found diverse applications in NMR, including in selective excitation sequences [126], polarization transfer schemes [127], NMR quantum computing [128, 129], spectral editing sequences [130, 131, 132], and anisotropic diffusion [133, 134]. Previous work using 2D multiple-quantum correlation schemes focused on combining spin state selection and multiple quantum coherence excitation in order to accurately determine homonuclear couplings and to achieve spectral simplification of complex scalar coupled spectra [135, 136, 137, 138, 139]. Other work in this direction involved the use of maximum-quantum NMR to demix severely overlapping 2D spectra and to speciate mixtures of phenolic molecules [140, 141].

This chapter describes a novel multiple-quantum/single-quantum correlation scheme to resolve overlaps along the diffusion dimension in a mixture of small molecules with severely overlapped NMR signals. The pulse scheme is similar in intent to those of several 3D DOSY variants that append/prepend a diffusion sequence to a homonuclear 2D COSY or TOCSY scheme. A two-dimensional Fourier transform of the correlation experiment followed by an inverse Laplace transform along the third diffusion dimension,

results in a set of 2D correlation subspectra, with signals appearing at the diffusion coefficients of the individual components of the mixture. There are very few experiments that use multiple-quantum correlated spectroscopy to resolve signal overlaps in a 3D DOSY experiment [142]. The pulse sequence is demonstrated on two model mixtures namely, a mixture of fluorinated amino acids and a mixture of small organic molecules. The fluorine nuclear spin has a high gyromagnetic ratio (and hence good sensitivity) and a large chemical shift anisotropy (and hence a large spectral peak dispersion) and is becoming increasingly important in NMR studies of ligand-protein binding and drug discovery assays. Spectra of good resolution and sensitivity are obtained with this 3D MQ-DOSY (multiple quantum diffusion ordered spectroscopy) method, leading to an accurate determination of the diffusion coefficients of individual components of the mixtures. This 3D DOSY variant pulse scheme will be of value for a large range of applications ranging from binding studies using diffusion to separation of subspectra of complex molecular mixtures.

4.2 MQ NMR

MQ spectroscopy is a powerful tool in the simplification of spectral analysis as well as in providing new information on molecular spin dynamics. MQ NMR has a large number of applications, and it has been applied to heteronuclear as well as homonuclear coupled spin systems with *J* coupling, dipolar and quadrupolar interactions. MQ transitions have been observed in liquids, solids and liquid crystals. The definition of the coherence is based on the expansion of the time-dependant wave function $|\Psi(t)\rangle$ in terms of stationary basis function $|\Psi_i\rangle$.

$$|\Psi(t)\rangle = \sum_{i=1}^{N} C_i(t)\,|\Psi_i\rangle \tag{4.1}$$

Where $C_i(t)$ are the time dependant coefficients and N is the dimension of the Hilbert space. A coherence between states Ψ_r and Ψ_s exists when the ensemble average of the

product of coefficients

$$\rho_{rs}(t) = \overline{C_r(t)C_s^*(t)} \tag{4.2}$$

does not vanish. The element $\rho_{rs}(t)$ are tabulated in the form of a hermitian N $\times$ N matrix which is known as density matrix. In high field NMR the Zeeman interaction causes the splitting of the energy levels according to the field direction and the difference between magnetic quantum numbers [143, 144].

$$\Delta m_{rs} = m_r - m_s = \pm 1 \tag{4.3}$$

In weakly coupled spin 1/2 systems, a density matrix element is essentially the same as a classical transverse magnetization vector m_{rs},

$$m_{xrs}(t) = Re\{\rho_{rs}(t)\} \tag{4.4}$$

$$m_{yrs}(t) = -Im\{\rho_{rs}(t)\} \tag{4.5}$$

MQ coherences are related to the off-diagonal elements of the density matrix ρ (the n quantum coherences) [143, 144]. A MQ coherence describes the transition between two eigenstates where the well known selection rule $\Delta m = \pm 1$ is violated. MQ transitions occur when states in nonadjacent Zeeman manifolds are placed in coherent superposition. The various transitions are shown in Figure 4.1 which shows in schematic form the energy level diagram of a system of N coupled spin 1/2 nuclei . An "allowed" SQ transition is one in which the quantum number changes by ± 1. A MQ transition has no such restriction, it can be N quantum or even zero quantum. In single quantum spectroscopy only one spin flips while in an N quantum transition multiple spins flip. This multiple flip involves a simultaneous absorption or emission of n photons. When extending this consideration from the two spin system to a multiple spin system when $\Delta m_{rs} \neq \pm 1$, "forbidden" coherences appear [145]. In liquids it is caused by indirect spin spin coupling and in solids by direct dipolar coupling. The MQ NMR by creating high order multiple quantum coherences can simplify the spectra. To characterize the

coherence we can use the raising and lowering operator $\hat{I}^+$ and $\hat{I}^-$, respectively.

$$\hat{I}^+ = \hat{I}_x + i\hat{I}_y \tag{4.6}$$

$$\hat{I}^- = \hat{I}_x - i\hat{I}_y \tag{4.7}$$

Application of these operators to the spin functions yields the spin function of the next higher or next lower magnetic quantum number n,

$$\hat{I}^+\beta = [\hat{I}_x + i\hat{I}_y]\beta = \frac{1}{2}\alpha - i^2\frac{1}{2}\alpha = \alpha \tag{4.8}$$

A double quantum coherence where two nuclei change their spin orientation at the same time is characterized by the product $\hat{I}^+\ \hat{I}^+$ or $\hat{I}^-\ \hat{I}^-$, and the product of the form $\hat{I}^+\ \hat{I}^-$ or $\hat{I}^-\ \hat{I}^+$ describes zero quantum coherences. A mixing period is required to convert the MQ coherences into single quantum coherences.

4.3 2D MQ/SQ Correlation NMR

In NMR spectroscopy one observes only transitions for which the change in the absolute value of the magnetic quantum number is one. Such transitions are referred to as single quantum transitions. Coherence between the states $|\alpha\alpha\rangle$ and $|\beta\beta\rangle$ shown in Figure 4.3 are called double quantum (DQ) coherence, and between the states $|\alpha\beta\rangle$ and $|\beta\alpha\rangle$ called ZQ coherence. Such transitions are "forbidden" and cannot be detected directly. The MQ experiment typically employs a method of indirect detection using two-dimensional spectroscopy and then records their response to either naturally occurring or externally manipulated local fields. To study the time evolution of the multiple quantum (MQ) coherence the two dimensional experiment experiment has been constructed where time t_1 is increased step by step. A multiple quantum experiment can be separated into four periods: preparation, evolution, mixing and detection (Figure 4.2). During the preparation period of length τ the system is brought into an initial state by the action of a propagator $U(\tau)$ upon the density matrix $\rho(0)$. During the evolution pe-

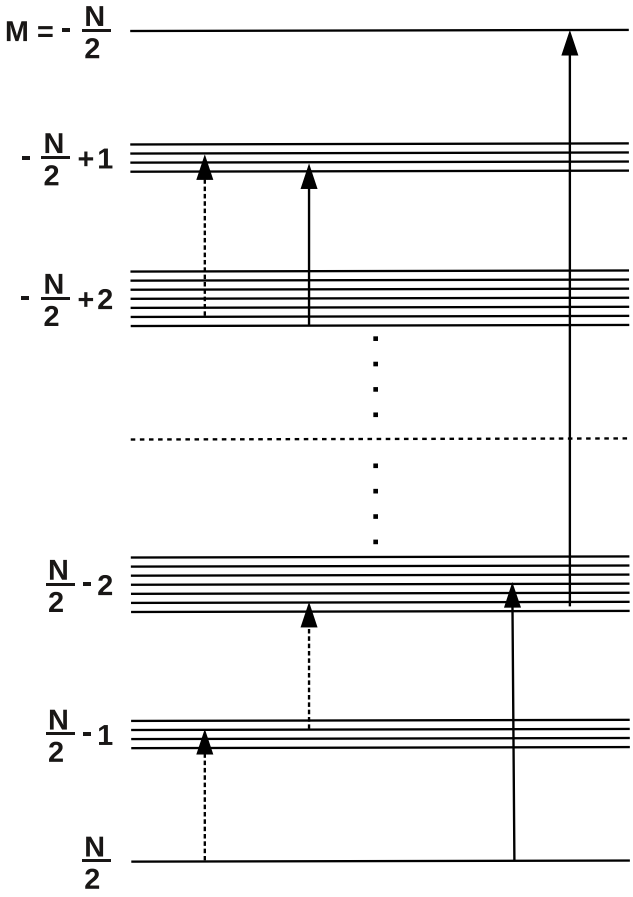

Figure 4.1: The energy level diagram of a system of N coupled spin 1/2 nuclei. The solid arrows indicate “forbidden” MQ transitions, the dashed arrows are “allowed” single-quantum transitions. The $\Delta m = -1$ solid arrow indicates a transition forbidden by symmetry.

riod of length t_1, the coherent states evolve under the influence of the time independent Hamiltonian H_1.

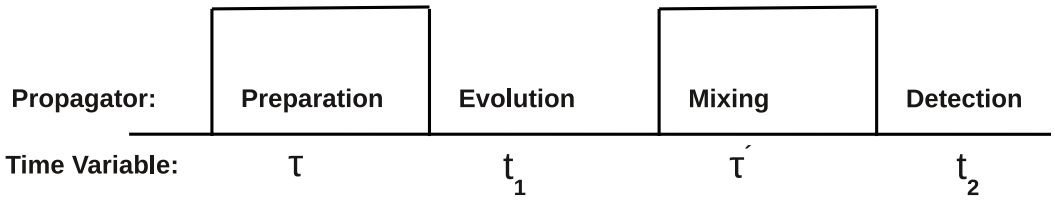

Figure 4.2: A block diagram of two dimensional NMR experiment divided into four periods, indicating the separation of time domains.

During the mixing period of length τ', transfer of coherence between states of the system are affected by the operator V(τ'). During the detection period of length t_2, coherent states of the system are detected as they evolve under the influence of the time independent Hamiltonian H_2.

For a system of two spin-1/2 nuclei, the double-quantum coherence (DQ), and zero-quantum coherence (ZQ) are represented by product operators in which both spins have transverse components. For example, the operator $2\hat{I}_x\hat{S}_y$ can be expressed as:

$$2\hat{I}_x\hat{S}_y = 2\ \tfrac{1}{2}\left(\hat{I}^+ + \hat{I}^-\right)\ \tfrac{1}{2i}\left(\hat{S}^+ - \hat{S}^-\right)$$

$$= \frac{1}{2i}\left(\hat{I}^+\hat{S}^+ - \hat{I}^-\hat{S}^-\right) \ + \ \frac{1}{2i}\left(-\hat{I}^+\hat{S}^- + \hat{I}^-\hat{S}^+\right) \tag{4.9}$$

The first term in the second line of the above equation $\left(\hat{I}^+\hat{S}^+ - \hat{I}^-\hat{S}^-\right)$, represents a DQ coherence $(\Delta m = 2)$ and the second term $\left(-\hat{I}^+\hat{S}^- + \hat{I}^-\hat{S}^+\right)$ is a ZQ coherence $(\Delta m = 0)$. MQ coherences can be prepared by suitable combinations of pulses and free-precession periods. In the product operator formalism, DQ coherence and ZQ coherence can be obtained by suitable combinations of two-spin product operators.

$$\frac{1}{2}\left(\hat{I}^+\hat{S}^+ + \hat{I}^-\hat{S}^-\right) = \frac{1}{2}\left(2\hat{I}_x\hat{S}_x - 2\hat{I}_y\hat{S}_y\right) = DQ_x \tag{4.10}$$

$$\frac{1}{2i}\left(\hat{I}^+\hat{S}^+ - \hat{I}^-\hat{S}^-\right) = \frac{1}{2}\left(2\hat{I}_x\hat{S}_y + 2\hat{I}_y\hat{S}_x\right) = DQ_y \tag{4.11}$$

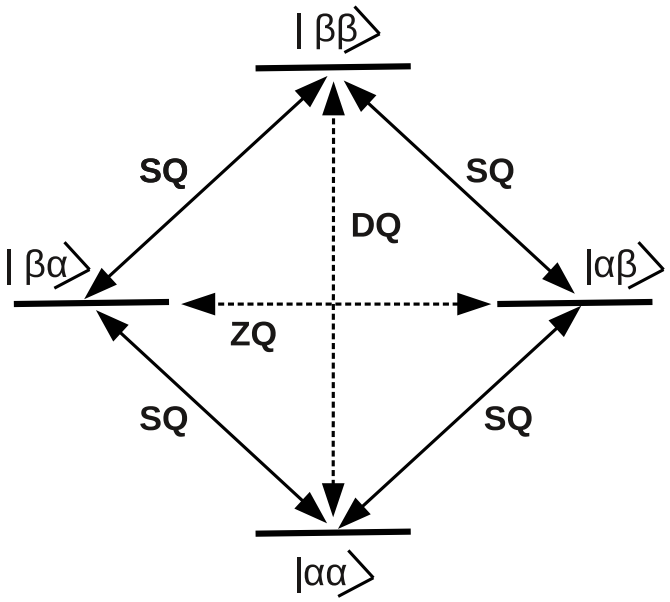

Figure 4.3: The energy levels of a two spin system with equivalent spins of Zeeman energy levels for the states $|\alpha\alpha\rangle$,$|\beta\beta\rangle$, $|\beta\alpha\rangle$,$|\alpha\beta\rangle$. The allowed single quantum (SQ) transitions and "forbidden" zero quantum (ZQ) and double quantum(DQ) transitions are indicated.

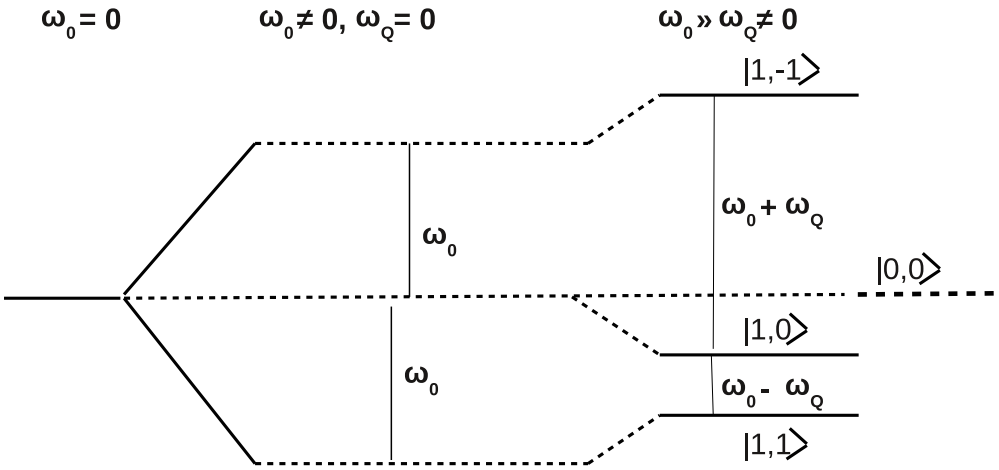

Figure 4.4: Energy level diagram of the spin pair including the effect of the dipolar coupling. The two single quantum transitions ω_{12} and ω_{23} of the three level spin system are separated by $2\omega_Q$ which depends on the dipolar coupling strength. The eigenstates of the Hamiltonian are superpositions of the states $|\alpha\alpha\rangle$,$|\beta\beta\rangle$, $|\beta\alpha\rangle$,$|\alpha\beta\rangle$, called symmetric (triplet) and antisymmetric (singlet) states. The energy levels of the triplet states $|1,1\rangle = |\alpha\alpha\rangle$,$|1,-1\rangle = |\beta\beta\rangle$ and $|1,0\rangle = \frac{1}{\sqrt{2}}(|\alpha\beta\rangle + |\beta\alpha\rangle)$ are shifted compared to the Zeeman levels.

$$\frac{1}{2}\left(\hat{I}^{+}\hat{S}^{-}+\hat{I}^{-}\hat{S}^{+}\right)=\frac{1}{2}\left(2\hat{I}_x\hat{S}_x+2\hat{I}_y\hat{S}_y\right)=ZQ_x \tag{4.12}$$

$$\frac{1}{2i}\left(\hat{I}^{+}\hat{S}^{-}-\hat{I}^{-}\hat{S}^{+}\right)=\frac{1}{2}\left(2\hat{I}_y\hat{S}_x-2\hat{I}_x\hat{S}_y\right)=ZQ_Y \tag{4.13}$$

Pure DQ coherence precesses at the sum of the chemical shifts of the two spins during a delay *t*, and a pure ZQ coherence precesses at the difference of the chemical shift. Two-spin multiple quantum coherence does not evolve under the influence of the scalar coupling of the two spins involved in the coherence (Figure 4.4).

4.4 Experimental Section

Materials & Methods: All the samples were obtained from Sigma Aldrich and used without further purification. The mixture of fluorinated amino acids, henceforth denoted Mixture 1, was prepared by dissolving 12 mg of 3-fluoro-DL-valine, 8 mg of 4-fluoro-L-phenylalanine and 6 mg of 5-fluoro-L-tryptophan in 400 μl of D_2O, at a concentration of 0.23 M. The mixture of small molecules, henceforth denoted Mixture 2, was prepared by dissolving 10 mg of glucose, 20 μl of 1-propanol and 15 μl of 3-methyl-1-butanol in 400 μl of D_2O, at a concentration of 0.23 M. The structure of all the small molecules used in this study is given in Figure 4.5.

2D ^{1}H and ^{19}F DOSY: 2D DOSY experiments were performed using the BPPSTE sequence [28, 43, 30]. The duration of the total diffusion encoding sine-shaped gradient pulse δ was 2 ms. The gradient recovery delay after each gradient pulse was set to 200 μs. The maximum gradient strength is 53.5 G/cm. The gradient strength was incremented in 16 steps between 2% and 95% of the maximum value, with each step corresponding to a separate experiment. The diffusion interval Δ was set at 100 ms. A relaxation delay of 1 s was used between successive experiments. Lorentz-Gauss resolution enhancement with exponential time constants of 0.3 s and 0.1 s respectively, was used in the initial Fourier transformation. The data were fitted to extract the diffusion coefficients, using the procedure described in Chapter 1.

3D MQ-DOSY pulse sequence: The pulse sequence for the 3D MQ-DOSY experiment

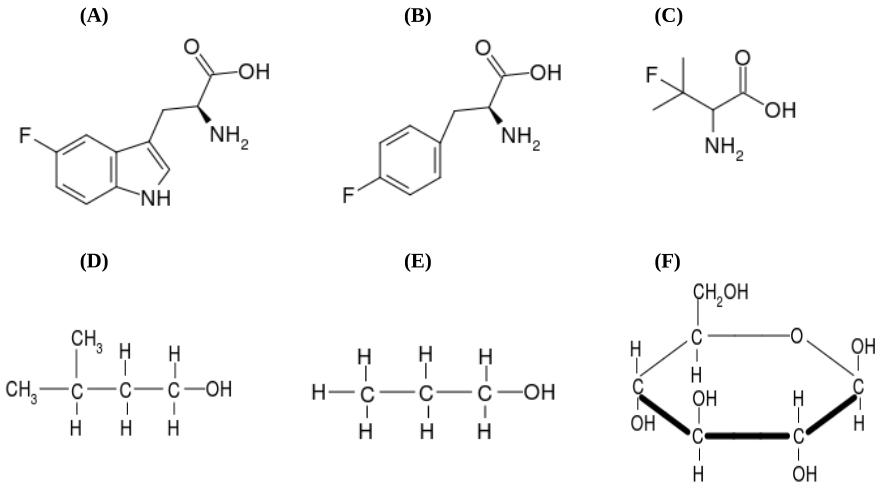

Figure 4.5: Structures of individual molecules. Mixture 1 consists of ^{19}F-labeled amino acids with a single fluorine substituent either on an aromatic ring as in (A) 5-fluoro-L-tryptophan, (B) 4-fluoro-L-phenylalanine or with an aliphatic fluorine substituent as in (C) 3-fluoro- DL-valine. Mixture 2 consists of the small molecules (D) 3-methyl-1-butanol, (E) 1-propanol and (F) glucose.

is given in Figure 4.6. The scheme begins with a bipolar stimulated echo sequence for diffusion with a pair of diffusion encoding/decoding gradients, homospoil gradients and a delay for eddy currents dissipation. A MQ/SQ correlation scheme is appended to the diffusion sequence. If molecular diffusion has occurred, the signal is accordingly attenuated after the stimulated-echo sequence. This SQ magnetization then evolves into various MQ under the standard $90^\circ - \tau - 180^\circ - \tau - 90^\circ - t_1 - 90^\circ - t_2$ multiple-quantum excitation sequence. The interval $\tau = 1/4J_{HH}$ is set according to the homonuclear J couplings present. After the t_1 evolution period, the final 90° detection pulse is sandwiched between two gradients G_1 and G_2 for selection of the MQ of the desired order. The ratio of the gradients is set to $G_2 = nG_1$ where n is the order of the coherence. For phase sensitive detection the phase of the second proton pulse is incremented according to the States-TPPI method.

4.5 Results and Discussion

Spectral patterns in MQ/SQ correlations: The correlation peaks pattern in the 2D NMR spectrum becomes progressively simpler as the order of the MQ coherence in-

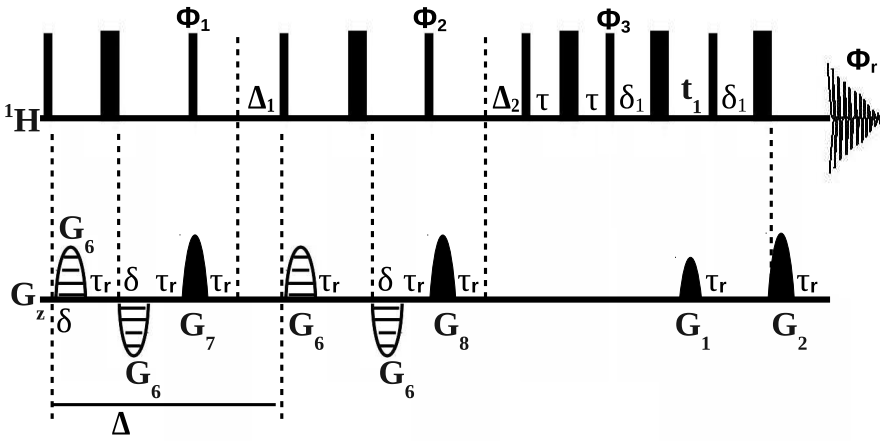

Figure 4.6: Pulse sequence for 3D MQ-DOSY multiple-quantum correlated diffusion ordered experiment. Narrow and wide pulses correspond to pulse flip angles of $90°$ and $180°$, respectively. Phase cycling is $\phi_1 = x, -x; \phi_2 = 4(x), 4(-x); \phi_3 = x, x, -x, -x; \phi_r = 2(x, -x), 2(-x, x)$. Phases if not indicated otherwise are all applied along the x axis. The delay Δ is for the diffusion interval while δ is the length of the gradient and G_6 is the strength of the diffusion encoding gradient and τ_r denotes gradient recovery times. The delay τ is optimized for the uniform excitation of homonuclear MQ of the desired coherence order and the gradient ratio is correspondingly set to $G_2 = NG_1$ for excitation of the Nth quantum. G_7 and G_8 are homospoil gradients set to 17.13% and 13.17% (of the maximum strength), respectively. Δ_1 and Δ_2 are delays introduced so that the total time including rf and gradient lengths and delays, adds up to the diffusion time Δ and δ_1 is a small delay equal to the length of G_1 plus τ_r.

creases. However, there is a concomitant decrease in the efficiency of the MQ excitation, since the efficiency depends on the strengths of the scalar couplings in the specific systems under consideration. The delay τ in the middle of the MQ excitation interval has to be optimized to obtain maximum signal intensity. In principle the amplitude of a DQ coherence in a weakly scalar coupled two-spin system is proportional to $\sin(\pi J\tau)$ and the maximum amplitude should emerge at $\tau = 1/2J$. In reality since molecules contain a range of spin coupling networks of varied strengths the MQ excitation efficiency has to be empirically optimized for each specific system. This is done by varying the τ delay in a series of steps (keeping the t_1 evolution period fixed to 3 μs, in a 1D version) and retaining that value for which the antiphase magnetization obtained is a maximum. The J_{HH} was varied in the range 3-16 Hz for all the molecules. The 2D MQ/SQ data set consisted of 1024 $\times$ 128 data points with spectral widths of 5.99 ppm and 16 ppm in the direct and indirect dimensions, respectively. The number of scans was 32 for each t_1 increment with a relaxation delay of 2 s between scans. The time domain data was zero-filled to 2048 and 1024 in the SQ and MQ dimensions, respectively.

The number of transitions for the nth order spectrum in a system of m coupled spins is given by [126, 135]

$$2m!/(m-n)!(m+n)!... \tag{4.14}$$

For a DQ coherence ($\Delta n = \pm 2$) two of the spins flip simultaneously from the $|\alpha\rangle$ to the $|\beta\rangle$ state and vice versa, while for the highest quantum ($m = n$) there is a single transition. The three protons (two of which are equivalent) of the fluorinated amino acid 5-fluoro-L-tryptophan form the MM'X part of a 4 spin AMM'X spin system (with the fluorine spin being labeled A, leading to six lines i.e a doublet of a triplet for the fluorine multiplet in Figure 4.7). The resulting *J* couplings are measured to be J_{AM}= 9.6 Hz, J_{MX}= 5.4 Hz, J_{AX}= 3.1 Hz. The four protons (with two equivalent pairs) of the fluorinated amino acid 4-fluoro-L-phenylalanine form the MM'XX' part of a 5 spin AMM'XX' spin system (with the fluorine spin being labeled A, leading to nine lines i.e a triplet of a triplet for the fluorine multiplet in Figure 4.7, seven of which are resolved in the 1D spectrum). The resulting *J* couplings are measured to be J_{AM}= 5.3 Hz, J_{MX}= 9.3 Hz, J_{AX}= 14 Hz, $J_{M'X}$= 7.2 Hz. The eight protons (with two equivalent

methyl groups) of the fluorinated amino acid 3-fluoro-DL-valine form the A_3B_3MM' part of a nine spin $A_3B_3MM'X$ spin system (with the fluorine spin being labeled X). The resulting J couplings are measured to be J_{AB}= 10 Hz, J_{AM}= 7.2 Hz, J_{AX}= 12.1 Hz, J_{MX}=6.2 Hz, $J_{M'X}$=4.2 Hz. In a DQ/SQ correlation experiment on the fluorinated aminoacid systems, there are several types of homonuclear proton DQ coherences such as MX, M'X, MX' etc., resulting from the antiphase magnetization immediately after the second 90° pulse. In the indirect DQ dimension the magnetization evolves at the sum of the chemical shifts of the active spins and under the effect of the total sum of all the passive couplings. The rationale for analysis of MQ/SQ correlations for the small molecules in Mixture 2 (glucose, pentanol and butanol) is similar to that already discussed for the fluorinated amino acids.

1D Proton & Fluorine Spectra: The 1D ^{1}H and ^{19}F spectra of the mixture of amino acids 3-fluoro-DL-valine, 4-fluoro-L-phenylalanine and 5-fluoro-L-tryptophan (Mixture 1), and the 1D ^{1}H spectra of the mixture of glucose, 1-propanol and 3-methyl-1-butanol (Mixture 2) are shown in Figures 4.7 (A), (B) and (C), respectively. The proton spectra of the mixtures show considerable overlap in the resonances, while the fluorine chemical shifts are well resolved. It has been previously noted that since 19F has a large chemical shift anisotropy, fluorinated small molecules are good model systems with well-resolved peaks and good signal-to-noise ratios [146, 147].

2D DOSY Analysis: Diffusion-encoded experiments in this work used the LEDBPGP type of pulse sequences since the longitudinal encoding-decoding (LED) approach leads to minimal loss of magnetization. It has been shown that using sinusoidal shaped gradients in PFG-NMR experiments leads to reduced eddy current effects as compared to rectangular gradients. The 2D ^{1}H and ^{19}F DOSY of Mixture 1 and the 2D ^{1}H DOSY spectrum of Mixture 2 are shown in Figures 4.8 (A), (B), and (C), respectively. The solvent signals in the proton DOSY spectra are clearly separated along the diffusion dimension. However, there is considerable overlap amongst the proton DOSY spectra of both mixtures. While the fluorine chemical shifts are well resolved along the chemical shift dimension in Figure 4.8(B), the peaks are completely overlapped along the DOSY dimension. The analysis of the standard 2D DOSY spectra leads to the conclusion that a 3D DOSY type of experiment is required in order to achieve separation along

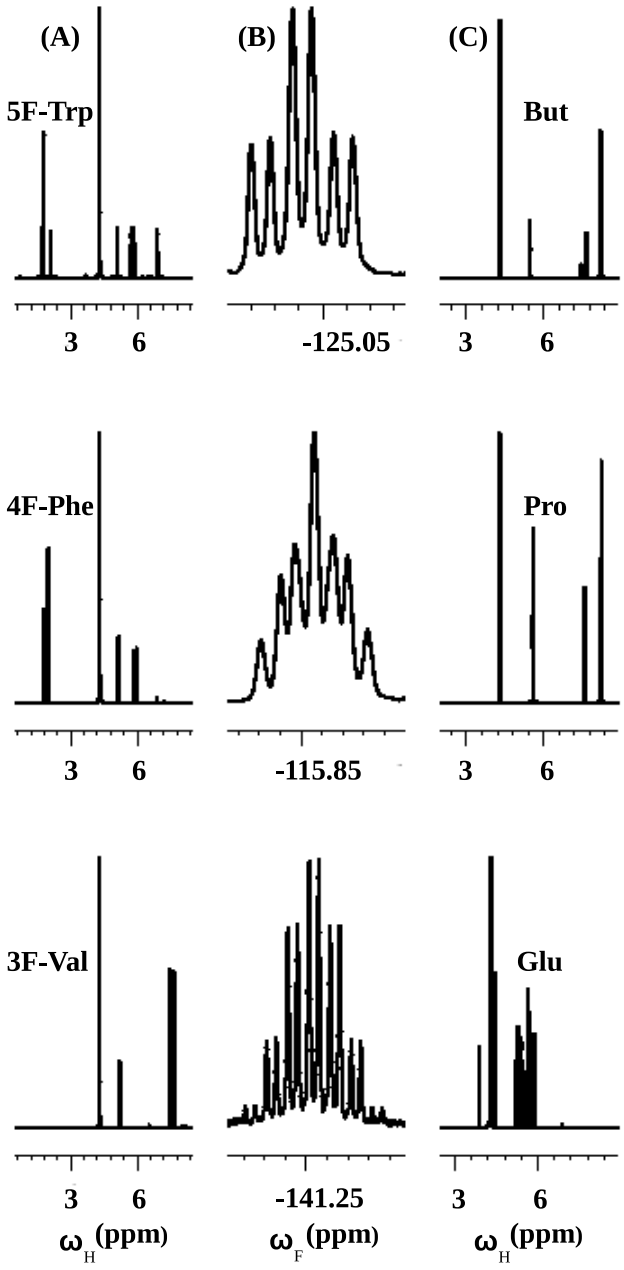

Figure 4.7: 600 MHz 1D (A) ^{1}H spectra of Mixture 1 and the individual fluorinated amino acid components, (B) ^{19}F spectra of Mixture 1 and its individual fluorinated amino acid components, and (C) ^{1}H spectra of Mixture 2 and its individual small molecule components. 16 scans were collected for the proton and the fluorine spectra, with 8192 complex points for each scan. Spectra were apodized with a 0.3 Hz exponential line-broadening function, baseline corrected and zero-filled. The vertical scaling factor was adjusted to keep the noise level the same in all spectra.

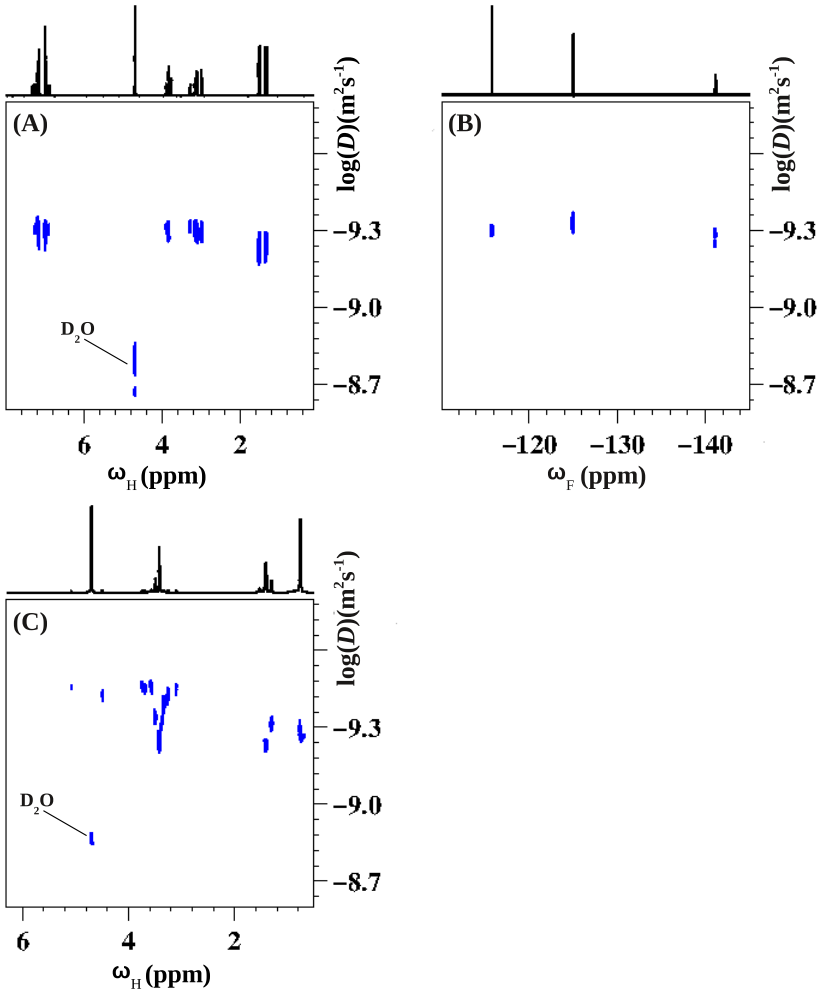

Figure 4.8: 600 MHz spectra of (A) 2D ^{1}H DOSY of Mixture 1 (B) 2D ^{19}F DOSY of Mixture 1 and (C) 2D ^{1}H DOSY of Mixture 2 measured using the bipolar pulse pair stimulated echo sequence. 16 transients were acquired for each of 16 values of the pulsed field gradient strength, incremented in equal steps from 2.68 to 50.83 Gcm^{-1}. The D_2O solvent signals are marked in the proton DOSY spectra in (A) and (C). Proton and fluorine chemical shifts (in ppm) are indicated along the x axis and diffusion units ($\log\left(D/\mathrm{m^2s^{-1}}\right)$) on the y axis.

the diffusion dimension and to obtain accurate estimates of the diffusion coefficients of individual components of the mixtures.

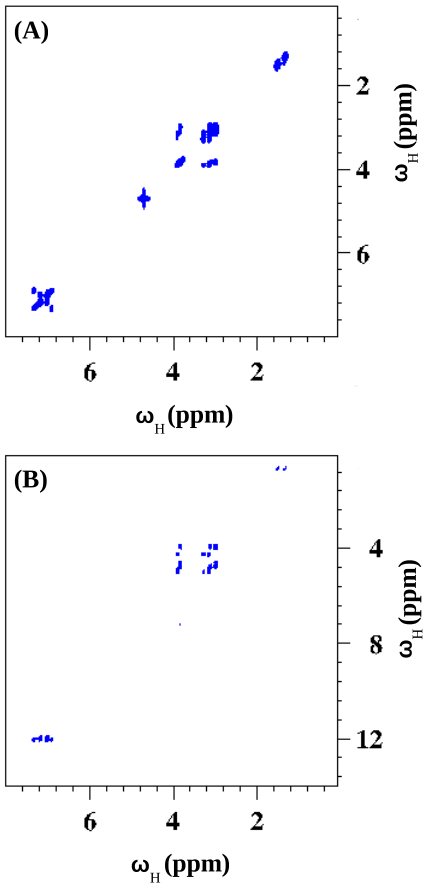

Figure 4.9: (A) 600 MHz 2D SQ-SQ correlation (ordinary COSY) spectrum of Mixture 1. The size of the data matrix is 2048 $\times$ 1024 and the number of t_1 increments is 128. (B) 600 MHz 2D SQ-DQ spectrum of Mixture 1, correlating DQ and SQ coherences along the F_1 and F_2 dimensions, respectively.

2D MQ Experiments: The 2D MQ/SQ correlation spectra of Mixtures 1 and 2 are shown in Figures 4.9 and 4.10, respectively. The spectra in Figures 4.9(A) and 4.10(A) show the SQ/SQ correlation (the normal COSY experiment). The optimization of the τ interval for MQ excitation is performed on a 1D version of the pulse sequence to obtain the best intensity and uniform excitation of the desired MQ coherence on each mixture. The final pair of sine-shaped gradients sandwiching the 90° detection pulse are used to select the desired MQ order, while dephasing all other unwanted coherences. The spectra in Figures 4.9(B) and 4.10(B) show the SQ/DQ correlations of Mixtures 1

and 2, respectively. The gradient ratio in Figures 4.9(B) and 4.10(B) has been set to 1:2 to select the DQ. The spectra in Figures 4.9(B) and 4.10(B) show simplified spectral patterns and have almost as good a sensitivity as compared to the standard COSY spectra. While we did perform the experiments to select higher order ($n > 2$) MQ/SQ correlations (spectra not shown), the intensity of the peaks decreased dramatically with increasing MQ order, and were hence of limited utility for the 3D MQ-DOSY scheme. The DQ correlation spectra on the other hand, were an optimal compromise, leading to reduction in number of peaks and hence spectral complexity as compared to the standard COSY whilst at the same time retaining adequate signal-to-noise.

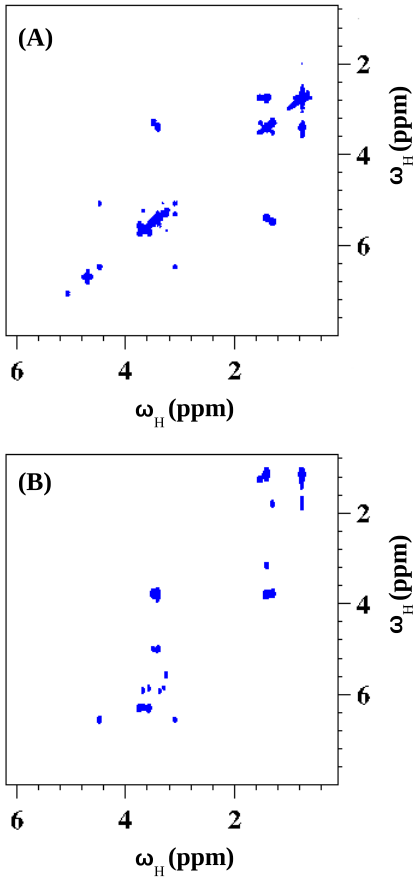

Figure 4.10: (A) 600 MHz 2D SQ-SQ correlation (ordinary COSY) spectrum of Mixture 2. The size of the data matrix is 2048 $\times$ 1024 and the number of t_1 increments is 128. (B) 600 MHz 2D SQ-DQ spectrum of Mixture 2, correlating DQ and SQ coherences along the F_1 and F_2 dimensions, respectively.

3D MQ-DOSY Experiments: Figures 4.11 and 4.12 show the 2D DQ subspectra ex-

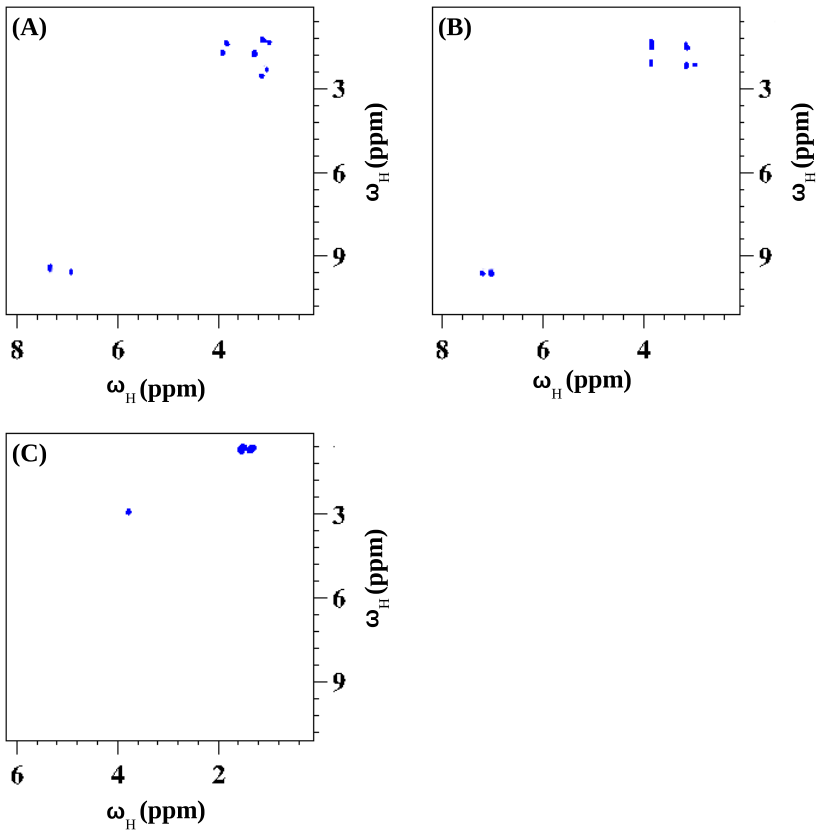

Figure 4.11: SQ-DQ planes extracted from the 3D MQ-DOSY experiment for each molecule in Mixture 1. 2D SQ-DQ subspectra of (A) 5-fluoro-L-tryptophan, (B) 4-fluoro-L-phenylalanine and (C) 3-fluoro-DL-valine extracted from the respective 3D experiments for diffusion coefficient ranges of 1.6 - 2.0 $\times 10^{-10}$ m^2/s, 5.2 - 5.8 $\times 10^{-10}$ m^2/s, and 6.0 - 6.6 $\times 10^{-10}$ m^2/s, respectively.

Table 4.1: Table of diffusion coefficients $D(\times 10^{-10}$ m^{2}s$^{-1})$ of individual components of Mixture 1 and Mixture 2 extracted from the 2D subspectra of the 3D MQ-DOSY experiment on each mixture and compared to the diffusion coefficients measured from the 2D ^{1}H DOSY and the 2D ^{19}F DOSY experiment on each individual component. Uncertainties in D values reflect the standard errors in the fits.

Molecule	D(^{1}H DOSY)	D(^{19}F DOSY)	D(3D MQ-DOSY)
5F-Tryptophan	1.86 ± 0.03	1.93 ± 0.03	1.8 ± 0.04
4F-Phenylalanine	5.42 ± 0.03	5.75 ± 0.04	5.5 ± 0.01
3F-Valine	6.08 ± 0.07	6.47 ± 0.02	6.3 ± 0.02
Glucose	3.47 ± 0.09	—-	3.25 ± 0.04
Propanol	8.51 ± 0.04	—-	8.5 ± 0.07
Butanol	7.24 ± 0.08	—-	7.3 ± 0.09

tracted from the 3D MQ-DOSY experiments on Mixtures 1 and 2, respectively. 2D projections of 3D DOSY spectra are reconstructed by integrating the 2D lineshapes between defined limits in the diffusion domain, with peak regions larger than those used for volume integration. To get clean diffusional separation, 16 transients for each of 8 gradient levels were acquired with a total experiment time of 5h 39min. A diffusion coefficient is computed by varying the gradient strengths in a series of experiments, merged into a single 3D experiment and each DQ/SQ correlation thus becomes diffusion tagged. The resolution of the 3D MQ-DOSY experiment is clearly able to separate the individual diffusing components. Each subspectrum in Figures 4.11 and 4.12 contains signals only from the particular mixture component. he diffusion coefficients computed from the 3D subspectra in Figure 4.11 turn out to be 1.8 $\times 10^{-10}$ m^2/s, 5.5 $\times 10^{-10}$ m^2/s, and 6.3 $\times 10^{-10}$ m^2/s for 5-fluoro-L-tryptophan, 4-fluoro-L-phenylalanine and 3-fluoro-DL-valine, respectively. The diffusion coefficients computed from the 3D subspectra in Figure 4.12 turn out to be 3.25 $\times 10^{-10}$ m^2/s, 8.5 $\times 10^{-10}$ m^2/s, and 7.3 $\times 10^{-10}$ m^2/s, for glucose, 1-propanol and 3-methyl-1-butanol, respectively. The mean diffusion coefficients obtained from the analysis of the subspectra in the 3D MQ-DOSY experiments on Mixture 1 and Mixture 2 are given in Table 4.1. The diffusion coefficients of the individual components of both mixtures extracted from the 2D ^{1}H DOSY (and 2D ^{19}F DOSY for the fluorinated aminoacids) experiments are also shown for comparison. The

3D diffusion ordered experiments on the mixtures and the 2D diffusion ordered experiments on the individual components show comparable diffusion coefficients, implying that the 3D MQ-DOSY experiment is a viable scheme for separating signals from different components in a mixture along a diffusion dimension. While 3D COSY-DOSY

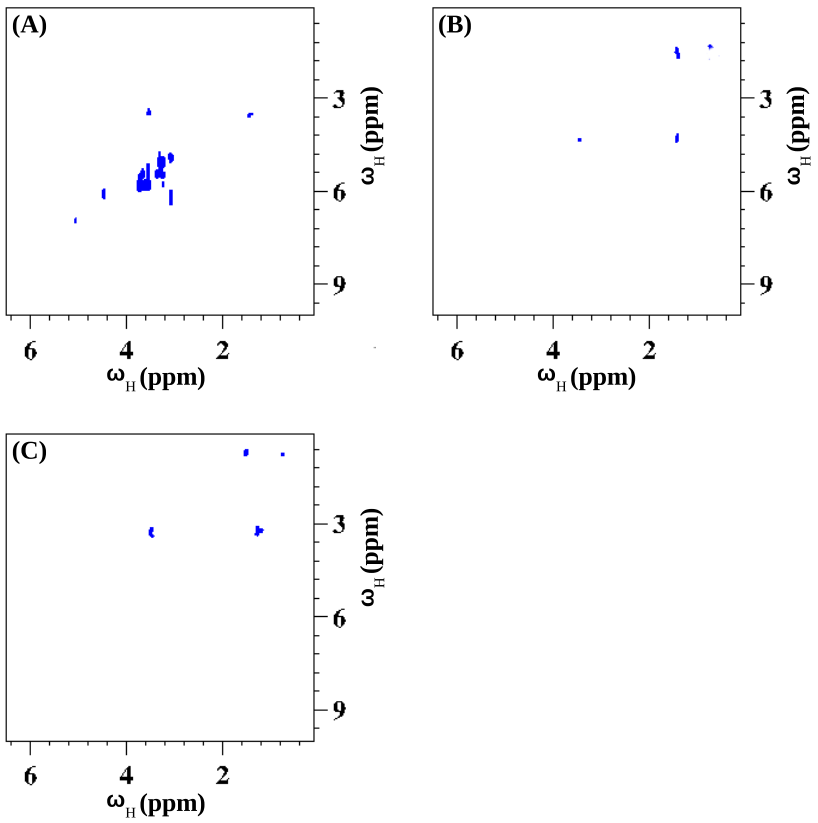

Figure 4.12: SQ-DQ planes extracted from the 3D MQ-DOSY experiment for each molecule in Mixture 2. 2D SQ-DQ subspectra of (A) glucose, (B) 1-propanol and (C) 3-methyl-1-butanol extracted from the respective 3D experiments for diffusion coefficient ranges of 3.0 - 3.5 $\times 10^{-10}$ m^2/s, 8.2 - 8.8 $\times 10^{-10}$ m^2/s, and 7.0 - 7.6 $\times 10^{-10}$ m^2/s, respectively.

experimental schemes have the advantage of high sensitivity, the spectra for complex mixtures of small molecules suffer from strong singlet peaks along the diagonal leading to poor resolution and hence ambiguities in fitting of the diffusion coefficients to the data. The MQ-DOSY methods described here retain the sensitivity advantage of homonuclear proton 3D DOSY experiments while at the same time have fewer peaks than SQ correlation spectra (standard DOSY-COSY). This leads to less spectral crowding and hence more robust monoexponential fits to the Stejskal-Tanner equation and hence more accurate estimates of the diffusion coefficient.

4.6 Conclusions

A versatile three-dimensional diffusion-edited NMR experiment is described in this chapter, that concatenates a multiple-quantum/single-quantum correlation scheme with a diffusion-ordered pulse sequence. The experiment is demonstrated on mixtures of small molecules with similar diffusion coefficients and is able to resolve severely overlapped signals along the third dimension. The subspectra of individual components of the mixtures are well separated and their diffusion coefficients can hence be extracted with a greater degree of accuracy as compared to the standard 2D DOSY (diffusion ordered spectroscopy) experiments.

Diffusion NMR experiments can help separate individual components of a mixture along a diffusion ordered dimension. This work describes the incorporation of a novel multiple-quantum/single-quantum correlation scheme into a diffusion ordered pulse sequence. The resulting 3D scheme achieves good resolution of severely overlapped multiplets and leads to the accurate estimation of diffusion coefficients. The efficacy of the experiment has been demonstrated on mixtures of small molecules. This 3D MQ-DOSY sequence has potential applications in spectral simplification of biomacromolecular complexes and multi-component mixtures.

CHAPTER 5

Using ^{19}F NMR to Resolve Diffusion Coefficients of Fluorinated Drugs in a Micellar Matrix

5.1 Background and Motivation

NMR PFG-based pulse sequences are widely used to study the diffusion characteristics and hence the molecular mobility of different systems [148]. ^{19}F NMR is a tool used for the quantitative analysis of various fluorinated molecules, given the fact that the ^{19}F spin-1/2 nucleus has high sensitivity and a large chemical shift range which minimizes signal overlap. Incorporation of a fluorine substituent in drug molecules favorably impacts the metabolic stability and binding affinity of the molecule and is hence an important part of the drug discovery process. Fluorine NMR has been used for the structure and configuration of fluorinated steroids, to perform NMR based binding assays, to characterize chain ends and branching structures in fluoropolymers, to estimate the fluorine chemical shift anisotropy tensor and use it for structural characterization, and to quantify fluorinated drug metabolites in biofluids [153, 154]. Performing a diffusion measurement of a drug molecule (ligand) in the presence of protein gives information about how the drug binds to the protein. Fluoroquinolones enters the bacterial cells and accumulate within and the diffusion process modulates this cellular accumulation. The lipid bilayer is a major component involved in the inner membrane of gram-negative bacteria and membrane of gram-positive organism. The important feature of membrane lipids is their amphipathic character indicated by the polar or hydrophilic head group and the non-polar or hydrophobic group.

This chapter focuses on the diffusion properties of prulifloxacin and pazufloxacin which are fluoroquinolone antibiotics that exhibit strong activity against both gram-positive and gram-negative bacteria. Fluoroquinolones play an important role in the treatment of serious bacterial infections, particularly community-acquired infections.

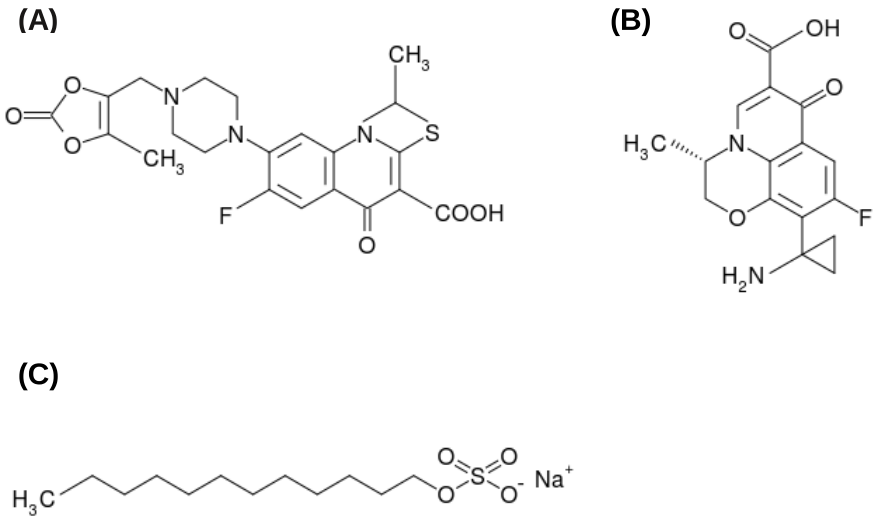

Figure 5.1: Chemical structures of (A) Prulifloxacin (B) Pazufloxacin (C) SDS micelles.

Fluoroquinolones generally show concentration dependent bacteria killing activity that depends on the ratio of maximum drug concentrations to minimum inhibitory concentration. The structures of these two fluoroquinolones and the sodium dodecyl sulfate (SDS) micelle are shown in Figure 5.1. Both prulifloxacin, 6-fluoro-1-methyl-7-[4-(5-methyl-2-oxo-1,3-dioxolen-4-yl) methyl-1-piperazinyl]-4-oxo-4H-[1,3] thiaceto [3, 2-a] quinoline-3-carboxylic acid and pazufloxacin, 10-(1-aminocyclopropyl)-9-fluoro-3-methyl-7-oxo-1H,7H-[1,3] oxazino [5,4.3] quinoline-carboxylic acid are widely used in the treatment of various bacterial infections. The mechanism of action of many fluoroquinolone drugs is not yet fully understood, and hence understanding the stereochemistry of fluoroquinolone drugs is essential to understand their interaction with DNA and gyrase enzymes. Previous studies have focused on the drug loading and diffusion properties of R_f-hydrogels for small anticancer drugs has been probed using molecular and ^{19}F spin diffusion NMR. ^{1}H NMR was used to determine polymer degradation, drug release mechanisms and drug-polymer hydrogen bonding interactions and it was found that the mechanism of drug release is controlled by solvent removal and polymer degradation. Complex mixtures of fluorinated molecules and fluorinated chemical fragments are increasingly being used in biochemical and binding assays for drug discovery. It is hence important to determine the fluorine chemical shifts and the diffusion coefficients of the individual binder molecules in the chemical mixture formed either by adding to-

gether single compounds or by chemical synthesis. This chapter also focuses on the utility of the ^{1}H-^{13}C 3D COMPACT-IDOSY experiment (described in Chapter 3) to accurately quantify the diffusion coefficient of each component drug in the drug mixture. We have also used 1D ^{31}P and ^{19}F diffusion experiments to study the drug loading and diffusion properties of both pazufloxacin and prulifloxacin in DPPC lipid bilayers.

5.2 Micelle Assisted DOSY

If the components of a mixture are of similar molecular weights (i.e. very close self-diffusion coefficients), the standard 2D DOSY method will fail to resolve them along the diffusion dimension. A new set of methods called matrix-assisted DOSY have been designed to circumvent this problem. The method relies on the differential chemical interactions of the molecules with a slow diffusion matrix, such as SDS micelles [149]. The analysis of mixtures of components of similar size and similar diffusion coefficients by conventional DOSY is difficult [72]. High resolution in DOSY requires both that mixture components have different diffusion coefficient and their signals do not overlap. So in DOSY experiments component of similar size and structure are difficult or impossible to resolve. In DOSY the average diffusion coefficients for different components may be manipulated by the addition of co-solutes or co-solvents. However, changing the matrix in which solute diffuse, by introducing a co-solute which interacts differentially with different substrates, can allow separation [150]. It has been shown that performing DOSY in a matrix with which the analytes interact differentially can resolve signals from similar compounds that would otherwise show the same diffusion. This method is is known as Matrix Assisted Diffusion Ordered NMR Spectroscopy (MAD). MAD methods have great potential for the analysis of complex mixtures. In such a matrix-assisted DOSY experiment, the interaction of the analytes with the matrix modulates the average diffusion coefficients, as different mixture components bind to the matrix extents, it also sometimes helps to resolve the spectral overlap by causing differential chemical shift change [151]. It was also shown that isomers that have little or no difference in diffusion coefficient in simple solution may readily be resolved in DOSY experiments on solutions containing micelles or reversed micelles [152].

For our experiment we have used sodium dodecyl sulfate (SDS) micelles in the mixture of prulifloxacin and pazufloxacin. MAD-DOSY spectra should reflect differences in diffusion caused by differential binding of the drugs to SDS. However, we did not observe significant changes in the diffusion coefficients of the drugs and hence concluded that MAD-DOSY did not work for our mixture of fluorinated drugs.

5.3 Experimental Methods

Sample Preparation: Pazufloxacin, prulifloxacin, SDS and 1,2-dipaalmitoyl-sn-glycero-3-phosphocholine (DPPC) compounds were obtained from Sigma Aldrich and were used without further purification. Three different types of samples were prepared: for free diffusion in solution, for diffusion in a micellar matrix and for restricted diffusion inside DPPC bilayers. The samples used for free solution diffusion experiments were prepared by mixing individual drugs (each having concentration 12 mM) separately in 500 μl of DMSO-d6 as solvent. The drug mixture was prepared by mixing both drugs (12 mM each) in 500 μl of DMSO-d6. For samples of individual drugs in SDS, 12mM of drug and 100 mM of SDS were added to 500 μl of DMSO. For drug mixture in micellar sample 12 mM of each drug and 100 mM of SDS were taken. For samples inserted in DPPC, desired quantity of DPPC and drug were dissolved in chloroform. The solvent was evaporated with a stream of nitrogen so as to deposit a lipid film on the inner walls of the container. The last traces of solvent were removed by vacuum drying for at least 1 hour. Hydration and processing steps were performed at 50 °C, which is above the DPPC gel-fluid melting temperature (T_m = 42 °C). The films were hydrated with PBS:D2O (90:10) (pH-7.4), incubated for 1 hour, and sonicated for 2 hours. The lipid concentration was maintained at 50 mM and the drug concentration was kept at 25 mM.

Experimental Parameters:

All experiments were performed at ambient temperature (in an air-conditioned room at 22 °C) to avoid errors due to convection gradients.

The 1D ^{1}H spectra of the mixture of prulifloxacin and pazufloxacin and its individ-

ual components with obtained with experimental parameters: number of scans = 16, SW = 20.55 ppm, D1 = 1 s and processed with SI = 32k and LB = 0.30 Hz. The 1D ^{19}F spectra of the drug mixture and its individual components were recorded with number of scans =16, TD = 132 K, SW = 75.46 ppm, D1 = 1 s and processed with SI = 260 K and LB = 0.30 Hz. The 1D ^{19}F spectra of the drugs inserted in DPPC were collected with number of scans = 1024, SW = 75.46 ppm, D1 = 2 s and processed with SI = 2 k and LB = 0.30 Hz. The 1D ^{31}P spectra of the drug mixture in DPPC were collected with number of scans =16, TD = 65 k, SW = 39.77 ppm, D1 = 5 s and processed with SI = 32 k and LB = 1.0 Hz. The 1D ^{1}H spectra of the drug mixture in DPPC were collected using a 1D sequence with water suppression using excitation sculpting with gradients, with number of scans =1024, SW = 20.55 ppm, D1 = 1 s, a homospoil gradient = 1 ms and processed with SI = 4 k and LB = 0.30 Hz.

^{31}P NMR: Broadband proton decoupled 1D ^{31}P NMR spectra were recorded at 161.9 MHz using a single pulse excitation and WALTZ proton decoupling during the signal acquisition.

2D ^{1}H and ^{19}F DOSY: For 2D DOSY NMR spectra the bipolar pulse pair stimulated echo (BPPSTE) sequence was used with a maximum gradient of 53.5 G/cm and a total diffusion-encoding pulse width (δ) of 2 ms. The gradient recovery delay was set to 200 μs and a diffusion delay (Δ) = 50-200 ms was used for the different samples. Sixteen experiments were recorded with gradient intensity linearly sampled from 2 to 95%. All data were processed using Topspin 2.1 software and fitted using the procedure described in Chapter 1.

5.4 Results and Discussion

Figure 5.2 shows the 1D proton and ^{19}F spectra of the mixture of prulifloxacin and pazufloxacin and the individual drugs. Closer inspection reveals that the proton spectra of the mixture show overlaps in the resonances, while the fluorine chemical shifts are well resolved. Figure 5.3 (A-C) depicts the 2D ^{1}H and 2D ^{19}F DOSY spectra of the mixture of prulifloxacin and pazufloxacin in DMSO-d6 and in SDS micelles. The presence of 100 mM SDS, leads to only a slight decrease in diffusion coefficient (approximately

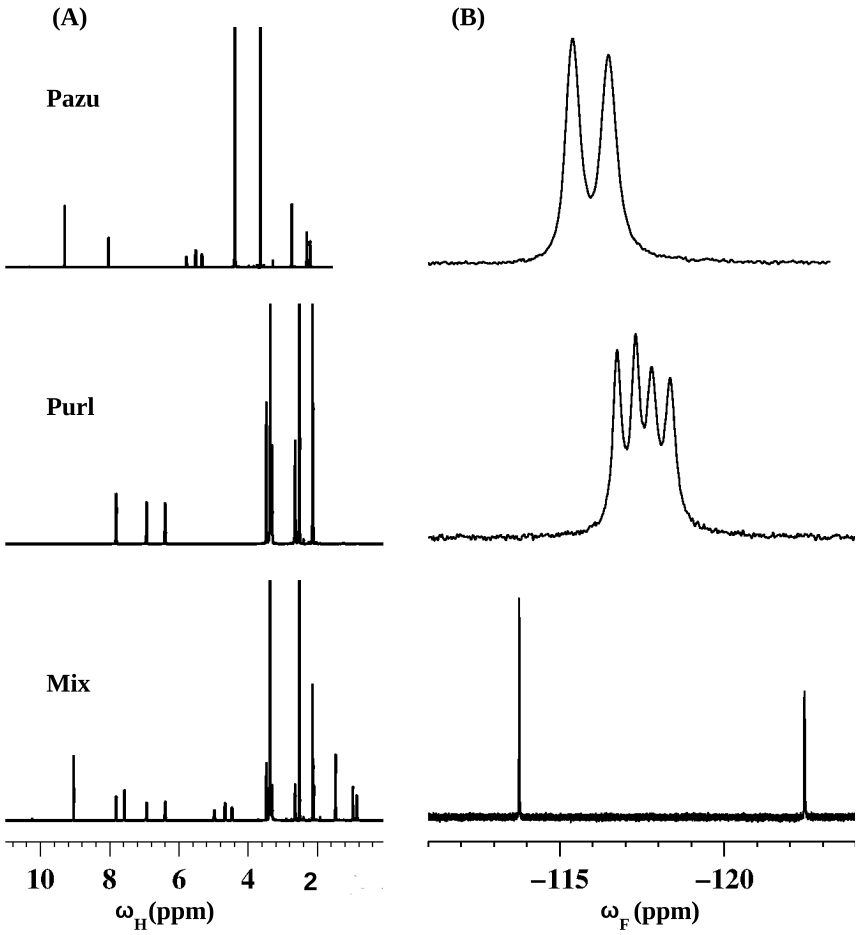

Figure 5.2: (A) ^{1}H spectra of a mixture of prulifloxacin and pazufloxacin and the individual drug components (B) ^{19}F spectra of a mixture of prulifloxacin and pazufloxacin and the individual components.

Table 5.1: Diffusion coefficients of prulifloxacin and pazufloxacin extracted from 2D ^{1}H DOSY and 2D ^{19}F DOSY spectra of the individual drugs.

Molecule	D ^{1}H ($\times 10^{-10}$ m^2 s^{-1})	D ^{19}F ($\times 10^{-10}$ m^2 s^{-1})
Prulifloxacin	1.94 ± 0.04	1.91 ± 0.02
Pazufloxacin	2.45 ± 0.01	2.31 ± 0.01

10%) for the drug mixture, which cannot be attributed to any differential drug binding or micellar formation. We hence conclude that the MAD-DOSY experiment did not work for our system of fluorinated drugs and we would hence have to resort to 3D-DOSY schemes, to resolve the individual diffusion components. The "LEDBPGP" type of pulse sequences were used to record the 2D DOSY spectra, which uses bipolar gradient pulses to eliminate any background gradients that would lead to additional unwanted echoes. The analysis of the NMR derived self-diffusion coefficients for prulifloxacin and pazufloxacin from ^{1}H DOSY and ^{19}F DOSY are tabulated in Table 5.1. The fluorine chemical shifts are well resolved in the spectra as well as in the fluorine DOSY spectra. The presence of SDS in the MAD-DOSY spectra did not lead to differential drug binding as evidenced from Figure 5.3 and hence the 2D MAD-DOSY experiment has not worked for our system of fluorinated drug mixture.

Figure 5.4 shows the 1D ^{1}H, ^{13}C and ^{19}F NMR spectra and peak assignment for prulifloxacin. The chemical shift values of proton, carbon and fluorine nuclei for this drug are given in Table 5.2. The ^{1}H NMR spectra of investigated fluoroquinolones showed signals for aromatic and non-aromatic protons in the molecules. Carboxylic proton (COOH) for prulifloxacin was observed as a singlet at 14.68 ppm in the spectra. For the aromatic part of ^{1}H NMR spectra, the characteristic splitting pattern due to the presence of fluorine atom (F29) was observed. The H5 proton in ^{1}H NMR spectra appears as doublet at 7.8 ppm, split by the fluorine atom through three bonds, with coupling constant $3J_{H-F}$ = 13.7 Hz. The signal for proton H_2 appears at 6.39 ppm, split into doublet through four bonds by the fluorine atom with coupling constant $4J_{H-F}$ = 6.1 Hz. The signal for H14, H18 appears at 3.3 ppm and for H15, H17 appears at 2.64 ppm. H14, H18 protons are coupled to H15, H17 protons through three bonds with coupling constant $3J_{H-H}$ = 8.4 Hz. Similarly H11 proton appears at 3.47 ppm and H27 proton appears at 2.13 ppm, being coupled to each other through three bonds with coupling constant $3J_{H-H}$ = 6.1 Hz. H19 proton appears as singlet at 3.35 ppm in the

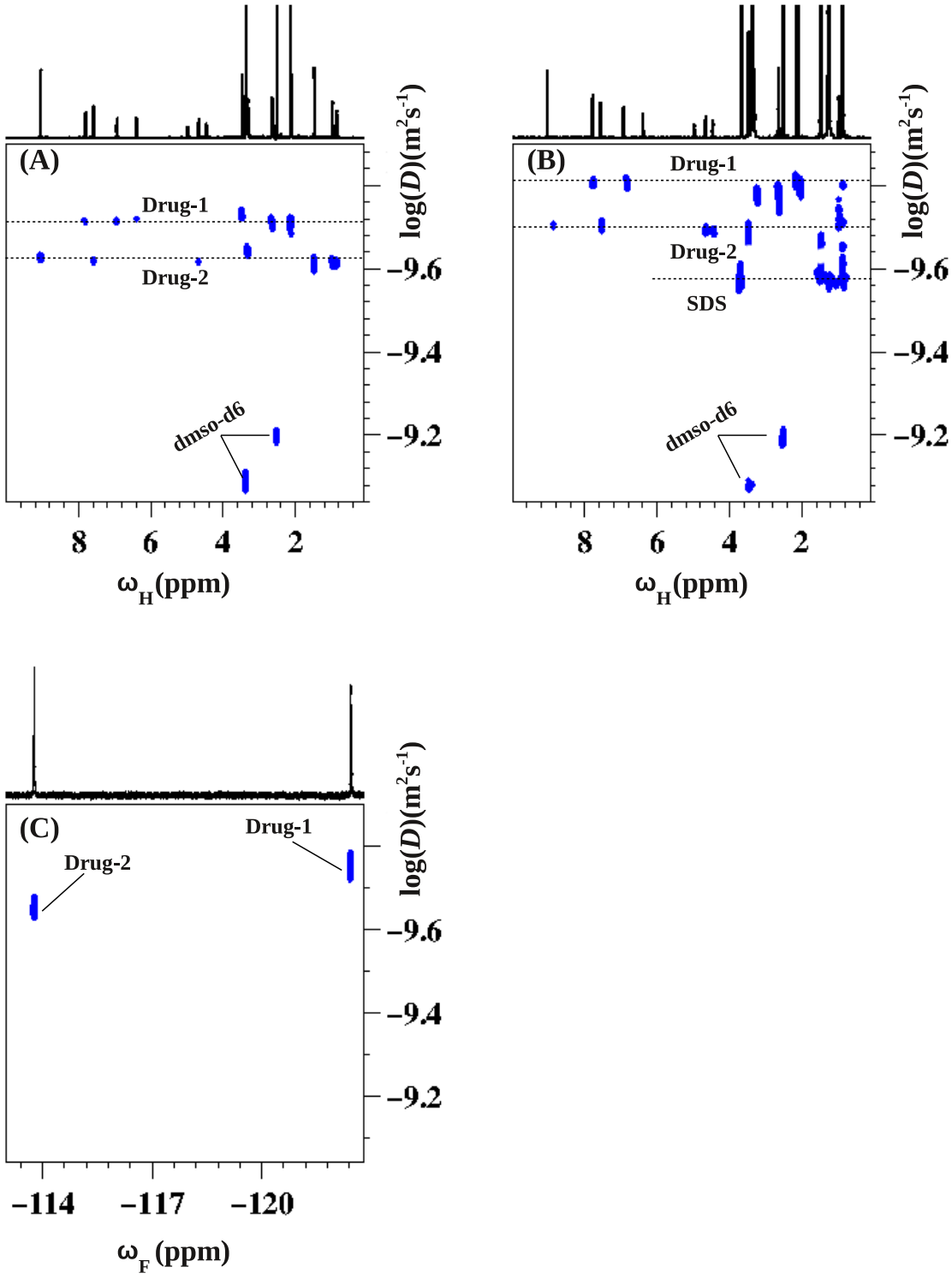

Figure 5.3: Proton DOSY spectra of the (A) Mixture of prulifloxacin and pazufloxacin in DMSO-d6. (B) Mixture of prulifloxacin and pazufloxacin in DMSO-d6 with the addition of 100 mM SDS. (C) 2D ^{19}F spectra of prulifloxacin and pazufloxacin in DMSO-d6. The label Drug 1 refers to prulifloxacin and the label Drug 2 refers to pazufloxacin.

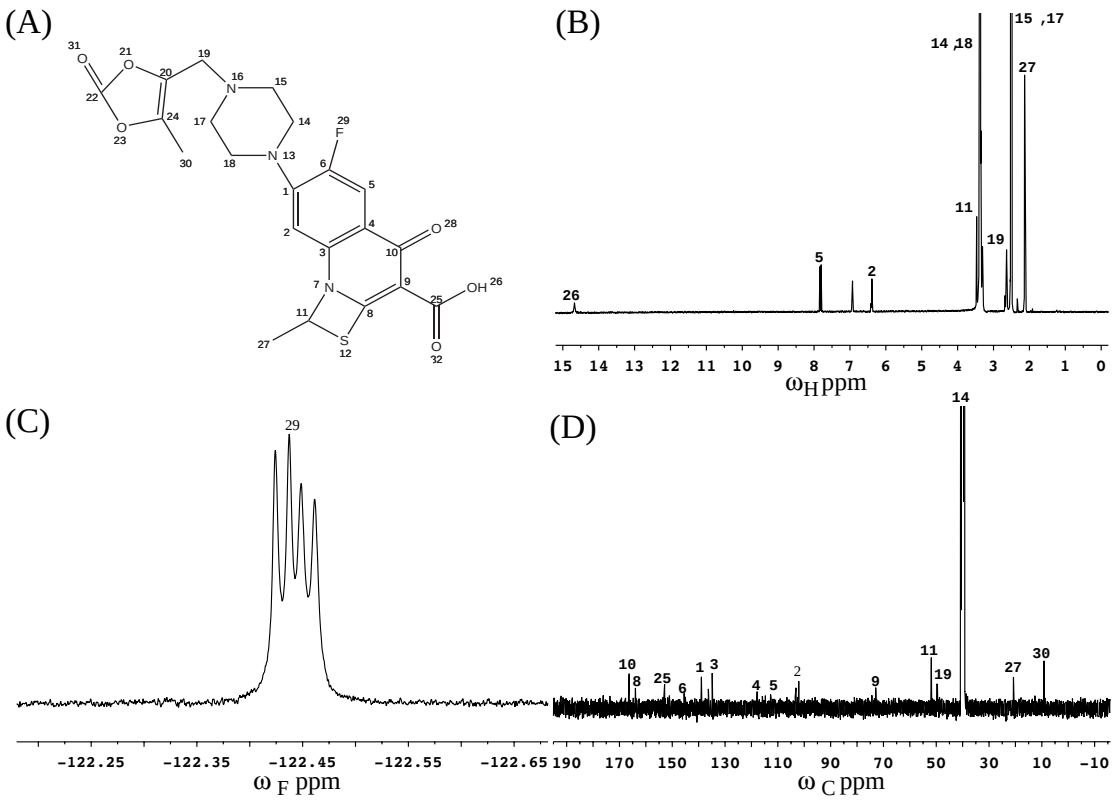

Figure 5.4: (A) Structure of prulifloxacin. (B) Peak assignment of the proton NMR spectrum of prulifloxacin in DMSO-d6. (C) Peak assignment of the carbon NMR spectrum of prulifloxacin in DMSO-d6. (D) Peak assignment of the fluorine NMR spectrum of prulifloxacin in DMSO-d6.

spectrum.

Figure 5.5 shows the 1D ^{1}H,^{13}C and ^{19}F NMR analysis for pazufloxacin. The chemical shift values of proton,carbon and fluorine nuclei for this drug are given in Table 5.3. The characteristic splitting pattern due to the presence of fluorine atom was also observed in pazufloxacin. The H2 proton in ^{1}H NMR spectra appears as a doublet split by the fluorine atom through three bonds and with coupling constant $3J_{H-F}$ = 10.15 Hz. H8 proton appears at 9.07 ppm as a singlet. NH_2 proton (H17) appears at 5.01 ppm. H15 and H16 protons appears at 0.99 ppm and 0.88 ppm respectively, being coupled to each other through three bonds, with coupling constant $3J_{J-H}$ = 6.5 Hz. H18 proton appears at 1.49 ppm as doublet due to splitting by H13 proton and being coupled to it through three bonds with coupling constant $3J_{H-H}$ = 6.8 Hz. H12 proton appears at 4.4 ppm, also being coupled to H13 proton through three bonds and coupling constant $3J_{H-H}$ = 11.4 ppm. H13 proton appears at 3.38 ppm and is coupled to both H18 and

Table 5.2: ^{1}H,^{13}C and ^{19}F chemical shift values (in ppm) of prulifloxacin.

Hydrogen	Chemical Shift (ppm)
H2	6.39
H5	7.80,7.84
H11	3.47
H14,H18	3.31
H15,H17	2.64
H19	3.35
H26	14.68
H27	2.13
Carbon	Chemical Shift (ppm)
C1	138.95
C2	102.09
C3	134.86
C4	117.84
C5	114.72
C6	145.48
C8	163.94
C9	72.92
C10	166.33
C11	51.86
C14	40.15
C19	49.81
C25	152.90
C27	20.74
C30	9.17
Fluorine	Chemical Shift (ppm)
F29	-122.44,-122.46

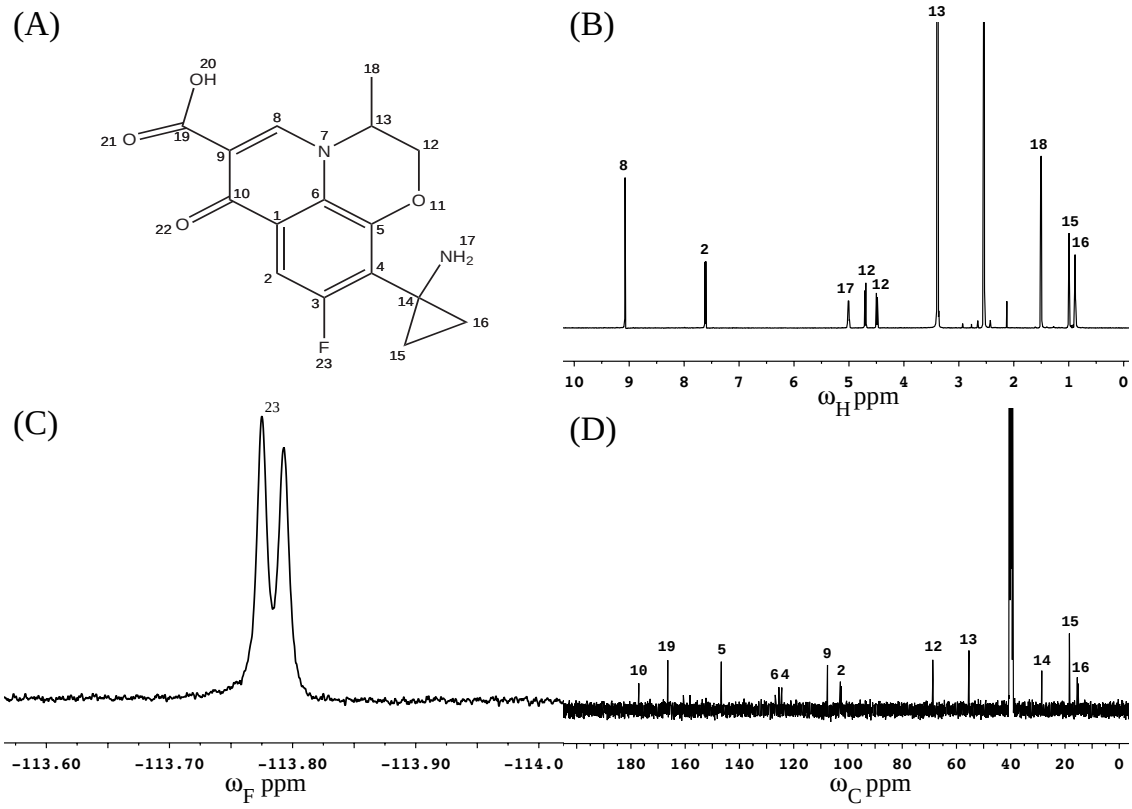

Figure 5.5: (A) Structure of pazufloxacin (B) Peak assignment of the proton NMR spectrum of pazufloxacin in DMSO-d6. (C) Peak assignment of the carbon NMR spectrum of pazufloxacin in DMSO-d6. (D) Peak assignment of the fluorine NMR spectrum of pazufloxacin in DMSO-d6.

H12 protons.

The effect of prulifloxacin and pazufloxacin on the mobility of phosphate headgroups of DPPC was studied by ^{31}P NMR. Figure 5.6 (A-C) shows the 1D ^{19}F, ^{31}P and ^{1}H spectra of the mixture of prulifloxacin and pazufloxacin inserted inside DPPC membrane mimetic. The 1D spectra shows that the drug signals are broadened, as compared to pure form. The broadening of the signals arises due to an exchange at an intermediate time scale between the bound and free form. The spin lattice relaxation times *(T_1)* and the spin-spin relaxation times *(T_2)* are measures of the overall tumbling and segmental motions in the molecule. Prulifloxacin and pazufloxacin contain both proton and fluorine groups which make it convenient to use both ^{1}H and ^{19}F signals to study their diffusion character in the DPPC lipid membrane. A diffusion ^{1}H NMR and ^{31}P NMR experiment was conducted on a sample of DPPC, prulifloxacin with DPPC and pazufloxacin with DPPC. The observed diffusion coefficients of prulifloxacin and

Table 5.3: ^{1}H,^{13}C and ^{19}F chemical shift values (in ppm) of pazufloxacin.

Hydrogen	Chemical Shift (ppm)
H2	6.39
H5	7.80,7.84
H11	3.47
H14,H18	3.29
H15,H17	2.52
H19	2.64
H26	14.68
H27	2.13
Carbon	Chemical Shift (ppm)
C1	138.95
C2	102.09
C3	134.86
C4	117.84
C5	114.72
C6	145.48
C8	163.94
C9	72.92
C14	28.55
C15	18.36
C16	15.4
C19	177.10
Fluorine	Chemical Shift (ppm)
F23	-113.77,-113.79

pazufloxacin with DPPC and the spin lattice relaxation times *(T_1)* and spin-spin relaxation times *(T_2)* are given in Table 5.4. The estimates of spin-spin relaxation times *(T_2)* from the NMR line-width indicate that the T_2 values are the order of 10-100 ms. Lower values of T_2 indicate that the both drugs lose their mobility and bind to lipid membrane, resulting in a loss of motional freedom. Lipid phosphorus exhibits large chemical shift anisotropy. ^{31}P NMR line shape is sensitive to different types of motions of lipid molecules. Figure 5.7 shows the results of a stimulated echo experiment on the phosphorus frequency by altering the gradient amplitude, results in signal decays with a high signal to noise ratio which is well suitable for fitting the self diffusion coefficient. We recorded a series of 1D NMR spectra with increasing gradient for diffusion measurements on the mixture of prulifloxacin and pazufloxacin with DPPC and compared the result to the diffusion coefficients obtained in the same experiment in the absence of DPPC as shown in Figure 5.8. The presence of DPPC reduced the translational diffusion rates of prulifloxacin and pazufloxacin. Figure 5.9 (A) shows the 2D HMBC spectra of the mixture of prulifloxacin and pazufloxacin. The projections onto the $\delta_C - \delta_H$ plane of the 3D COMPACT-IDOSY data for the diffusion coefficient range 1.5 to 2.0 $\times 10^{-10}$ m^2/s showing the signal of prulifloxacin is given in Figure 5.9(B) and for the diffusion coefficient range 2.2 to 3.0 $\times 10^{-10}$ m^2/s showing the signal of pazufloxacin is given in Figure 5.9(C). The spectra in the extracted 2D planes are well-resolved, leading to an improved accuracy in the estimation of the diffusion coefficients from this 3D DOSY experiment.

5.5 Conclusions

The determination of the stereochemistry of fluorinated drugs and the relative configuration of such drugs in liposomal drug carriers is crucial to understanding their biological activity. A set of 2D fluorine and proton DOSY, 2D MAD-DOSY and novel 3D heteronuclear DOSY experiments have been performed on a mixture of two quinolone antibacterial agents, pazufloxacin and prulifloxacin. The results of the different pulse sequences are compared on the basis of their ability to separate the drugs based on their molecular weights and accurate computation of their diffusion coefficients. The

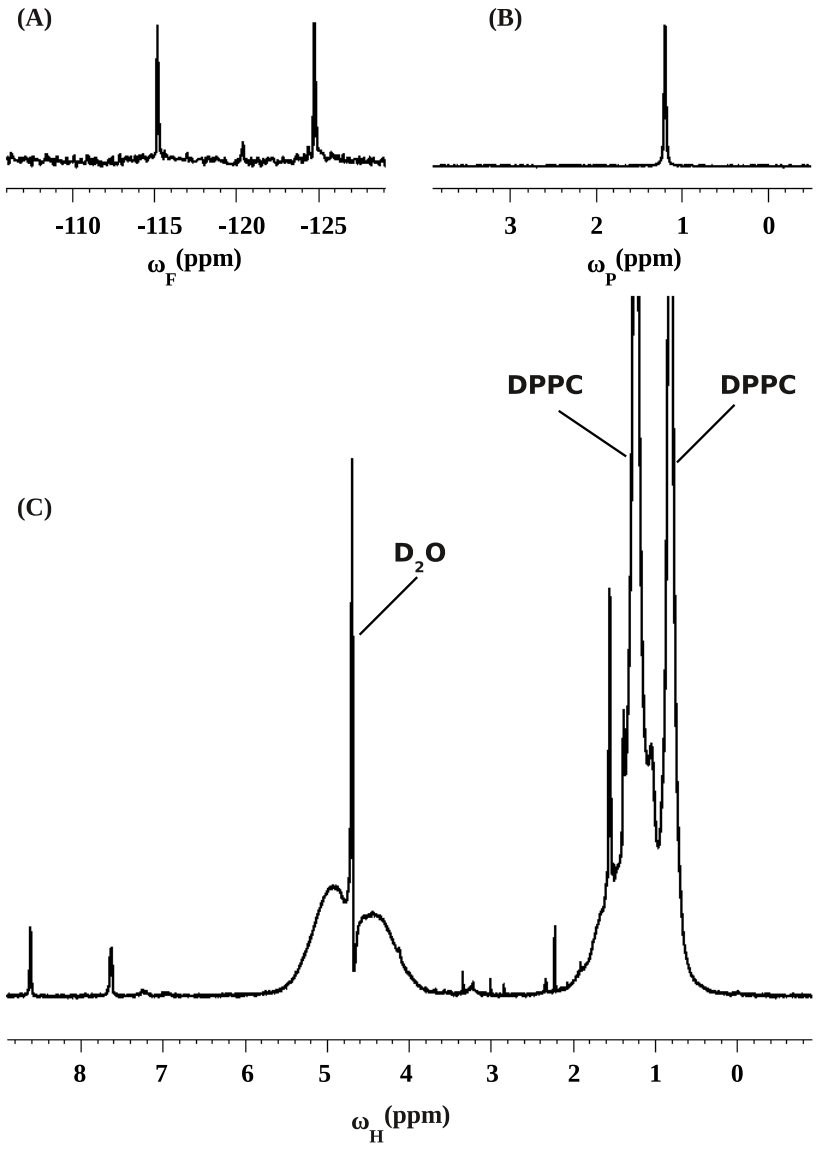

Figure 5.6: 1D (A) ^{19}F spectra of mixture of prulifloxacin and pazufloxacin in DPPC (B) ^{31}P spectra of mixture of prulifloxacin and pazufloxacin in DPPC. (C) ^{1}H spectra of mixture of prulifloxacin and pazufloxacin in DPPC.

Table 5.4: Relaxation rates and Diffusion coefficients D ($\times 10^{-11}$ m^2/s) of Prulifloxacin and Pazufloxacin inside DPPC, extracted from 2D ^{1}H DOSY, 2D ^{19}F DOSY and 2D ^{31}P DOSY spectra.

Drugs	Nuclei	T_1	T_2	Diffusion Coefficient
Prulifloxacin with DPPC	^{31}P	2.20 s	0.94 s	1.15 ± 0.03
	^{1}H	1.49 s	0.78 s	1.17 ± 0.02
	^{19}F	1.34 s	0.79 s	1.20 ± 0.01
Pazufloxacin with DPPC	^{31}P	1.05 s	0.63 s	1.56 ± 0.01
	^{1}H	1.79 s	0.17 s	1.52 ± 0.03
	^{19}F	1.36 s	0.15 s	1.54 ± 0.01
DPPC	^{31}P	2.85 s	0.15 s	1.62 ± 0.02
	^{1}H	1.95 s	0.68 s	1.60 ± 0.03

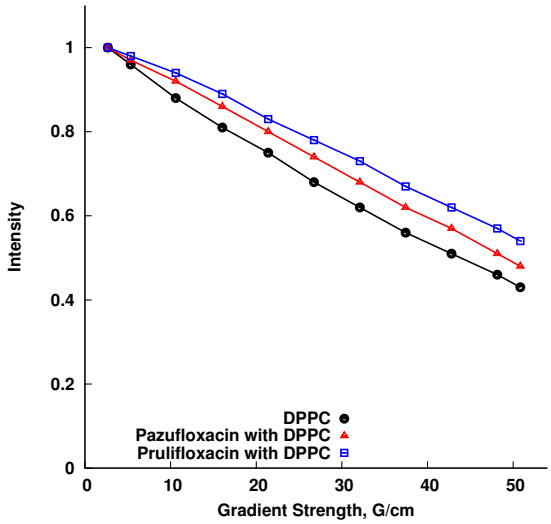

Figure 5.7: Experimental echo decay for the fluorinated drugs and drugs inserted in DPPC as measured by ^{31}P diffusion NMR. Data points represent DPPC alone (open circle with black line), pazufloxacin in DPPC (arrow with red line), and prulifloxacin in DPPC (square with blue line).

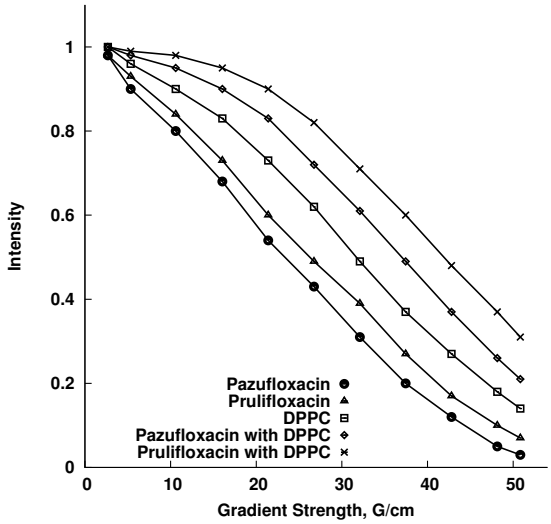

Figure 5.8: STE-PFG NMR intensity decays of prulifloxacin, pazufloxacin, prulifloxacin inserted in DPPC, pazufloxacin inserted in DPPC and DPPC alone. Differences in the decay rates indicate different diffusion coefficients measured for drugs in free form and when bound to DPPC.

2D DOSY and 2D MAD-DOSY experiments were not able to separate the individual diffusion coefficients of the drugs in the mixture and we hence had to resort to the 3D COMPACT-IDOSY experiment for accurate determination of the diffusion coefficients. The 3D COMPACT-IDOSY experiment will be useful in the deconvolution of complex mixtures of fluorinated molecules and in fluorinated ligand-binding assays. Drug loading and penetration into a phospholipid bilayer, which has important implications for drug delivery applications, was characterized using ^{31}P NMR and ^{19}F to measure the self-diffusion coefficients of the free and bound drugs. The incorporation of the fluorinated drugs inside the DPPC lipid bilayer was evidenced by the lowering of the translational self-diffusion coefficient as compared to that of the free drug. For instance, the diffusion coefficient (measured from ^{1}H DOSY) of prulifloxacin inside DPPC decreased by a factor of 10 as compared to its free form (1.17×10^{-11} m^2/s inside DPPC as seen in Table 5.4 and 1.94×10^{-10} m^2/s as seen in Table 5.1). The work described in this chapter will be of relevance for the elucidation of structure of new fluorinated drugs and binding studies of how changes in steric configuration cause changes in affinity at the receptor binding site, which are increasingly becoming important for clinical applications and in the polymer and pharmaceutical industries.

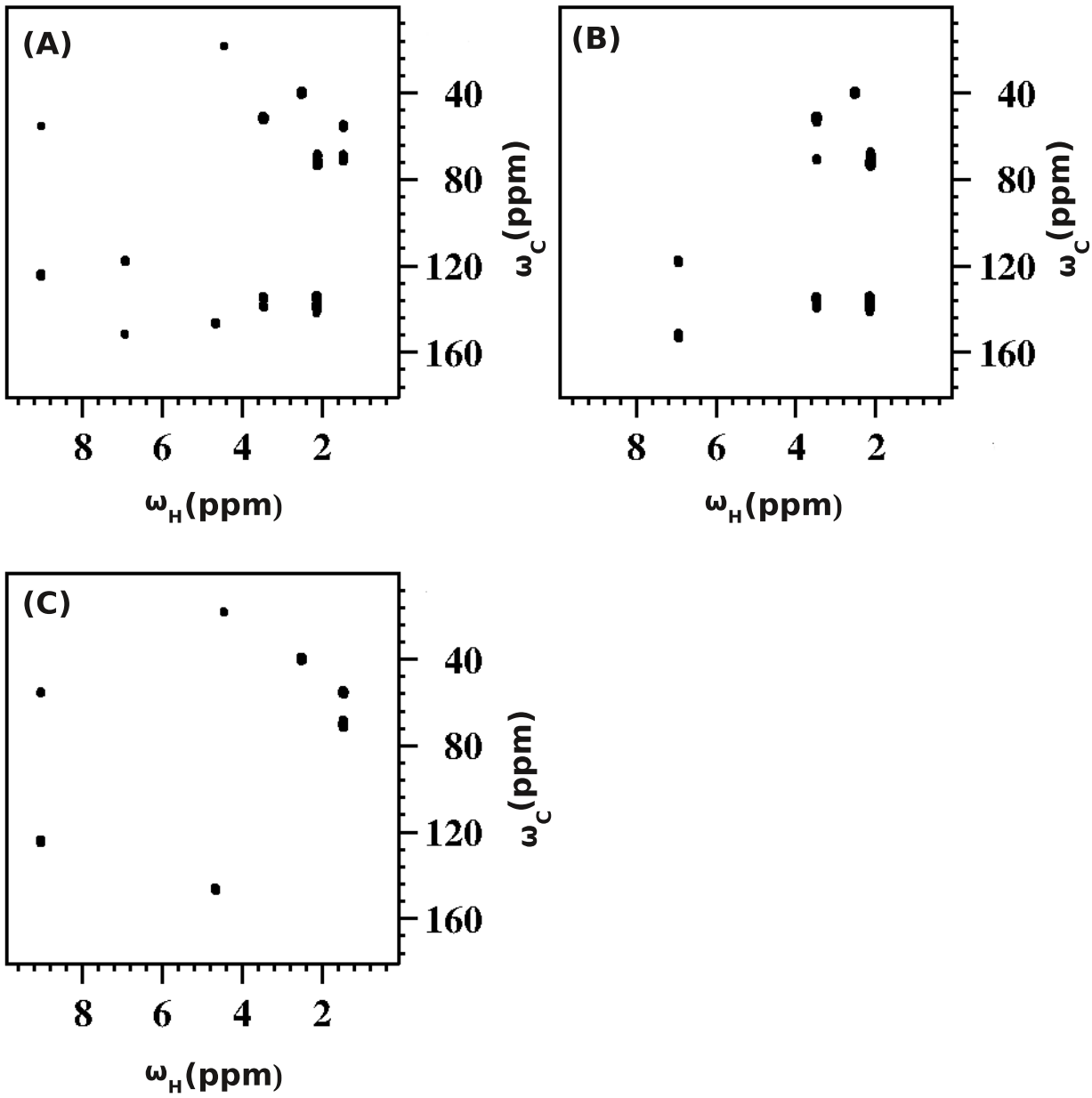

Figure 5.9: COMPACT-IDOSY data for a mixture of prulifloxacin and pazufloxacin (A) HMBC spectra (B) signals with diffusion coefficient between 1.5 to 2.0 $\times 10^{-10}\ \mathrm{m}^2/\mathrm{s}$, (prulifloxacin). (C) signals with diffusion coefficient between 2.2 to 3.0 $\times 10^{-10}\ \mathrm{m}^2/\mathrm{s}$, (pazufloxacin).

CHAPTER 6

Diffusion NMR Studies of Anti-Oxidants in DPPC Lipid Bilayers

6.1 Background and Motivation

Biological membranes provide an environment which is required for many biochemical processes. Different types of biological membranes have diverse lipid and protein compositions. A lipid bilayer, one of the main components of a biological membrane, provides mechanical stability and low permeability to ions and large molecules. The structural characteristic of the cell membrane is such that it behaves like a two-dimensional liquid, and its constituent molecules (membrane proteins and lipids), rapidly move about in the membrane plane, while phospolipids do not undergo free diffusion in the cellular plasma membrane. The diffusion of molecules in the complex cellular membrane is affected by membrane inhomogeneities and interactions with cytoplasm. All membrane components can freely diffuse along the plane of the membrane and the rate of their diffusion determines the kinetics of the membrane-associated biochemical reactions. The diffusion coefficient can be determined by NMR techniques such as PFGSE NMR. This chapter focuses on the interaction of two antioxidants α-tocopherol and curcumin with a phospholipid bilayer. Curcumin (1,7-Bis(4-hydroxy-3-methoxyphenyl)-1,6-heptadiene-3,5-dione) a natural polyphenol, found in the rhizomes of Curcuma longa, commonly called turmeric, exhibits anti-inflammatory, antineoplastic, and chemopreventive activities and has been shown to be pharmacologically safe even at high doses [156, 157]. Vitamin E (α-tocopherol) is a fat-soluble vitamin with antioxidant properties present in nuts, seeds, vegetables and whole grains. α-tocopherol, (2,5,7,8-Tetramethyl-2-[(4,8,12-trimethyltridecyl)]-6-chromanol) is an important lipid-soluble antioxidant, and it protects membranes from oxidation by reacting with lipid radicals produced in the lipid peroxidation chain reaction [158]. In a biological system, an antioxidant can be defined as any substance that when present at low concentrations

compared to that of an oxidizable substrate would significantly delay or prevent oxidation of that substrate [155]. Although oxidation reactions are crucial for life, they can also be damaging to plants and animals. The oxidizable substrate may be any molecule that is found in foods or biological materials, including carbohydrates, DNA, lipids, and proteins. Antioxidants may be classified according to their mechanism of action: primary or chain breaking antioxidants and secondary or preventive antioxidants. Some antioxidants exhibit more than one mechanism of activity and are therefore referred to as multiple-function antioxidants. Primary antioxidants are also referred to as type 1 or chain-breaking antioxidants. Secondary antioxidants are also classified as preventive or class 2 antioxidants. The main difference between these antioxidant types is that the secondary antioxidants do not convert free radicals into stable molecules. Antioxidants are widely used in dietary supplements and have been investigated for the prevention of diseases such as cancer, coronary heart disease and even altitude sickness. Antioxidants also have many industrial uses, such as preservatives in food and cosmetics and to prevent the degradation of rubber and gasoline. PFG NMR experiments in conjunction with molecular dynamics (MD) simulations, afford additional information on the mobility of lipid-soluble antioxidants, which has implications for the efficiency of radical scavenging in biological membranes [160].

6.2 DPPC Lipid Bilayers

DPPC is a phospholipid consisting of two palmitic acids and is the major constituent of pulmonary surfactants. Palmitic acid is the most common fatty acid found in animals, plants and microorganisms. Phospholipids are a class of lipids that are a major component of all cell membranes as they can form lipid bilayers. The majority of the lipid content in most eukaryotic and prokaryotic cells are phospholipids. Phospholipid bilayers are usually divided into two polar head group regions and one non-polar hydrocarbon region consisting of the phospholipid hydrocarbon chains. The identity of the phospholipid is therefore determined by the composition of headgroup and the length and saturation of the hydrocarbon tail. Phospholipid bilayers have been widely studied from different points of view because of the important role played in the structure

and function of biological membranes [159]. In the bilayer, a limited number of water molecules can penetrate into the head group regions.

6.3 Antioxidants and Lipid Interactions

Antioxidants are classified into two broad divisions, depending on whether they are soluble in water (hydrophilic) or in lipids (hydrophobic). The hydrophilic antioxidants react with oxidants in the cell cytosol and the blood plasma, while hydrophobic antioxidants protect cell membranes from lipid peroxidation. These compounds may be synthesized in the body or obtained from the diet.

6.4 Experimental Methods

^{1}H diffusion experiments were also performed on Bruker Avance 600 NMR spectrometer using Diff30 diffusion probe capable of generating magnetic field gradients of up to 1200 G/cm. To avoid probe heating and to stabilize the sample temperature the probe was cooled by a water circulation unit (BCU 20) and the temperature was maintained at $25\,^{\circ}\mathrm{C}$. A stimulated echo pulse field gradient sequence with a diffusion time of 100 ms and gradient pulse duration of 2.0 ms was applied. The gradient steps were varied in 32 steps to a maximum gradient amplitude of 1200 G/cm for DPPC, DPPC with curcumin and DPPC with α- tocoferol samples and in 16 steps upto 120 G/cm for other samples. The data evaluation was performed by fitting to the Stejskal-Tanner equation, as described in Chapter 1. The curcumin, alpha-tocoferol and DPPC samples were obtained from Sigma Aldrich and used without further purification. The sample was prepared by dissolving 2 mg of curcumin in 600 μl of DMSO-D6, at a concentration of 10 mM. The sample of α-Tocopherol was prepared by dissolving 50 μl in 600 μl of Acetone-D6. For samples in DPPC, desired quantity of DPPC and alpha-tocopherol/curcumin were dissolved in chloroform. The solvent was evaporated with a stream of nitrogen so as to deposit a lipid film on the inner walls of the container. The last traces of solvent were removed by vacuum drying for at least 1 hour. Hydration and processing steps were performed at $50\,^{\circ}\mathrm{C}$, which is above the DPPC gel-fluid melting temperature (T_m

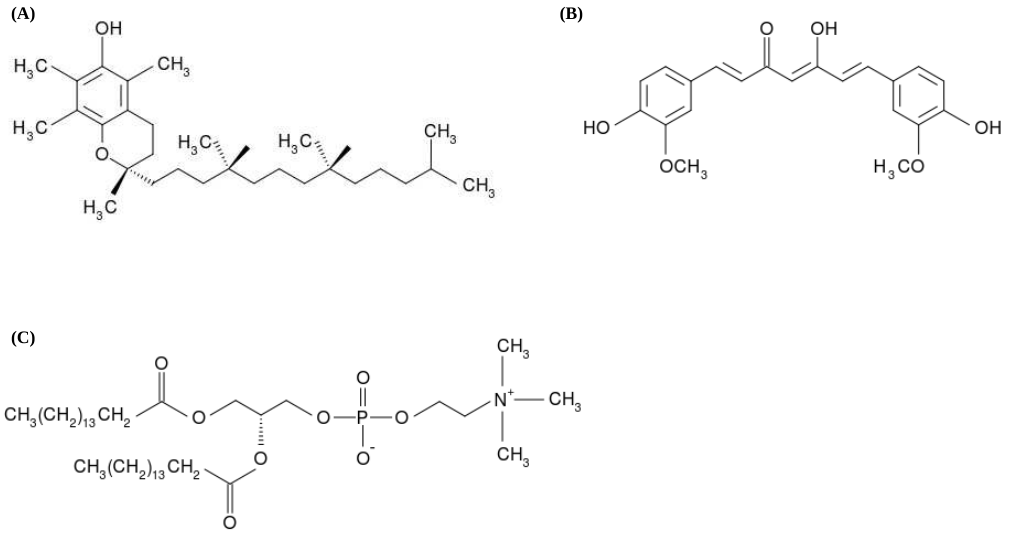

Figure 6.1: Structures of individual molecules.(A) α-Tocopherol (B) Curcumin (C) DPPC.

= $42\,^{\circ}\mathrm{C}$). The films were hydrated with 500 μl of PBS:D2O (90:10) (pH-7.4), incubated for 50 minutes, and sonicated for 2 hours. The lipid concentration was maintained at 25 mM and the alpha tocopherol/curcumin concentration was kept 12.5 mM. The structure of all the molecules used in this study is given in Figure 6.1.

6.4.1 1D Proton and Carbon spectra

1D ^{1}H experiments were carried out with a typical $\pi/2$ pulse length of 9.15 μs and a relaxation delay of 1 s. Fourier transform spectral parameters were 32K data points using a 8361 Hz spectral window. ^{13}C NMR were performed with a typical 90° pulse length of 14.60 μs. Proton decoupling was performed using WALTZ16. Standard methods were used for the acquisition of the 2D COSY, TOCSY, HMQC and HMBC spectra. The d2 delay for the HMQC and HMBC methods was 3.44 ms, corresponding to $^{1}J_{XH}$ of 145 Hz. The d6 HMBC delay was 60 ms, corresponding to $^{2,3}J_{XH}$ of 8.0 Hz. The TOCSY mixing time was set to 60 ms.

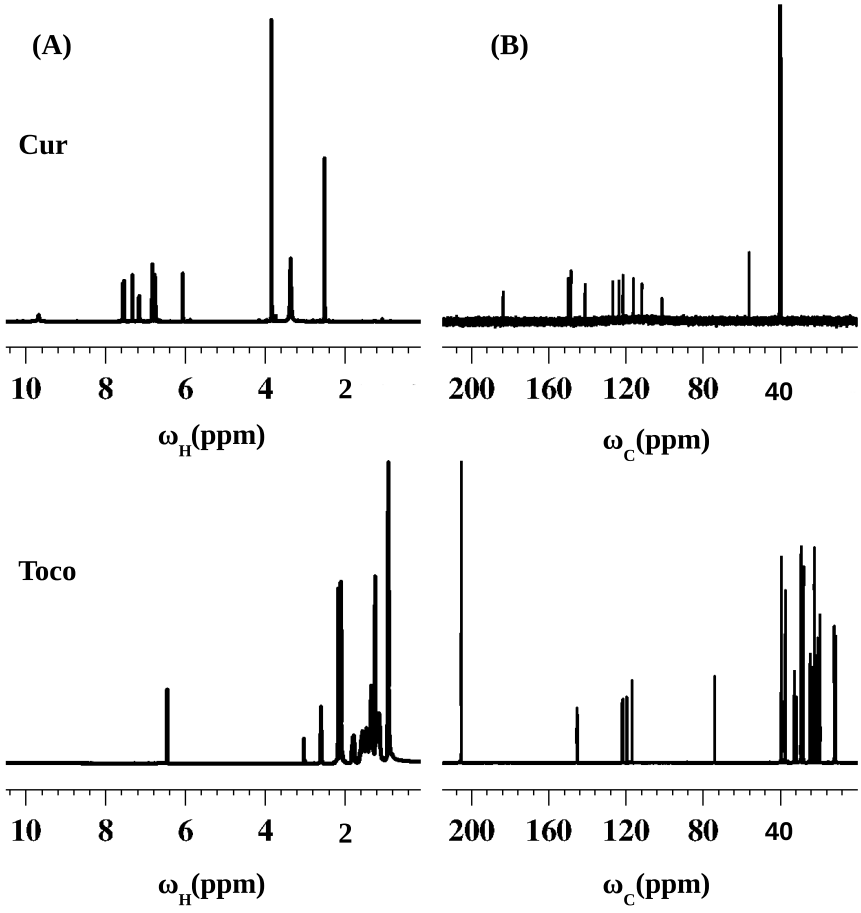

Figure 6.2: Fig (A) 1D ^{1}H NMR spectra of the curcumin and α-Tocopherol were acquired with 16 transients, 32K data points using a 8361 Hz spectral window and a relaxation delay of 1 s. (B) ^{13}C NMR spectra of the curcumin and α-tocopherol were acquired with 65K data points with number of scans 2K and relaxation delay of 2 s.

6.5 Results and Discussion

When a molecule is incorporated inside a lipid bilayer, the diffusion coefficient becomes anisotropic and may be represented in terms of a second-order symmetric diffusion tensor having tensor elements $D_\perp$ and $D_\parallel$, representing the diffusion perpendicular and parallel to the bilayer normal direction, respectively. Transforming to the laboratory frame defined by the applied pulsed-field gradients, the measured diffusion coefficient becomes

$$D_{zz} = D_\perp \sin 2\theta + D_\parallel \cos 2\theta \tag{6.1}$$

where θ is the angle between the bilayer normal and the direction of the applied field gradient. When the bicelles are aligned in the applied magnetic field with their bilayer normal perpendicular to the direction of the external magnetic field, and when the field gradient is applied parallel to the magnetic field, the above equation reduces to $D_{zz} = D_\perp$ which corresponds to lateral diffusion within the bilayer. Using PFG NMR, the lateral diffusion of molecules in the plane of the lipid bilayer can be measured. Here we describe PFGSE NMR-based methods on curcumin and α-tocopherol that bind with DPPC. The methods exploit the changes in either the relaxation rates or diffusion rates in free and bound conditions. Since these experiments employed a PFG-STE sequence, appropriate gradient strengths were determined which could discriminate between the antioxidants and DPPC lipid bilayers. At a low gradient strength of 1.2 G/cm, the NMR signals of the both the antioxidants and the DPPC are observed. However, at a high gradient strength of 1200 G/cm, the signals from the free compounds are completely eliminated, while those from the bilayers are reduced. To identify antioxidant that bind to DPPC from a mixture of nonbinding compounds with use of a diffusion-edited approach, several PFG-STE spectra were recorded and analyzed. First, a PFG-STE spectrum of the test compounds in the absence of DPPC was acquired at a low gradient strength. At this gradient strength, the resonances from all of the compounds are observed. Next, PFG-STE spectra of the compounds in the presence of DPPC were obtained at low and high gradient strengths. The corresponding *D* were estimated from the slopes of the straight lines fitted to the data.

Figure 6.2 shows the 1D ^{1}H and 1D ^{13}C NMR spectra of curcumin and α- toco-

pherol. The proton spectra of curcumin featured a proton singlet at δ 6.06 ppm due to the hydroxyl group. The methoxyl group of the both aromatic rings was confirmed by a proton singlet at δ 3.35 ppm and a proton multiplet centered between δ 6.69 to 6.82 ppm. The ^{13}C NMR spectra of curcumin shows resonances for all twenty-one carbons. The ^{13}C NMR spectrum showed a singlet at 183.3 ppm due to the presence of a carbonyl carbon. The presence of aromatic rings were confirmed by resonances ranging between δ 111.28 to 146.84 ppm. Figure 6.3 (A-D) shows the 2D NMR spectra from the experiments COSY, HMQC, TOCSY and HMBC on the curcumin molecule. Figure 6.4 (A-D) shows the 2D NMR spectra from the experiments COSY, HMQC, TOCSY, and HMBC on the α-tocopherol molecule. The ^{1}H-^{1}H COSY analysis gave cross-peaks for proton correlations. The HMQC experiment helped to confirm the ^{1}H-^{1}H and ^{13}C NMR chemical shift assignments. For instance, Figure 6.4(B) shows the aromatic protons at δ 6.49 to 7.35 ppm have direct connectivity with aromatic carbon at δ 116.92 to 121.06 ppm. The ^{1}H-^{1}H TOCSY analysis gave correlations between all the protons. The HMBC analysis led to multiple bond correlation information. Table 6.4 shows the diffusion coefficients of α- tocopherol and curcumin, which exhibit varying diffusion behavior in free and bound forms. Both α- tocopherol and curcumin when incorporated in the bilayer diffuse slower relative to their free forms in solution. The diffusion of the DPPC molecules is slower than that of the antioxidant in free forms, but the difference gets smaller at higher concentration. Since the headgroup of DPPC has got a much larger dipole moment than that of the antioxidants, the diffusion of DPPC will be effectively slowed down by these interactions.

Molecule	Diffusion Coefficient ($\times 10^{-10}$ m^{2}s^{-1})
α-Tocopherol	6.29 ± 0.03
Curcumin	1.85 ± 0.02
α-Tocopherol + DPPC	0.06 ± 0.04
Curcumin + DPPC	0.1 ± 0.03
DPPC	0.16 ± 0.01

Table 6.1: Table of the diffusion coefficients of the antioxidant molecules diffusing freely and inside DPPC, measured on the Diff30 probe.

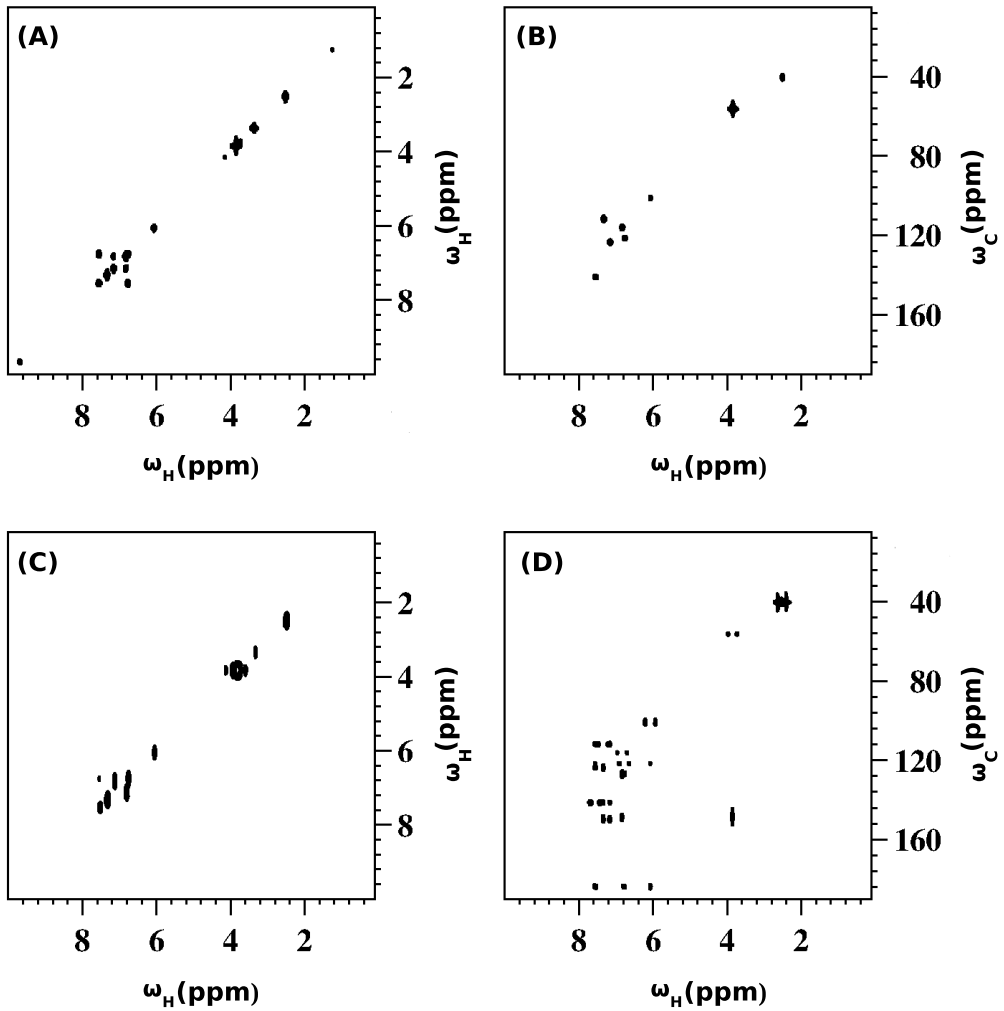

Figure 6.3: 600 MHz (A) 2D COSY spectrum of curcumin. The data matrix is 1024 $\times$ 1024 and the number of t_1 increments is 128. (B) 2D HMQC spectrum with a data matrix of 1024 $\times$ 1024 and the number of t_1 increments=128, the recycle delay is 1 s and ${}^{1}J_{XH}$ = 145 Hz. (C) 2D TOCSY spectrum. The data matrix is 1024 $\times$ 1024 and the number of t_1 increments is 256, the recycle delay is 2 s and the mixing time was set at 60 ms. (D) 2D HMBC spectrum. The data matrix is 1024 $\times$ 1024 and the number of t_1 increments is 256, the recycle delay is 2 s and ${}^{2,3}J_{XH}$ = 8.0 Hz.

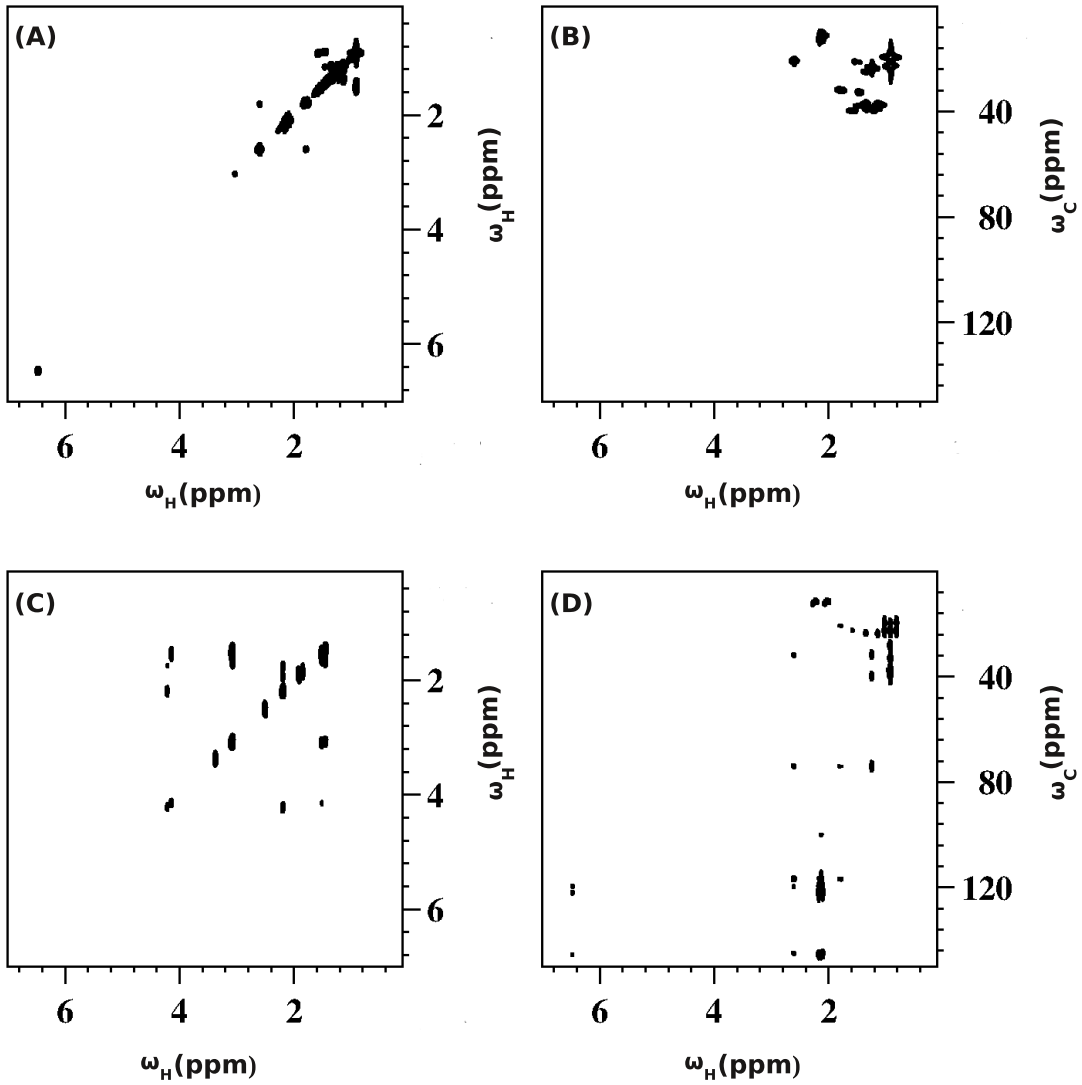

Figure 6.4: 600 MHz (A)2D COSY spectrum of α-Tocopherol. The data matrix is 1024 $\times$ 1024 and the number of t_1 increments is 128. (B) 2D HMQC spectrum. The data matrix is 1024 $\times$ 1024 and the number of t_1 increments is 128, the recycle delay is 1s and $^1J_{XH}$ = 145 Hz. (C) 2D TOCSY spectrum. The data matrix is 1024 $\times$ 1024 and the number of t_1 increments is 256, the recycle delay is 2 s and the mixing time was set at 60 ms. (D) 2D HMBC spectrum. The data matrix is 1024 $\times$ 1024 and the number of t_1 increments is 256, the recycle delay is 2 s and $^{2,3}J_{XH}$ = 8.0 Hz.

6.6 Conclusions

By using PFG NMR methods, we have investigated the influence of the lipid phase on the self-diffusion of antioxidants α-tocopherol and curcumin diffusing in a DPPC lipid bilayer system. The diffusion experiments were repeated on the Diff30 probe which can achieve much higher gradient strengths, to probe molecules with much slower diffusion. The experimental analysis described in this chapter is still in a preliminary stage and a more detailed analysis combined with MD simulations is required to reach quantitative conclusions about the data.

CHAPTER 7

Summary & Future Outlook

This thesis deals with the study of the translational self diffusion coefficients using pulsed field gradient NMR and the development of novel homonuclear and heteronuclear three dimensional DOSY-type pulse sequences. The designed schemes have been applied to mixtures of small molecules, fluorinated drug mixtures and biomolecules diffusing inside a lipid bilayer. Specifically, the work described in the thesis includes:

- A novel diffusion-edited 3D NMR experiment was designed that incorporates a BEST-HMQC pulse sequence prior to the 2D diffusion sequence. This pulse sequence provides a more sensitive and less time-consuming alternative to standard 3D HMQC-DOSY experiments. The feasibility of the technique is demonstrated on a mixture of amino acids, on a mixture of small molecules with similar diffusion coefficients, and on commercial gasoline.

- A new 3D diffusion-ordered heteronuclear NMR experiment COMPACT-IDOSY sequence was designed, which combines the 2D HMBC experiment (that evaluates long-range ^{13}C-^{1}H couplings) with the DOSY sequence in an IDOSY fashion. The experimental pulse scheme was implemented on a mixture of flavonoids rutin and quercetin. The scheme offers substantial reduction in experimental time, good sensitivity and excellent resolution of signal overlap, leading to the accurate determination of translational diffusion coefficients of individual components in the mixture.

- A versatile three-dimensional diffusion-edited nuclear magnetic resonance experiment (3D MQ-DOSY) has been developed that concatenates a multiple-quantum, single-quantum correlation scheme with a diffusion-ordered pulse sequence. The experiment is demonstrated on mixtures of small molecules with similar diffusion coefficients and is able to resolve severely overlapped signals along the third dimension.

- The diffusion coefficients of individual fluorinated drug molecules prulifloxacin and pazufloxacin have been estimated using both 2D proton and fluorine DOSY, 3D COMPACT-IDOSY and micelle-assisted DOSY. The diffusion of each drug inside a lipid bilayer has also been investigated using proton, carbon and phosphorus diffusion and relaxation measurements.

- The lateral and translational self diffusion of antioxidants inside a lipid bilayer such as DPPC has been of much recent interest. This thesis reports a diffusion study of of two antioxidants α-tocoferol and curcumin inside the DPPC bilayer. PFG NMR experiments were performed by using the high gradient strengths available on the special rf Diff30 probe.

The future prospects for extensions of the work described in this thesis include: To use the 3D DOSY methods developed to study protein diffusions in a crowding environment such as ficoll or dextran. Under crowded conditions, diffusion is dominated by the solution viscosity [161]. Hence glycerol can be added to the protein with buffer, to mimic the diffusion of a protein of much larger size and much slower diffusion [162]. Another direction of interest is the application of non-uniform sampling (NUS) protocols to diffusion pulse sequences. The advantage of NUS is that it frequently affords high resolution spectra from much smaller data sets as compared to conventional uniform sampling [163, 164].

APPENDIX A

Diffusion Probe Calibration & Diffusion Data Processing

This Appendix describes protocols to install the diffusion probe and procedures to process diffusion data. The Bruker diffusion Diff30 probe is a single nucleus probe, with a ^{1}H radiofrequency coil insert with an inner diameter of 5 mm. Magnetic field gradients of up to 12 T/m can be generated. Such high gradient amplitudes are required for studies of high molecular weight or viscous samples with small diffusion coefficients. To avoid probe heating and to control sample temperature, the probe is cooled by flowing water and the temperature is usually maintained at $25\,^{\circ}\mathrm{C}$.

A.1 Installing the probe

- Slowly insert Diff30 probe and alternatively fasten two screws under probe.
- Connect all cables: For Diff30- Two RF Cables, pics cable is not required. In addition the following are required: Air cable-BCU extreme unit, heater cable, gradient cable, one sensor cable.
- Type in “edhead” command. In edhead dialog choose “Diff30” probe, click define as current probe button, and finally click exit button.
- Type “edte” command, turn on button in edte dialog.
- Type in “edprosol” command, confirm the pulse widths and power cables were all changed to fit the “Diff30” probe.
- Type “ha” to see the accessible hardware. Once it shows the relevant information, press “ok”.
- Type “ii” (initialize interface) a few times, wait till it finishes.
- Type “setpre” command go to files-read default.
- Do the RT shimming (doped water) in “gs mode”.
- The probe setup is performed in 3 major steps:

(a) The setup of the spectroscopic parameters, i.e rf pulse length, rf power, spectral width and receiver gain.

(b) The setup of the diffusion parameters, gradient pulse length and maximum amplitude, the diffusion time and the receiver gain, which is a function of the echo time.

(c) The setup of the 2D measurement parameters, number of gradient steps,number of scans and number of repetitions.

A.2 Gradient calibration

Before carrying out diffusion measurements the only way to calibrate such gradients exactly is to measure the diffusion coefficients of a well known sample carefully and compare the results with the standard literature values. Usually one will use a water sample for this calibration, the best way is to use the Bruker standard sample called "Doped water", which is 1% H_2O in D_2O with 0.1g/l $GdCl_3$. For the proton diffusion coefficient of this sample the values of D_2O, 1.872 $\times 10^{-9}$ m^2/s measured at room temperature (298K) can be used, because the sample is practically D_2O, H_2O is only used as a tracer. If this is not available, we can use normal demineralized water. The water must be doped by using 1g/l $CuSo_4$. In this case use the value of diffusion coefficients of H_2O, 2.031 $\times 10^{-9}$ m^2/s measured at room temperature (293K) [88]. A scaling factor known as the gradient calibration constant (GCC) must be adjusted such that results from diffusion experiments standard samples yield the correct value. The GCC is determined by comparing the "old" value (i.e., the value of GCC applied during calibration experiments), with the value of *D* and the known value of diffusion coefficient from the literature D_{lit}.

$$GCC_{new} = \sqrt{\frac{D}{D_{lit}}} \times GCC_{old} \tag{A.1}$$

This value of GCC is stored using "setpre" command.

A.3 Temperature calibration

Diffusion coefficients of liquid samples are strongly temperature dependent. Temperature calibration can be performed by using an NMR temperature standard, e.g. one of the Bruker "Temperature calibration" samples. The common method to perform this calibration is to observe the chemical shift separation between the OH resonances and CHn resonances in either Methanol or Ethylene Glycol. Methanol in Methanol-d4 is used for low- temperature calibration and Ethylene Glycol in DMSO-D6 is used for temperatures above ambient.

The edte window has a wide variety of features including temperature control, monitoring corrections, and many more. To open the temperature control window, simply type "edte". Switch to the correction tab and press the "Edit" button in the linear correction line. Select "Slope/Offset calculation." Enter in the two sample and target temperatures in units of K and select "Calculate Slope and Offset." Press "OK." Select "Apply." If necessary, select "Activate" in the linear correction line. It is possible to control the settings of the monitoring window by selecting "Monitoring settings" at the bottom of the screen.

A.4 Processing 3D DOSY Data with Bruker Topspin2.1

NMR data in this thesis were processed using Bruker Topspin 2.1 software. To extract the diffusion data from the DOSY experiments, the baseline of all the spectra were corrected and the threshold was adjusted such that all signals of interest were above it. 3D DOSY processing must always be preceded by cross-peak definition that can be done either automatically by the software or manually. Cross-peaks can then be redefined, excluded, and combined via the process panel and the interactive spectrum display, allowing the operator to include only the peaks of interest in the diffusion analysis.

Command "dosy2d" is for the processing of a 2D DOSY experiment, which is a set of 1D spectra weighted by the diffusion coefficients. The outcome of the DOSY processing is that the chemical shift information displayed along x axis is obtained by FFT of the time domain data whereas the diffusion coefficients plotted along the y axis

are calculated by an ILT..

The command “dosy3d” is for a 3D DOSY data set, which is a set of 2D spectra weighted by the diffusion coefficients. Usage of the DOSY module is quite simple. First acquire a DOSY experiment either 2D or 3D. Then process it in a regular fashion along the spectroscopic axes. There are three directions for a 3D DOSY dataset as the F_3, F_2 (DOSY dimension) and F_1 direction. F_3 is always the acquisition direction. For processed data, F_2 and F_1 are always the second and third direction, respectively. The name of a 3D processing command expresses the direction in which it works. The command “tf_3” processes a 3d dataset in the F_3 direction (acquisition direction). tf_3 transforms time domain data (FID) in to frequency domain data (spectrum) by Fourier transformation.

Each row of the F_3 time domain data is baseline corrected according to BC_mod. This parameter takes the value “single” meaning the average intensity of the last quarter of the FID detected on single channel. Linear prediction is done according to ME_mod. This parameter takes the value “Lpfr”meaning forward prediction can be used to extend truncated FIDs. Each row is multiplied with a window function according to WDW. This parameter usually takes the value “sine”. Each row is phase corrected according to PH_mod. This parameter takes the value “pk”, for PH_mod = pk, tf_3 applies the values of PHC0 and PHC1. If phase values are not known by typing “xfb” on the 3D data to process a 23 or 13 plane, after doing a phase correction value in the 2D dataset, store the phase value to 3D.

The size of the processed data is determined by the processing parameter SI. A typical value for SI is TD/2. Before running “tf_3” the processing parameter SI in all three directions F_3, F_2 and F_1 must be set. “tf_3” stores the data in subcube format. It automatically calculates the subcube sizes such that one row (F_3) of subcubes fits in the available memory. After that type the command “tf_1”. In 3D DOSY processing “tf_1” only works, when data have already been processed with “tf_3”. The command “tf_1” processes a 3D dataset in the F1 direction. This transforms time domain data (FID) into frequency domain data (spectrum) by Fourier transformation. Depending on the processing parameters BC_mod, WDW_mod, ME_mod and PH_mod,“tf_1” also performs baseline correction, window multiplication, linear prediction and spectrum phase cor-

rection. After that type the command “dosy3d” to get 3d transform or type “eddosy” to open windows to set up processing parameters, type xlist= difflist, enter appropriate value for Disp$_{min}$ (lower display limit) and Disp$_{max}$ (upper display limit). Also enter value for Gdist (ms) = Gradient distance (big Delta) and Glen (ms) = Gradient length (little delta) from DOSY experiment, enter $\gamma = 4257.700$ for proton DOSY. Press “click start fitting” button to perform fitting and at the end the 3D DOSY plot is displayed. The 3D-DOSY processing method gives pseudo-3D data, where the diffusion coefficient axis is appended to usual 2D spectra, such as COSY, HMQC, and HMBC. The slice data of the 3D spectra with respect to the diffusion coefficient give the 2D spectra of the individual components. The commands “r12”, “r13” and “r23” read a plane from 3D processed data and store it as a 2D dataset. In Topspin select “procpars” tab and click on “Extract Slice” in popup menu. This opens the dialog box that offers several options, each of which selects a certain command for execution.

Furthermore set the three parameters namely plane orientation, plane number and destination proc number. **Plane orientation**: set F1-F3. This parameter determines the commands “r13” is executed. **Plane number**: the maximum plane number depends on the SI value in the direction orthogonal to the plane orientation. **Destination procno**: can put any number (example 999) where the output 2D dataset is stored. The processing state of the output 2D data relates to the processing state of the input 3D data. An extracted plane can processed with 2D processing commands like xfb, xf2, xf1 etc.

A.4.1 Error estimation

Measuring the absolute value of diffusion coefficient is very difficult because of uncertainties in gradient calibration, uncertainties in temperature. For calculating errors we did a set of 1D experiments (pulseprogram:stebpgp1s1d) and data were collected with different gradient strengths (2 to 95%) on 600 MHz Bruker Avance NMR. The intensity of the attenuated signal was calculated and the experimental data were fitted to the Stejskal-Tanner equation by using GNU plot. GNU plot is a powerful tool for data plotting and error analysis. Open the files in GNU plot by using the experimental determined values, plot the data in a linear graph, use linear fit to find the slope and

% Gradient	Gradient (Gauss/cm)
2	1.09
5	2.73
10	5.44
20	10.9
30	16.4
50	27.25
100	54.5

Table A.1: Each gradient percent corresponds to a gradient value in units of Gauss/cm.

then the percent gradient can be converted to an absolute gradient strength. Sample experimental values are listed in the Table.

After determining the gradient value for each percent gradient plot in I/I_0 vs square of the gradient, the slope can help with finding the diffusion coefficient by using the following equations.

$$D = -m/\gamma^2 \times \delta^2 \times (\Delta - \delta/3))) \tag{A.2}$$

In this example the value of δ equals to 0.60 ms to 100 ms and Δ has value of 100 ms to 200 ms. To determine the reliable size of the random error of the spectral repetitions, a single spectrum of the solvent was chosen as target. The standard errors σ_D have been calculated using exponential fitting of the signal attenuation data and estimating the errors in the relative diffusion coefficient.

Consider a function f(t), 0 $\leq$ t $\leq$ t*, represented at discrete times t_i by $f'(t_i)$ = y_i with standard deviation σ_{y_i}, and the total integration interval is $t* = Mh$, where t_i = (i-1) $\times$ Δt and $i = 1....M + 1$. The standard deviations σ_{y_i} and the variance σ_F^2 is

$$\sigma_F^2 = \left(\frac{\partial F}{\partial y_1}\right)^2 \sigma_{y_1}^2 + \left(\frac{\partial F}{\partial y_1}\right)^2 \sigma_{y_2}^2 + ... + \left(\frac{\partial F}{\partial y_M}\right)^2 \sigma_{yM}^2 \tag{A.3}$$

$$= \sum_{i=1}^{M} \left(\frac{\partial F}{\partial y_i}\right)^2 \sigma_{y_i}^2 = \sum_{i=1}^{M} h^2 \sigma_{y_i}^2 \tag{A.4}$$

Where = $h = \Delta$t.

$$\frac{\sigma_D}{\sigma_m} = \frac{-1}{[\gamma^2 \times \delta^2 \times (\Delta - \delta/3)]} \tag{A.5}$$

For both PFGSE and PFGSTE, the standard deviation for Δ and δ are

$$\frac{\sigma_D}{\sigma_\Delta} = \frac{-1}{[\gamma^2 \times \delta^2 \times (\Delta - \delta/3)^2]} \tag{A.6}$$

$$\frac{\sigma_D}{\sigma_\delta} = \frac{-m}{[3\gamma^2 \times \delta^2 \times (\Delta - \delta/3)^2]} + \frac{2m}{\gamma^2 \times \delta^2 \times (\Delta - \delta/3)]} \tag{A.7}$$

Therefore

$$\sigma_{D_{sample}} = \sqrt{\left[\left(\frac{\sigma_D}{\sigma_m}\right) \times \sigma_m\right]^2 + \left[\left(\frac{\sigma_D}{\sigma_\Delta}\right) \times \sigma_\Delta\right]^2 + \left[\left(\frac{\sigma_D}{\sigma_\delta}\right) \times \sigma_\delta\right]^2} \tag{A.8}$$

A.5 The DOSY Toolbox Kit

Some of the diffusion data in this thesis was also processed using the DOSY Toolbox opensource software package (http://dosytoolbox.chemistry.manchester.ac.uk/dosytoolbox).

A reference 2D NMR spectrum was recorded on the Bruker Avance-III 600-MHz spectrometer, by setting the value of gradient strengths, spectral widths, diffusion time intervals, number of scan and gradient duration. For processing, the DOSYToolbox program was run using the shell script “run_DOSYToolbox09_Linux32.sh”, giving the location of the v710 directory as an argument. The main window will then open, which provides access to all processing capabilities via processing panels and menus. A data set is then imported using the “file” menu. The following tools help in processing the imported DOSY data.

1. “Spectrum number” panel is used to display the different gradient levels.
2. “Phase correction” panel is used for zero and first order phase correction applied using the slide bars.
3. “Plot control” panel is used to zoom, expand, and scale the spectra and the FIDs.

4. “Standard processing” panel is used to set the number of points for the Fourier transformation, the window function and the reference peak.

5. “Corrections” panel is used to set the baseline correction and reference deconvolution. Clicking the “FIDDLE” button applies the reference deconvolution. The “center” button sets the center frequency of the signal.

6. “Advanced processing” panel, click the “Process” button for running the method with current settings.

7. “DOSY” button gives access to both the standard DOSY as well as to multi-exponential fitting. This leads to two dimensions, one dimension gives information about chemical shift and second gives information about diffusion coefficients.

REFERENCES

[1] J. Kowalewski and L. Mäler. *Nuclear spin relaxation in liquids: Theory, experiments, and applications*. Taylor and Francis, 2006.

[2] L. Emsley and G. Bodenhausen. Optimization of shaped selective pulses for NMR using a quaternion description of their overall propagators. *J.Magn.Reson*, 97:135, 1992.

[3] E. Kupce, J. Boyd, and I. D. Campbell. Short selective pulses for biochemical applications. *J.Magn.Reson*, 106B:300, 1995.

[4] C. P. Slichter. *Principles of Magnetic Resonance*. Springer Berlin., 1978.

[5] K. Wüthrich. *NMR of proteins and nucleic acids*. Wiley, 1986.

[6] R. R. Ernst, G. Bodenhausen, and A. Wokaun. *Principles of Nuclear Magnetic Resonance in One and Two Dimensions*. Oxford University Press, 1987.

[7] Atta-ur-Rahman. *Nuclear Magnetic Resonance: Basic Principles*. Springer, 1986.

[8] T. C. Pochapsky and S. S. Pochapsky. *NMR for Physical and Biological Scientists*. Garland Science, 2006.

[9] P. T. Callaghan. *Principles of Nuclear Magnetic Resonance Microscopy*. Oxford University Press, 1994.

[10] H. Günther. *NMR Spectroscopy: Basic Principles, Concept, and application in Chemistry*. John Wiley and Sons, 1992.

[11] E. Fukushima and S. B. W. Roeder. *Experimental Pulse NMR: A Nuts and Bolts Approach*. Addison-Wesley, 1993.

[12] J. B. Lambert and E. P. Mazzola. *Nuclear Magnetic Resonance Spectroscopy: An Introduction to Principles Applications, and Experimental Methods*. Pearson Prentice Hall, 2003.

[13] Q. Teng. *Structural Biology: Practical NMR Applications*. Springer, 2005.

[14] J. Keeler. *Understanding NMR Spectroscopy*. John Wiley and Sons, 2010.

[15] R. Freeman. *Spin Choreography: Basic Steps in High Resolution NMR*. Pearson Prentice Hall, 1997.

[16] M. H. Levitt. *Spin Dynamics: Basic of Nuclear Magnetic Resonance*. Pearson Prentice Hall, 2008.

[17] G. S. Rule and T. K. Hitchens. *Fundamentals of Protein NMR Spectroscopy*. Cambridge University Press, 2006.

[18] R. L. Vold, J. S. Waugh, M. P. Klein, and D. E. Phelps. Measurement of spin relaxation in complex systems. *J. Chem. Phys.*, 48:3831, 1968.

[19] H. Y. Carr and E. M. Purcell. Effects of diffusion on free precession in nuclear magnetic resonance experiments. *Phys. Rev.*, 94:630–638, 1954.

[20] S. Meiboom and D. Gill. Modified spin-echo method for measuring nuclear relaxation times. *Rev. Sci. Instrum*, 29:688, 1958.

[21] E. L. Cussler. *Diffusion: Mass Transfer in Fluid Systems*. Cambridge University Press, 2009.

[22] G. B. Arfken, H. J. Weber, and F. E. Harris. *Mathematical Methods for Physicists, Sixth Edition: A Comprehensive Guide*. Academic Press, 2005.

[23] W. S. Price. *NMR studies of Translational Motion: Principles and Applications*. Cambridge University Press, 2009.

[24] P. T. Callaghan, S. L. Codd, and J. D. Seymour. Spatial coherence phenomena arising from translational spin motion in gradient spin-echo experiments. *Concepts Magn. Reson. Part A*, 11:181–202, 1999.

[25] J. Crank. *The Mathematics of Diffusion, Second Edition*. Oxford University Press, 1980.

[26] W. S. Price. Pulsed-field gradient nuclear magnetic resonance as a tool for studying translational diffusion: Part II. experimental aspects. *Concepts Magn. Reson. Part A*, 10:197–237, 1998.

[27] H. J. V. Tyrrell and K. R. Harris. *Diffusion in Liquids: A Theoretical and Experimental Study*. Butterworth-Heinemann, 1984.

[28] C. S. Johnson. Diffusion ordered nuclear magnetic resonance spectroscopy:principles and applications. *Prog. Nuc. Magn. Reson*, 34:203, 1999.

[29] W. S. Price. Pulsed field gradient nuclear magnetic resonance as a tool for studying translational diffusion: Part I. basic theory. *Concepts. Magn. Reson*, page 299, 1997.

[30] M. D. Pelta, H. Barjat, G. A. Morris, A. L. Davis, and S. J. Hammond. Pulse sequences for high-resolution diffusion-ordered spectroscopy (HR-DOSY). *Magn. Reson. Chem*, 36:706–714, 1998.

[31] S. Viel, F. Ziarelli, and S. Caldarelli. Enhanced diffusion-edited NMR spectroscopy of mixtures using chromatographic stationary phases. *Proc. Natl. Acad. Sci. USA*, 100:9696, 2003.

[32] S. Caldarelli. Chromatographic NMR: A tool for the analysis of mixtures of small molecules. *Magn. Reson. Chem*, 45:S48–S55, 2007.

[33] S. Viel and S. Caldarelli. Improved 3D DOSY-TOCSY experiment for mixture analysis. *Chem. Comm*, 7:2013–2015, 2008.

[34] A. M. Torres, G. Zheng, and W. S. Price. J-compensated PGSE: An improved NMR diffusion experiment with fewer phase distortions. *Magn. Reson. Chem*, 48:129, 2009.

[35] E. O. Stejskal and J. E. Tanner. Spin diffusion measurements: Spin-echoes in the presence of a time-dependent field gradient. *J. Chem. Phys.*, 42:288–292, 1965.

[36] E. L. Hahn. Spin echoes. *Phys. Rev.*, 80:580–594, 1950.

[37] K. I. Momot and P. W. Kuchel. PFG NMR diffusion experiments for complex systems. *Concepts. Magn. Reson*, 28A:249–269, 2006.

[38] J. Keeler, R. T. Clowes, A. L. Davis, and E. D. Laue. Pulsed-field gradients: Theory and practice. *Prog. Nuc. Magn. Reson*, 239:145–207, 1994.

[39] H. C. Torrey. Bloch equations with diffusion terms. *Phys. Rev.*, 104:563–565, 1956.

[40] H. Walderhaug, O. Söderman, and D. Topgaard. Self-diffusion in polymer systems studied by magnetic field-gradient spin-echo NMR methods. *Prog. Nuc. Magn. Reson*, 56:406–425, 2010.

[41] B. Antalek. Using PGSE NMR for chemical mixture analysis:Quantitative aspects. *Concepts. Magn. Reson*, 30A:219, 2007.

[42] P. Stilbs. Fourier transform pulsed-gradient spin-echo studies of molecular diffusion. *Prog. Nuc. Magn. Reson*, 19:1–45, 1987.

[43] D. H. Wu, A. D. Chen, and C. S. Johnson, Jr. An improved diffusion-ordered spectroscopy experiment incorporating bipolar-gradient pulses. *Journal of Magnetic Resonance, Series A*, 115:260–264, 1995.

[44] P. J. Basser. Inferring microstructural features and the physiological state of tissues from diffusion-weighted images. *NMR Biomed.*, 8:333–344, 1995.

[45] P. C. Lauterbur. Image formation by induced local interactions: Examples employing nuclear magnetic resonance. *Nature*, 242:190–191, 1973.

[46] W. S. Price. Pulsed-field gradient nuclear magnetic resonance as a tool for studying translational diffusion: Part 1. basic theory. *Concepts Magn. Reson. Part A*, 9:299–336, 1997.

[47] W. S. Price. Applications of pulsed gradient spin-echo NMR. diffusion measurements to solution dynamics and organization. *Diffusion Fundamentals*, 2:112.1–112.19, 2005.

[48] K. Hayamizu, Y. Aihara, H. Nakagawa, T. Nukuda, and W. S. Price. Ionic conduction and ion diffusion in binary room-temperature ionic liquids composed of [emim][bf4] and libf4. *J. Phys. Chem. B*, 108:19527–19532, 2004.

[49] O. Söderman and P. Stilbs. NMR studies of complex surfactant systems. *NMR Biomed.*, 26:445–482, 1994.

[50] A. M. Weljie, A. P. Yamniuk, H. Yoshino, Y. Izumi, and H. J. Vogel. Protein conformational changes studied by diffusion NMR spectroscopy: Application to helix-loop-helix calcium binding proteins. *Protein Sci.*, 12:228–236, 2003.

[51] K. I. Momot and P. W. Kuchel. Pulsed field gradient nuclear magnetic resonance as a tool for studying drug delivery systems. *Concepts Magn. Reson. Part A*, 19A:51–64, 2003.

[52] B. P. Mayer, C. A. Valdez, S. Hok, S. C. Chinn, and B. R. Hart. 31P-edited diffusion-ordered ^{1}H nmr spectroscopy for the spectral isolation and identification of organophosphorus compounds related to chemical weapons agents and their degradation products. *Anal. Chem.*, 84:10478–10484, 2012.

[53] S. Viel, F. Ziarelli, G. Pages, C. Carrara, and S. Caldarelli. Pulsed field gradient magic angle spinning NMR self-diffusion measurements. *J.Magn.Reson*, 190:113, 2008.

[54] N. N. Yadav, A. M. Torres, and W. S. Price. An improved approach to calibrating high magnetic field gradients for pulsed field gradient experiments. *J.Magn.Reson*, 194:25, 2008.

[55] C. Carrara, S. Viel, C. Delaurent, F. Ziarelli, G. Excoffier, and S. Caldarelli. Chromatographic NMR in NMR solvents. *J.Magn.Reson*, 194:303, 2008.

[56] S. Caldarelli. Chromatographic NMR. *Ann. Rep. NMR Spect*, 73:159, 2011.

[57] D. Li, G. Kagan, R. Hopson, and P. G. Williard. Formula weight prediction by internal reference diffusion ordered NMR spectroscopy (DOSY). *J. Am. Chem. Soc*, 131:5627, 2009.

[58] T. Brand, E. J. Cabrita, and S. Berger. Intermolecular interaction as investigated by NOE and diffusion studies. *Prog. Nuc. Magn. Reson*, 46:159, 2005.

[59] T. Brand, E. J. Cabrita, G. A. Morris, R. Gunther, H. J. Hofmann, and S. Berger. Residue specific NH exchange rates studied by NMR diffusion experiments. *J.Magn.Reson*, 187:97–104, 2007.

[60] A. M. Krause-Heuer, N. J. Wheate, W. S. Price, and J. Aldrich-Wright. Diffusion-based studies on the self-stacking and nanorod formation of platinum(II) intercalators. *Chem. Comm*, 10:1210, 2009.

[61] D. G. Regan and P. W. Kuchel. Simulations of molecular diffusion in lattices of cells: Insights for NMR of red blood cells. *Biophysical Journal*, 83:161, 2002.

[62] N. J. Wheate, P. G. A. Kumar, A. M. Torres, J. R. Aldrich-Wright, and W. S. Price. Examination of cucurbit[7]uril and its host-guest complexes by diffusion nuclear magnetic resonance. *J. Phys. Chem. B*, 112:2311, 2008.

[63] S. Viel, M. Mazarin, R. Giordanengo, T. N. T. Phan, L. Charles, S. Caldarelli, and D. Bertin. Improved compositional analysis of block copolymers using diffusion ordered NMR spectroscopy. *Anal. Chim. Acta*, 654:45, 2009.

[64] A. Ambrus and D. Yang. Diffusion-ordered nuclear magnetic resonance spectroscopy for analysis of DNA secondary structural elements. *Analytical Biochem*, 367:56, 2007.

[65] J. Yan, A. D. Kline, H. Mo, E. R. Zartler, and M. J. Shapiro. Epitope mapping of ligand-receptor interactions by diffusion NMR. *J. Am. Chem. Soc*, 124:9984, 2002.

[66] S. R. Inglis, M. J. Mcgann, W. S. Price, and M. M. Harding. Diffusion NMR studies on fish antifreeze proteins and synthetic analogues. *FEBS Lett*, 580:3911, 2006.

[67] W. S. Price. Protein association studied by NMR diffusometry. *Current Opinion in Colloid and Interface Science*, 11:19–23, 2006.

[68] B. A. Becker, K. F. Morris, and C. K. Larive. An improved method for suppressing protein background in PFG NMR experiments to determine ligand diffusion coefficients in the presence of receptor. *J.Magn.Reson*, 181:327, 2006.

[69] M. Nilsson, A. M. Gil, I. Delgadillo, and G. A. Morris. Improving pulse sequences for 3D diffusion-ordered NMR spectroscopy:âĂL'2DJ-IDOSY. *Analytical Chem*, 76:5418–5422, 2004.

[70] M. Nilsson, A. M. Gil, I. Delgadillo, and G. A. Morris. Improving pulse sequences for 3D DOSY: COSY-IDOSY *Chem. Comm*, pages 1737–1739, 2005.

[71] J. M. Newman and A. Jerschow. Improvements in complex mixture analysis by NMR: DQF-COSY iDOSY *Analytical Chem*, 79:2957–2960, 2007.

[72] H. Barjat, G. A. Morris, and A. G. Swanson. A three-dimensional DOSY-HMQC experiment for the high-resolution analysis of complex mixtures. *J.Magn.Reson*, 131:131–138, 1998.

[73] M. J. Stchedroff, A. M. Kenwright, G. A. Morris, M. Nilsson, and R. K. Harris. 2D and 3D DOSY methods for studying mixtures of oligomeric dimethylsiloxanes. *Phys. Chem. Chem. Phys*, 6:3221, 2004.

[74] B. Vitorge and D. Jeanneat. NMR diffusion measurements in complex mixtures using constant time HSQC-iDOSY and computer optimized spectral aliasing for high resolution in the carbon dimension. *Analytical Chem*, 78:5601, 2006.

[75] K. Vermillion and N. P. J. Price. Stable isotope-enhanced two and three-dimensional diffusion ordered ^{13}C NMR spectroscopy (SIE-DOSY ^{13}C NMR). *J.Magn.Reson*, 198:209, 2009.

[76] S. W. Provencher. CONTIN:a general purpose constrainted regularization program for inverting NOISY linear algebraic and integral equations. *Comput. Phys. Commun*, 27:229, 1982.

[77] M. Delsuc and T. E. Malliavin. Maximum entropy processing of DOSY NMR data. *Analytical Chem*, 70:2146, 1998.

[78] M. Nilsson, M. A. Connell, A. L. Davis, and G. A. Morris. Biexponential fitting of diffusion-ordered NMR data: Practicalities and limitations. *Analytical Chem*, 78:3040, 2006.

[79] P. Schanda, H. Van. Melckebeke, and B. Brutscher. Speeding up three-dimensional protein NMR experiments to a few minutes. *J. Am. Chem. Soc*, 128:9042, 2006.

[80] E. Lescop, P. Schanda, and B. Brutscher. A set of BEST triple-resonance experiments for time-optimized protein resonance assignment. *J.Magn.Reson*, 187:163, 2007.

[81] E. Lescop, T. Kern, and B. Brutscher. Guidelines for the use of band-selective radiofrequency pulses in hetero-nuclear NMR: Example of longitudinal-relaxation-enhanced BEST-type ^{1}H-^{15}N correlation experiments. *J.Magn.Reson*, 203:190, 2010.

[82] P. Schanda and B. Brutscher. Very fast two-dimensional NMR spectroscopy for real time investigation of dynamic events in proteins on the time scale of seconds. *J. Am. Chem. Soc*, 127:8014, 2005.

[83] P. Schanda, E. Kupce, and B. Brutscher. SOFAST-HMQC experiments for recording two-dimensional heteronuclear correlation spectra of proteins within a few seconds. *J. Bio. NMR*, 33:199, 2005.

[84] P. Schanda and B. Brutscher. Hadamard frequency encoded SOFAST-HMQC for ultrafast two-dimensional protein NMR. *J.Magn.Reson*, 178:334, 2006.

[85] T. Kern, P. Schanda, and B. Brutscher. Sensitivity enhanced IPAP-SOFAST-HMQC for fast-pulsing 2D NMR with reduced radiofrequency load. *J.Magn.Reson*, 190:333–338, 2008.

[86] G. Zheng, T. Stait-Gardner, P. G. Anil Kumar, A. M. Torres, and W. S. Price. PGSTE-WATERGATE:an STE-based PGSE NMR sequence with excellent solvent suppression. *J.Magn.Reson*, 191:159, 2008.

[87] G. Zheng and W. S. Price. Simultaneous convection compensation and solvent suppression in biomolecular NMR diffusion experiments. *J. Bio. NMR*, 45:295, 2009.

[88] M. Holz, S. R. Heila, and A. Sacco. Temperature-dependent self-diffusion coefficients of water and six selected molecular liquids for calibration in accurate ^{1}H NMR PFG measurements. *Phys. Chem. Chem. Phys.*, 2:4740–4742, 2000.

[89] E. Kupce and R. Freeman. Wideband excitation with polychromatic pulses. *J.Magn.Reson*, 108A:268, 1994.

[90] M. A. McCoy and L. Mueller. Nonresonant effects of frequency-selective pulses. *J.Magn.Reson*, 99:18, 1992.

[91] G. S. Kapur and S. Berger. Simplification and assignment of proton and two-dimensional hetero-correlated NMR spectra of petroleum fractions using gradient selected editing pulse sequences. *Fuel*, 81:883, 2002.

[92] J. Burri, R. Crockett, R. Hany, and D. Rentsch. Gasoline composition determined by ^{1}H NMR spectroscopy. *Fuel*, 83:187, 2004.

[93] A. S. McLachlan, J. J. Richards, A. R. Bilia, and G. A. Morris. Constant time gradient HSQC-iDOSY: practical aspects. *Magn. Reson. Chem*, 47:1081, 2009.

[94] C. A. Steinbeck and B. F. Chmelka. Rapid ^{1}H-^{13}C-resolved diffusion and spin-relaxation measurements by NMR spectroscopy. *J. Am. Chem. Soc*, 127:11624, 2005.

[95] P. Wurtz, P. Permi, N. C. Nielsen, and O. W. Sørensen. Clean-HMBC:suppression of strong-coupling induced artefacts in HMBC spectra. *J.Magn.Reson*, 194:89, 2008.

[96] S. Meier, B. O. Petersen, J. O. Duus, and O. W. Sørensen. Recent progress in heteronuclear long-range NMR of complex carbohydrates: 3D H2BC and Clean HMBC. *Carbohydrate Research*, 344:2274, 2009.

[97] T. E. Burrow, R. G. Enriquez, and W. F. Reynolds. The signal/noise of an HMBC spectrum can depend dramatically upon the choice of acquisition and processing parameters. *Magn. Reson. Chem*, 47:1086, 2009.

[98] K. Furihata, M. Tashiro, and H. Seto. High-resolution HMBC (HR-HMBC) a new method for measuring heteronuclear long-range coupling constants. *Magn. Reson. Chem*, 48:179, 2010.

[99] K. Furihata, M. Tashiro, and H. Seto. Bird J resolved HMBC and bird high resolution HMBC pulse sequences for measuring heteronuclear long-range coupling constants and proton-proton spin coupling constants in complicated spin systems. *Magn. Reson. Chem*, 49:53, 2011.

[100] W. Schoefberger, J. Schlagnitweit, and N. Muller. Recent developments in heteronuclear multiple-bond correlation experiments. *Ann. Rep. NMR Spect*, 72:1, 2011.

[101] T. D. W. Claridge and I. Pérez-Victoria. Enhanced ^{13}C resolution in semi-selective HMBC: A band-selective constant-time HMBC for complex organic structure elucidation by NMR. *Org. Biomed. Anal*, 1:3632, 2003.

[102] J. Furrer. A robust sensitive and versatile HMBC experiment for rapid structure elucidation by NMR: IMPACT-HMBC. *Chem. Comm*, 46:3396, 2010.

[103] J. F. K. Limtiaco, D. J. Langeslay, S. Beni, and C. K. Larive. Getting to know the nitrogen next door: HNMBC measurements of amino sugars. *J.Magn.Reson*, 209:323, 2011.

[104] E. Kupce and R. Freeman. Fast multidimensional NMR by polarization sharing. *Magn. Reson. Chem*, 45:2, 2007.

[105] M. F. Summers, L. G. Marzilli, and A. Bax. Complete ^{1}H and ^{13}C assignments of coenzyme B12 through the use of new two-dimensional NMR experiments. *J. Am. Chem. Soc.*, 108:4285–4294, 1986.

[106] K. Furihata and H. Seto. Decoupled HMBC (D-HMBC), an improved technique of HMBC. *Tetrahedron Lett.*, 36:2817–2820, 1995.

[107] A. J. Benie and O. W. Sørensen. HAT HMBC: A hybrid of H2BC and HMBC overcoming shortcomings of both. *J. Magn. Reson.*, 184:315–321, 2007.

[108] K. Furihata and H. Seto. Constant time HMBC (CT-HMBC), a new HMBC technique useful for improving separation of cross peaks. *Tetrahedron Lett.*, 39:7337–7340, 1998.

[109] J. Furrer. A robust, sensitive, and versatile HMBC experiment for rapid structure elucidation by NMR: IMPACT-HMBC. *Chem. Commun.*, 46:3396–3398, 2010.

[110] N. Birlirakis and E. Guittet. A new approach in the use of gradients for size-resolved 2D-NMR experiments. *J. Am. Chem. Soc*, 118:13083–13084, 1996.

[111] H. Kogler, O. W. Sørensen, G. Bodenhausen, and R. R. Ernst. Low-pass J filters. suppression of neighbor peaks in heteronuclear relayed correlation spectra. *J.Magn.Reson*, 55:157, 1983.

[112] A. Meissner and O. W. Sørensen. Economizing spectrometer time and broadband excitation in small-molecule heteronuclear NMR correlation spectroscopy. broadband HMBC. *Magn. Reson. Chem*, 38:981, 2000.

[113] D. O. Cicero, G. Barbato, and R. Bazzo. Sensitivity enhancement of a two-dimensional experiment for the measurement of heteronuclear long-range coupling constants by a new scheme of coherence selection by gradients. *J.Magn.Reson*, 148:209, 2001.

[114] A. Botana, J. A. Aguilar, M. Nilsson, and G. A. Morris. J-modulation effects in DOSY experiments and their suppression: The Oneshot45 experiment. *J.Magn.Reson*, 208:270, 2011.

[115] D. H. Wu, A. D. Chen, and C. S. Johnson, Jr. Three-dimensional diffusion-ordered NMR spectroscopy: the homonuclear COSY-DOSY experiment. *J.Magn.Reson*, 121A:88–91, 1996.

[116] W. H. Otto and C. K. Larive. Improved spin-echo edited NMR diffusion measurements. *J.Magn.Reson*, 153:273, 2001.

[117] L. H. Lucas, W. H. Otto, and C. K. Larive. The 2D-J-DOSY experiment: resolving diffusion coefficients in mixtures. *J.Magn.Reson*, 156:138–145, 2002.

[118] H. Zhang, R. Kerssebaum, and R. M. Gschwind. Improved applicability of DOSY experiments by high resolution probes combined with gradient amplifiers of diffusion units. *Magn. Reson. Chem*, 47:568, 2009.

[119] M. Shukla and K. Dorai. Resolving overlaps in diffusion encoded spectra using band-selective pulses in a 3D BEST-DOSY experiment. *J.Magn.Reson*, 213:69, 2011.

[120] A. A. Colbourne, G. A. Morris, and M. Nilsson. Local covariance order diffusion-ordered spectroscopy: A powerful tool for mixture analysis. *J. Am. Chem. Soc*, 133:7640–7643, 2011.

[121] A. K. Rogerson, J. A. Aguilar, M. Nilsson, and G. A. Morris. Simultaneous enhancement of chemical shift dispersion. *Chem. Comm*, 47:7063, 2011.

[122] D. P. Weitekamp. Time-domain multiple-quantum NMR. *Adv. Magn. Reson.*, 11:111, 1983.

[123] A. Wokaun and R. R. Ernst. Selective detection of multiple quantum transitions in NMR by two-dimensional spectroscopy. *Chem.Phys.Lett*, 52:407, 1977.

[124] D. N. Shykind, J. Baum, S. B. Liu, and A. Pines. Phase-incremented multiple quantum NMR experiments. *J.Magn.Reson*, 76:149, 1988.

[125] R. T. Syvitski, N. Burlinson, E. E. Burnell, and J. Jeener. Simultaneous selective detection of multiple quantum spectra. *J.Magn.Reson*, 155:251–256, 2002.

[126] K. Dorai and A. Kumar. Cascades of selective pulses on connected single-quantum transitions leading to the selective excitation of multiple-quantum coherences. *J.Magn.Reson*, A114:155, 1995.

[127] X. Zhu, S. Chen, Z. Chen, S. Cai, and J. Zhong. Simultaneous acquisition and effective separation of intermolecular multiple-quantum signals of different orders. *Chem.Phys.Lett*, 438:308, 2007.

[128] K. Dorai, Arvind, and A. Kumar. Implementing quantum logic operations, pseudo-pure states and the Deutsch-Jozsa algorithm using non-commuting selective pulses in NMR. *Phys. Rev. A*, 61:042306, 2000.

[129] N. Khaneja, F. Kramer, and S. J. Glaser. Optimal experiments for maximizing coherence transfer between coupled spins. *J.Magn.Reson*, 173:116–124, 2005.

[130] A. Lesage, C. Auger, S. Caldarelli, and L. Emsley. Determination of though-bond carbon-carbon connectivities in solid-state NMR using the inadequate experiment. *J. Am. Chem. Soc*, 119:7867, 1997.

[131] A. M. Dixon and C. K. Larive. NMR spectroscopy with spectral editing for the analysis of complex mixtures. *Appl. Spectrosc*, 53:426A, 1999.

[132] W. L. Meerts, C. A. DeLange, A. C. J. Weber, and E. E. Burnell. Evolutionary algorithms to solve complicated NMR spectra. *J. Chem. Phys*, 130:44504, 2009.

[133] D. Zax and A. Pines. Study of anisotropic diffusion of oriented molecules by multiple quantum spin-echoes. *J. Chem. Phys.*, 78:6333, 1983.

[134] L. E. Kay and J. H. Prestegard. An application of pulse-gradient double-quantum spin echoes to diffusion measurements on molecules with scalar-coupled spins. *J. Magn. Reson.*, 67:103–113, 1969.

[135] B. Baishya and N. Suryaprakash. Spin state selective detection of single quantum transitions using multiple quantum coherence: Simplifying the analyses of complex NMR spectra. *J. Phys. Chem. A*, 111:5211, 2007.

[136] B. Baishya and N. Suryaprakash. Spin selective multiple quantum NMR for spectral simplification, determination of relative signs, and magnitudes of scalar couplings by spin state selection. *J. Chem. Phys*, 127:214510, 2007.

[137] B. Baishya, G. N. M. Reddy, U. R. Prabhu, T. N. G. Row, and N. Suryaprakash. Simplifying the complex ^{1}H NMR spectra of fluorine-substituted benzamides by spin system filtering and spin-state selection: Multiple-quantum-single-quantum correlation. *J. Phys. Chem. A*, 112:10526, 2008.

[138] G. N. Manjunatha Reddy, T. N. Guru Row, and N. Suryaprakash . Discerning the degenerate transitions of scalar coupled ^{1}H NMR spectra: correlation and resolved techniques at higher quantum. *J.Magn.Reson*, 196:119–126, 2009.

[139] U. R. Prabhu and N. Suryaprakash. Selective homonuclear decoupling in ^{1}H NMR: Application to visualization of enantiomers in chiral aligning medium and simplified analyses of spectra in isotropic solutions. *J. Phys. Chem. A*, 114:5551–5557, 2010.

[140] G. N. Manjunatha Reddy and S. Caldarelli. Demixing of severely overlapping NMR spectra through multiple-quantum NMR. *Analytical Chem*, 82:3266–3269, 2010.

[141] G. N. M. Reddy and S. Caldarelli. Maximum-quantum (MAXQ) NMR for the speciation of mixtures of phenolic molecules. *Chem. Comm*, 47:4297, 2011.

[142] G. N. Reddy and S. Caldarelli. Identification and quantification of epa 16 priority polycyclic aromatic hydrocarbon pollutants by maximum-quantum NMR. *Analyst.*, 137:741–746, 2012.

[143] G. Bodenhausen. Multiple-quantun NMR. *Progress in Nuclear Magnetic Resonance Spectroscopy*, 14:137–173, 1981.

[144] G. P. Drobny. Multiple-quantun NMR: Studies of molecules in ordered phases. *Ann.Rev.Phys.Chem*, 36:451–489, 1985.

[145] T. J. Norwood. Multiple-quantum NMR methods. *Progress in Nuclear Magnetic Resonance Spectroscopy*, 24:295–375, 1992.

[146] K. Dorai and A. Kumar. Fluorine chemical shift tensors in substituted fluorobenzenes using cross correlations in NMR relaxation. *Chem.Phys.Lett*, 335:176, 2001.

[147] S. Begam Elavarasi and K. Dorai. Characterization of the 19F chemical shielding tensor using cross-correlated spin relaxation measurements and quantum chemical calculations. *Chem.Phys.Lett*, 489:248, 2010.

[148] K. F. Morris and C. S. Johnson. Diffusion-ordered two-dimensional nuclear magnetic resonance spectroscopy. *J. Am. Chem. Soc*, 114:3139, 1992.

[149] C. F. Tormena, R. Evans, S. Haiber, M. Nilsson, and G. A. Morris. Matrix-assisted diffusion-ordered spectroscopy: mixture resolution by NMR using SDS micelles. *Magn. Reson. Chem*, 48:550–553, 2010.

[150] R. W. Adams, J. A. Aguilar, J. Cassani, G. A. Morris, and M. Nilsson. Resolving natural product epimer spectra by matrix-assisted DOSY. *Org. Biomol. Chem*, 9:7062–7064, 2011.

[151] J. Cassani, M. Nilsson, and G. A. Morris. Flavonoid mixture analysis by matrix-assisted diffusion-ordered spectroscopy. *Journal of Natural Products*, 75:131–134, 2012.

[152] R. Evans, S. Haiber, M. Nilsson, and G. A. Morris. Isomer resolution by micelle-assisted diffusion-ordered spectroscopy. *Analytical Chem*, 81:4548, 2009.

[153] J. T. Gerig. Gradient-enhanced proton-fluorine NOE experiments. *Magn. Reson. Chem*, 37:647–652, 1999.

[154] J. T. Gerig. Fluorine NMR of proteins. *Prog. Nuc. Magn. Reson*, 26:293–370, 1994.

[155] B. Halliwell, M. A. Murcia, S. Chirico, and O. I. Aruoma. Free radicals and antioxidants in food and in vivo what they do and how they work. *Crit Rev Food Sci Nutr*, 35:7–20, 1995.

[156] A. Kunwar, A. Barik, R. Pandey, and K. I. Priyadarsini. Transport of liposomal and albumin loaded curcumin to living cells an absorption and fluorescence spectroscopic study. *Biochim Biophys Acta*, 1760:1513–1520, 2006.

[157] B. B. Aggarwal, A. Kumar, and A. C. Bharti. Anticancer potential of curcumin preclinical and clinical studies. *Anticancer Res*, 23:363–398, 2003.

[158] E. Herrera and C. Barbas. Vitamin E action, metabolism and perspectives. *J Physiol Biochem*, 57:43–56, 2001.

[159] J. J. López Cascales, T. F. Otero, A. J. Fernández Romero, and L. Camacho. Phase transition of a DPPC bilayer induced by an external surface pressure: from bilayer to monolayer behavior. a molecular dynamics simulation study. *Langmuir*, 22:5818–5824, 2006.

[160] R. Meyer, A. F. Sonnen, and W. M. Nau. Phase-dependent lateral diffusion of Îś-tocopherol in DPPC liposomes monitored by fluorescence quenching. *Langmuir*, 26:14723–14729, 2010.

[161] Y. Wang, L. A. Benton, V. Singh, and G. J. Pielak. Disordered protein diffusion under crowded conditions. *J. Phys. Chem. Lett.*, 3:2703, 2012.

[162] T. Didenko, R. Boelens, and S. G. Rüdiger. 3d DOSY-TROSY to determine the translational diffusion coefficient of large protein complexes. *Protein Eng Des Sel*, 24:99–103, 2011.

[163] M. Mobli and J. C. Hoch. Maximum entropy spectral reconstruction of non-uniformly sampled data. *Concepts Magn. Reson. Part A*, 32A:436–448, 2008.

[164] S. G. Hyberts, H. Arthanari, and G. Wagner. Applications of non-uniform sampling and processing. *Topics Curr. Chem.*, 316:125, 2012.